

**Characterization of the Multicopper Oxidase LPR1 and the P5-
Type ATPase PDR2 and their roles in the Phosphate Starvation
Response of *Arabidopsis thaliana***

Dissertation

zur Erlangung des
Doktorgrades der Naturwissenschaften (Dr. rer. nat.)

der

Naturwissenschaftlichen Fakultät I – Biowissenschaften –

der Martin-Luther-Universität

Halle-Wittenberg,

vorgelegt

von Herrn Marcus Heisters

geb. am 23.04.1985 in Eisleben

1. Gutachter: Prof. Steffen Abel, Martin-Luther-Universität Halle-Wittenberg
2. Gutachter: Prof. Gary Sawers, Martin-Luther-Universität Halle-Wittenberg
3. Gutachter: Prof. Thierry Desnos, CEA Cadarache

Tag der öffentlichen Verteidigung: 21.10.2019

Curriculum vitae

Marcus Heisters
Puschkinstraße 26
06108 Halle (Saale)

0162 7973710

Marcus.Heisters@googlemail.com

Geb. 23.04.1985
in Luth. Eisleben, Deutschland

Arbeitgeber und Tätigkeiten

Wissenschaftlicher Mitarbeiter

Seit September 2018

VEROVACCINES GmbH, Halle

Wissenschaftlicher Mitarbeiter /

Doktorand

Februar 2013 – August 2018

Leibniz-Institut für Pflanzenbiochemie, Halle
Abt. Molekulare Signalverarbeitung

*Thema: Characterization of the Multicopper Oxidase LPR1
and the P5-Type ATPase PDR2 and their roles in the
Phosphate Starvation Response of Arabidopsis thaliana*

Bildung

Studium

Oktober 2006 – März 2012

Studium der Biologie, Martin-Luther-Universität Halle-
Wittenberg

*Spezialisierungen: Mikrobiologie, Biochemie, Immunologie,
Pflanzenphysiologie*

Abschluss: Diplombiologe (1,6)

Schulbildung

Juni 2004

Abitur (2,1) am Martin-Luther-Gymnasium in Luth. Eisleben

Table of contents

I.	List of tables.....	v
II.	List of figures	v
III.	List of supplemental tables	vii
IV.	List of supplemental figures	vii
V.	List of abbreviations	vii
1	Introduction.....	1
1.1	The importance of phosphorus.....	1
1.2	General adaptations of plants to phosphate-deprived soils.....	1
1.3	The Phosphate Starvation Response of <i>Arabidopsis thaliana</i>	2
1.3.1	The systemic phosphate starvation response.....	2
1.3.2	The local phosphate starvation response	4
1.3.3	Function of LPR1 during phosphate starvation response	6
1.3.4	<i>PDR2</i> – The great unknown	9
1.4	Aims of this work.....	12
2	Results	12
2.1	<i>LPR1</i> encodes a ferroxidase and acts in phosphate starvation response	12
2.1.1	General regulation of LPR1 protein levels.....	12
2.1.1.1	LPR1 protein levels are elevated in <i>35S::LPR1</i> roots.....	12
2.1.1.2	Protein levels of LPR1 remain unchanged upon transfer to –Pi conditions.....	14
2.1.2	Determination of enzymatic ferroxidase activity of LPR1.....	15
2.1.2.1	Elevated ferroxidase activity in crude extracts of <i>35S::LPR1</i>	15
2.1.2.2	ferroxidase activity of roots grown on +Pi or -Pi medium	17
2.1.3	Confirmation of apoplastic localization of LPR1.....	18
2.1.4	Transient overexpression of GFP-tagged <i>LPR1</i> and <i>LPR2</i> constructs.....	20
2.1.5	Identification of putative iron and copper binding sites in LPR1	22

2.1.5.1	Site directed mutagenesis to inhibit the formation of the Fe ²⁺ -binding site and the T1 copper cluster of LPR1.....	24
2.1.5.2	Overexpression of mutated <i>LPR1</i> variants in <i>Nicotiana benthamiana</i>	26
2.1.5.3	Complementation of <i>lpr1</i> with generated variants of <i>35S::LPR1</i>	28
2.1.6	Different approaches to obtain active, purified LPR1 protein for subsequent biochemical analyses.....	30
2.1.6.1	Purification via the GFP-tag.....	30
2.1.6.2	Purification via antibody-coupled beads.....	33
2.1.6.3	Native purification from yeast.....	34
2.1.7	Determination of basic biochemical properties of LPR1 with crude extracts of transiently transformed tobacco leaves	36
2.1.8	Complementation of a yeast <i>fet3</i> -KO mutant with LPR1	39
2.2	<i>PDR2</i> encodes a P5-Type ATPase and acts in the phosphate starvations response	41
2.2.1	Cloning of the <i>PDR2</i> -locus into the gateway compatible pENTR vector	41
2.2.2	Subcellular localization of PDR2-GFP	43
2.2.2.1	Localization of PDR2-GFP after transient overexpression in <i>N. benthamiana</i>	44
2.2.2.2	Localization of PDR2-GFP in stably transformed <i>Arabidopsis</i> plants	46
2.2.3	Complementation of <i>pdr2</i> with <i>35S::PDR2-GFP</i>	47
2.2.3.1	No complementation of short root growth phenotype on low Pi	48
2.2.3.2	Complementation of silique phenotype.....	49
3	Discussion.....	51
3.1	The outcome of LPR1 function is limited to –Pi conditions	51
3.2	Identification of LPR1 as an apoplastic ferroxidase	53
3.3	Structure-function studies and biochemical properties of LPR1	54
3.4	Purification of LPR1	57
3.5	Complementation of a Δ <i>fet3</i> <i>S. cerevisiae</i> strain by <i>LPR1</i>	59
3.6	The regulatory function of PDR2 in the phosphate starvation response.....	61
3.7	Working model.....	63
3.8	Very recent findings	64

3.9	Outlook.....	65
3.10	Summary.....	66
3.11	Zusammenfassung.....	68
4	Materials and methods	70
4.1	Chemicals and other supplies.....	70
4.2	Media.....	70
4.2.1	Preparation of washed agar	70
4.2.2	Solid Medium for sterile growth of <i>Arabidopsis</i> seedlings.....	70
4.2.3	Murashige & Skoog medium for the growth of <i>Arabidopsis</i> cell cultures	71
4.2.4	Lysogeny broth medium.....	72
4.2.5	S.O.B. and S.O.C. medium	72
4.2.6	Preparation of YPD medium for cultivation of yeast cells.....	72
4.2.7	Preparation of Synthetic Defined (SD) medium.....	72
4.3	Plant cultivation and growth conditions	73
4.3.1	Sterile growth of <i>Arabidopsis</i> seedlings on agar plates	73
4.3.2	Cultivation of <i>Arabidopsis thaliana</i> and <i>Nicotiana benthamiana</i> on soil.....	73
4.3.3	Sterile growth of <i>Arabidopsis thaliana</i> suspension cultures.....	73
4.3.4	Stable transformation of <i>Arabidopsis</i> via the floral dip method.....	73
4.3.5	Transient transformation of <i>Nicotiana benthamiana</i> leaves	74
4.3.6	Determination of primary root growth of <i>Arabidopsis thaliana</i>	74
4.4	Bacterial and yeast general procedures.....	75
4.4.1	Cultivation of bacteria and yeast.....	75
4.4.1.1	Cultivation of <i>Escherichia coli</i>	75
4.4.1.2	Cultivation of <i>Agrobacterium tumefaciens</i>	75
4.4.1.3	Cultivation of <i>Saccharomyces cerevisiae</i>	75
4.4.1.4	Inducible gene expression in liquid <i>S. cerevisiae</i> cultures for protein production and complementation assays.....	75
4.4.2	Transformation of bacteria and yeast.....	76

4.4.2.1	Transformation of chemical competent <i>Escherichia coli</i> cells	76
4.4.2.2	Transformation of chemical competent <i>Agrobacterium tumefaciens</i> cells.....	76
4.4.2.3	Transformation of <i>Saccharomyces cerevisiae</i>	76
4.5	Molecular biological methods.....	77
4.5.1	DNA based methods.....	77
4.5.1.1	Isolation of plant DNA	77
4.5.1.2	Isolation of DNA from yeast	78
4.5.1.3	Isolation of plasmid DNA	78
4.5.1.4	Preparation of agarose gels for separation of DNA fragments.....	78
4.5.1.5	Purification of DNA fragments from agarose gels.....	78
4.5.1.6	Polymerase chain reaction (PCR)	78
4.5.1.7	Site directed mutagenesis of plasmids.....	79
4.5.2	RNA based methods	79
4.5.2.1	Isolation of plant RNA.....	79
4.5.2.2	First strand cDNA synthesis from RNA samples	79
4.5.2.3	Quantification of specific mRNA levels using quantitative Realtime-PCR (qRT-PCR)	79
4.6	Protein biochemistry methods.....	80
4.6.1	Extraction from proteins from different organisms.....	80
4.6.1.1	Total protein extraction from plant material	80
4.6.1.2	Total protein extraction of <i>Arabidopsis thaliana</i> cell cultures.....	80
4.6.1.3	Extraction of cell wall proteins from suspension cultured <i>Arabidopsis thaliana</i> cells	81
4.6.1.4	Total protein extraction from yeast cells	81
4.6.2	Determination of total protein content of samples	82
4.6.3	Protein separation via SDS-PAGE (Laemmli, 1970)	82
4.6.4	Staining of SDS Gels with Coomassie Brilliant Blue	82
4.6.5	Analysis of protein samples via Western Blot	82
4.6.6	Stripping of nitrocellulose membranes after western blot analysis	83

4.6.7	Determination of specific ferroxidase activity of a protein sample via Ferrozine assay	84
4.6.8	De-glycosylation assay	84
4.6.9	Enrichment and purification of proteins	85
4.6.9.1	Protein purification via GFP-Trap (Chromotek)	85
4.6.9.2	Protein purification via Immunoprecipitation (IP) using antibody-coupled agarose beads	85
4.7	Microscopic analysis	86
4.7.1	Confocal laser scanning microscopy (cLSM)	86
5	References	87
6	Appendix	94
6.1	Eidesstattliche Erklärung / Declaration under Oath	94
6.2	Supplemental tables	95
6.3	Supplemental figures	96

I. List of tables

Table 1:	Transgenic and mutant plant lines	ix
Table 2:	Bacterial strains	ix
Table 3:	Overview of all amino acid exchange variants of LPR1 generated	25
Table 4:	Composition of Solid Medium (SM)	70
Table 5:	Composition of Murashige & Skoog medium (MS)	71
Table 6:	MS medium supplements for <i>Arabidopsis</i> cell cultures	71
Table 7:	Composition of Lysogeny broth (LB) medium	72
Table 8:	Composition of Super Optimal Broth medium	72

II. List of figures

Figure 1:	General molecular mechanisms and genes involved in the <i>Arabidopsis</i> primary root response to Pi-deprived medium	5
Figure 2:	The ectopic overexpression of <i>LPR1</i> causes an ectopic accumulation of Fe, callose and ROS in Pi-deprived roots resembling a <i>pdr2</i> -like phenotype	7
Figure 3:	Phylogenetic tree of multicopper oxidases (MCOs)	8
Figure 4:	Working model of PDR2 and LPR1 acting together to orchestrate the local PSR	11

Figure 5: Protein levels of LPR1 in different genetic backgrounds.....	13
Figure 6: Levels of LPR1 in Col-0 roots after transfer to -Pi medium.	15
Figure 7: Specific ferroxidase activity of protein extracts from whole roots of different <i>Arabidopsis thaliana</i> genotypes.....	16
Figure 8: Specific ferroxidase activity of <i>Arabidopsis</i> roots grown on + or - Pi conditions.	17
Figure 9: Determination of LPR1 levels in different fractions of <i>Arabidopsis</i> suspension cultures.	19
Figure 10: Determination of LPR1 levels in cell walls of <i>Arabidopsis</i> suspension cultures after transfer to + and -Pi conditions.	20
Figure 11: Transient overexpression of <i>Sp~GFP~LPR1</i> and <i>Sp~GFP~LPR2</i> in <i>N. benthamiana</i>	22
Figure 12: Multiple sequence alignment of LPR1, LPR2, Fet3p and Fet5p.	23
Figure 13: Predicted structure of LPR1 including putative ligand binding sites based on Fet3p modeled with the PHYRE2 and 3DLigandSite servers.	24
Figure 14: Specific ferroxidase activity of crude extracts of <i>N. benthamiana</i> transiently expressing different LPR1 variants.	26
Figure 15: Analysis of mRNA levels of different <i>LPR1</i> variants after transient expression in <i>N. benthamiana</i>	27
Figure 16: Primary root growth of <i>lpr1</i> plants transformed with different variants of <i>LPR1</i>	29
Figure 17: Protein levels and ferroxidase activities of GFP-LPR1 prior and after purification via GFP-Trap.....	32
Figure 18: Purification of untagged LPR1 using LPR1 antibody coupled to Protein A beads.....	34
Figure 19: Detection of LPR1 in different fractions of <i>S. cerevisiae</i> overexpressing LPR1 or Fet3.	35
Figure 20: Determination of basic biochemical properties of LPR1 using crude extracts of transiently transformed tobacco leaves.....	37
Figure 21: Complementation of Δ fet3 with <i>LPR1</i> , <i>Fet3</i> and a chimeric variant of both.	40
Figure 22: Amplification and test digestion of genomic <i>PDR2</i> from <i>Arabidopsis</i> in pENTR/D-TOPO. ...	43
Figure 23: Subcellular localization of PDR2-GFP in <i>N. benthamiana</i>	45
Figure 24: Localization of PDR2-GFP in roots of <i>Arabidopsis</i>	46
Figure 25: Primary root growth of <i>pdr2-2</i> lines overexpressing PDR2-GFP.	48
Figure 26: Siliques of <i>Col-0</i> , <i>pdr2</i> and three different <i>pdr2</i> lines transformed with <i>35S::PDR2-GFP</i>	50
Figure 27: Assembly and function of the Fet3p-Ftr1 Fe uptake system in <i>S. cerevisiae</i>	60
Figure 28: Working model of the interplay between PDR2 and LPR1 during the phosphate deficiency response in the SCN of <i>Arabidopsis</i> primary roots.....	63

III. List of supplemental tables

Supplemental table 1: General primers and their respective sequences used in this work.....	95
Supplemental table 2: Overview of all generated LPR1 variants and the primers used for site directed mutagenesis.	95

IV. List of supplemental figures

Supplemental Figure 1: AA sequence of <i>Arabidopsis</i> LPR1 including ER signal peptide and antibody binding epitope.	96
Supplemental figure 2: LPR1 levels in Col-0 and <i>pdr2</i> roots upon transfer to -Pi medium	96
Supplemental figure 3: Decreasing amount of A570nm min-1 in different 35S::LPR2 lines.	97
Supplemental figure 4: Ferrozine activity of tobacco leaves transiently expressing GFP, LPR1-GFP and LPR2-GFP.	97
Supplemental figure 5: Protein levels of LPR1 in different genetic backgrounds.....	98
Supplemental figure 6: <i>LPR1</i> mRNA levels in Col-0 and <i>lpr1 lpr2</i> roots.....	98
Supplemental figure 7: LPR1 levels in roots of Col-0 and SALK_095658 (<i>lpr1-2</i>).....	99
Supplemental figure 8: Western Blot of Deglycosylation Assays of total root extracts from <i>Arabidopsis</i> seedlings.	99
Supplemental figure 9: Semi-quantitative RT-PCR of LPR1 in suspension cultures.....	100
Supplemental figure 10: Western Blot probed with Anti-LPR1 AB after transient expression of 35S::LPR1 variants in tobacco.	100
Supplemental figure 11: Native LPR1 and chimeric constructs generated for expression in yeast and complementation of a Δ fet3 strain.	100

V. List of abbreviations

2,4 D	2,4-dichlorophenoxyacetic acid
AB	Antibody
BPS	Bathophenanthrolinedisulfonate
BR	Brassinosteroid
CDS	Coding sequence
cLSM	Confocal laser scanning microscopy
dat	Days after transfer

dag	Days after germination
DTT	Dithiothreitol
ECL	Enhanced chemiluminescence
EDTA	Ethylenediaminetetraacetic acid
EtOH	Ethanol
EVC	Empty vector control
ER	Endoplasmic reticulum
EZ	Elongation zone
ICP-MS	Inductively-coupled plasma mass spectrometry
LiOAc	Lithiumacetate
MCO	Multicopper oxidase
MES	2-(N-morpholino)ethanesulfonic acid
MW	Molecular weight
PAGE	Polyacrylamide gel electrophoresis
PBS	Phosphate buffered saline
Pi	Inorganic phosphate
PM	Plasma membrane
pp-insP	inositol-pyrophosphates
PSR	Phosphate starvation response
PWC	Post-wash control
q-PCR	quantitative polymerase chain reaction
qRT-PCR	Quantitative real time polymerase chain reaction
RAM	Root apical meristem
ROS	Reactive oxygen species
RPM	Rounds per minute
RT	room temperature
SCN	Stem cell niche
SD	Standard deviation
SDM	Site directed mutagenesis
SDS	Sodium dodecyl sulfate
Sp	Signal peptide
TBS	Tris buffered saline
TEM	Transmission electron microscopy
TF	Transcription factor
TPC	Total protein control

Tris	2-Amino-2-(hydroxymethyl)propane-1,3-diol
Ura	Uracil
WB	Western Blot

Table 1: Transgenic and mutant plant lines: For each mutant or transgenic line, the affected gene, the corresponding protein, the type of mutation and the background ecotype is depicted. In case of T-DNA insertion lines, the corresponding SALK-lines are indicated.

Genotype	Genomic locus	Encoded Protein	Type of mutation	T-DNA insertion line	Ecotype
<i>lpr1-1</i>	At1G23010	LPR1	T-DNA Insertion	SALK_016297	Col-0
<i>lpr1-2</i>	At1G23010	LPR1	T-DNA Insertion	SALK_095658	Col-0
<i>lpr2-1</i>	At1g71040	LPR2	T-DNA Insertion	SALK_091930	Col-0
<i>pdr2-1</i>	At5G23630	PDR2	Point mutation	T699I	Col-0
<i>pdr2-2</i>	At5G23630	PDR2	T-DNA insertion	SALK_077682	Col-0
<i>35S::LPR1</i>	At1G23010	LPR1			Col-0
<i>35S::LPR2</i>	AT1G71040	LPR2			Col-0

Table 2: Bacterial strains: Bacterial strains with their corresponding genotypes and reference are shown.

Species	Strain	Chromosomal genotype	Reference
<i>Escherichia coli</i>	Top10	F ⁻ mcrA Δ (mrr-hsdRMS-mcrBC) Φ 80lacZ Δ M15 Δ lacX74 recA1 araD139 Δ (ara leu) 7697 galU galK rpsL (StrR) endA1 nupG	Invitrogen
<i>Escherichia coli</i>	Db3.1	gyrA462 endA1 Δ (sr1-recA) mcrB mrr hsdS20 glnV44 (=supE44) ara14 galK2 lacY1 proA2 rpsL20 xyl5 leuB6 mtl1	Invitrogen

<i>Escherichia coli</i>	DH5α	<i>fhuA2 lac(del)U169 phoA glnV44 Φ80'</i> <i>lacZ(del)M15 gyrA96 recA1 relA1 endA1 thi-1</i> <i>hsdR17</i>	
<i>Agrobacterium tumefaciens</i>	GV3101	C58, pMP90 (pTiC58DT-DNA)	Koncz and Schell (1986); (Plaxton and Tran, 2011)
<i>Agrobacterium tumefaciens</i>	GV3101::pMp90RK	C58, pMP90RK (pTiC58DT-DNA)	Koncz and Schell (1986)
<i>S. cerevisiae</i>	BY4741	MATa <i>his3Δ1 leu2Δ0 met15Δ0 ura3Δ0</i>	(Brachmann et al., 1998)

1 Introduction

1.1 The importance of phosphorus

Phosphorus (P) is one of the most important elements for life. Among many other functions, its most highly oxidized form, inorganic phosphate (Pi), is a core structural component of DNA and RNA. It assumes crucial functions as an effector molecule in metabolism, in post-translational modification of proteins and is a central carrier of chemical energy in all organisms. Thus, its significance for life cannot be overestimated (Bowler et al., 2010). The pivotal function of Pi is based on its chemistry, allowing the formation of phosphoanhydride bonds that are energy rich and kinetically stable on the one hand (Schroeder et al., 2006), but on the other hand, controlled enzymatic hydrolysis of phosphorylated products within milliseconds (Zhang et al., 1994). Because of these inherent chemical properties, plants must cope with various problems to acquire Pi from their environment soil. Although the total concentration of P in soil is usually quite high, the Pi is extremely rare in most soils around the world (Tiessen et al., 1995). Since Pi is easily adsorbed to various surfaces in the soil, and preferentially forms highly insoluble complexes with other metals like Fe or Al, its diffusion rate is very low ($< 10^{-12} \text{m}^2 \text{s}^{-1}$) (Lambers et al., 2015). Thus, the concentration of bioavailable Pi within most of the soils is $< 10 \mu\text{M}$ That is far less than Pi concentrations within a cell, that can easily reach mM ranges (Schachtman et al., 1998). Unlike mobile organisms, sessile plants are only able to utilize resources that are available in their immediate surroundings. They use high affinity phosphate transporters to take up Pi against a steep concentration gradient and therefore create Pi depletion zones around their roots. Thus, Pi availability is one of the most limiting factors in agriculture around the world (White and Hammond, 2008; Lopez-Arredondo et al., 2014). To overcome this problem, excessive P fertilization is used in 80 % of all agricultural areas. However, plants are only able to use 20 – 30 % of the fertilized Pi. The remaining Pi is lost to the soil, used by bacteria or flushed away leading to eutrophication of lakes and seas (Lopez-Arredondo et al., 2014). Since Pi resources are limited and the peak of P mining is forecast to occur within the next decades (Cordell et al., 2009; Porder and Ramachandran, 2013), the understanding of the plants P acquisition machinery is crucial for a future sustainable food production.

1.2 General adaptations of plants to phosphate-deprived soils

Since Pi limitation is a common stress factor in many soils, plants have evolved several strategies to adapt to it. About 80% of all terrestrial plant species develop mycorrhizal associations to enhance their Pi acquisition from the soil (Kruger et al., 2015). However, the fungal Pi uptake system becomes less effective on strongly weathered soils, where Pi availability is severely depleted (Lambers et al., 2015). Instead, the adaptation of the root architecture is a mechanism ubiquitously used by all plants

when facing low Pi conditions. The formation of cluster roots (or proteoid roots) by Proteaceae and other families enables the growth on soils that are extremely low on nutrients. Therefore, the roots form clusters of closely spaced, short lateral roots. The secretion of carboxylates like citrate and malate between these structures generate areas with local high concentrations of these compounds. Thus, they enable the access of low Pi amounts in the soil by solubilizing Pi bound to oxides and hydroxides of Fe and Al (Lambers et al., 2006). Since the abundance of Pi usually decreases in deeper layers of the soil, many plants use a strategy that is called topsoil foraging. When confronted with Pi depleted soil, the plant inhibits the primary root growth and favors the development and growth of higher-order roots and root hairs instead. Thus, the root surface in nutrient rich, shallow soil areas increases and as a consequence, the acquisition of Pi is drastically improved (Lynch and Brown, 2001). Besides the alteration of root system architecture, biochemical reactions are also triggered which lead to the secretion of various enzymes, i.e. phosphohydrolases and nucleases, to liberate Pi from macromolecules like DNA (Chen et al., 2000). Additionally, secreted carboxylates chelate cations like Fe^{3+} and Al^{3+} to release rock-bound Pi (Meyer et al., 2010). Recent studies also revealed the Pi status-dependent colonization of *Arabidopsis* roots by *Colletotrichum tofieldiae*, a fungal endophyte, on Pi-impooverished soils. The fungus develops a dense net of hyphae that mine Pi from otherwise insoluble substances. Root-associated hyphae thereby deliver Pi to the plant (Hiruma et al., 2016).

Thus, compared with other minerals, Pi limitation is the predominant driver of root system adaptations in plants (Gruber et al., 2013; Kellermeier et al., 2014).

1.3 The Phosphate Starvation Response of *Arabidopsis thaliana*

1.3.1 The systemic phosphate starvation response

Although the phosphate starvation response in plants has been studied for decades and many of the mechanisms that orchestrate the adaptation of plants to P limitation have been revealed, many aspects remain elusive. *Arabidopsis thaliana* has a fully sequenced genome, a short lifecycle and well-established seed libraries and transformation protocols that make handling and genetic manipulation straightforward. This marks *Arabidopsis* as an optimal model organism to study the molecular mechanisms of the phosphate starvation response (PSR) of *Brassicaceae* that helped to uncover the genetic and molecular networks that control the adaptations to altered phosphate availabilities in plants.

One of the key features of the PSR of *Arabidopsis* is the differentiation between two distinct pathways – the systemic and the local PSR (Thibaud et al., 2010). In the systemic response, the internal Pi status of the plant is perceived and integrated. Split-root assays revealed that, as long as

Pi levels in the plant are sufficient, the lack of external available Pi in the soil does not cause the activation of phosphate starvation inducible genes (Martin et al., 2000; Franco-Zorrilla et al., 2005). Additionally, a mutant with abolished activity of several high-affinity Pi transporters that has significantly low internal Pi levels exhibits constitutive expression of PSR genes, even when grown on high Pi medium (Gonzalez et al., 2005). Thereby, Pi itself seems to be directly involved in the systemic regulation of PSR genes, since the application of phosphite (Phi), a non-metabolized form of Pi that accumulates in the plant, suppresses the induction of those genes (Ticconi et al., 2001). Nevertheless, the long distance signaling between roots and shoots in Pi starved plants requires additional components and a complicated regulation network has been identified that coordinates the systemic PSR. *mir399* (miRNA399) was identified as a long-distance signaling molecule moving from shoot to root and thereby inhibiting the translation of PHO2, an E2 Ubiquitin conjugase enzyme. Consequently, PHO2-mediated repression of several PSR genes is abolished. Thus, *pho2* mutants accumulate high amounts of Pi in the shoot (Lin et al., 2008). *At4* and *IPS1*, two non-coding RNAs, are induced by Pi limitation. Both negatively regulate the inhibitory effect of *mir399* on *Pho2* mRNA levels by target mimicry. The co-induction of *At4*, *IPS2* and *mir399* alongside with their antagonistic effect on the PSR thereby provide a mechanism to fine-tune Pi homeostasis (Franco-Zorrilla et al., 2007).

The MYB transcription factor PHR1 also plays a pivotal role in the transcriptional regulation of many central genes (Rubio et al., 2001). The binding to PHR1 binding sequences (P1BS) thereby controlling the expression of a large subset of genes related to Pi starvation, among them the members of the *PHT1* and *PHO1* families, encoding for high affinity Pi transporters as well as members of the *SPX* family that are involved in the regulation of Pi homeostasis (Stefanovic et al., 2007; Duan et al., 2008; Karthikeyan et al., 2009). Structure-function studies of several SPX domain containing proteins suggest that inositol-pyrophosphates (pp-InsP) bind with μM affinity to the SPX domain and therefore serve as a proxy to determine intracellular Pi levels (Wild et al., 2016). The activity of PHR1 is thereby also regulated by SPX1. Under Pi sufficient conditions, InsP6 is bound to SPX1 preventing the binding of PHR1 to DNA and thereby inhibiting the activation of PSR-related genes (Qi et al., 2017).

Consequently, the outcome of the altered gene expression due to activation of the systemic PSR is quite diverse. Besides the above mentioned induction of genes encoding for high-affinity Pi transporters, metabolic pathways are adjusted to maintain physiological Pi concentrations in the cells (Ticconi and Abel, 2004). The accumulation of anthocyanin and starch is used to recycle Pi from already synthesized compounds (Plaxton and Tran, 2011) and phospholipids of membranes are replaced by sulfo- and galactolipids to reallocate the containing phosphate to other metabolic

pathways (Yu et al., 2002; Frentzen, 2004). The secretion of various enzymes i.e. phosphatases, phosphohydrolases and nucleases also contribute to the mobilization of Pi from insoluble organic or inorganic compounds.

In summary, the systemic PSR primarily aims to recycle and redistribute already assimilated Pi resources as a response to low internal Pi levels to maintain all relevant metabolic processes. However, the expression of genes encoding high affinity Pi transporters and secreted enzymes in the roots is also considered as a part of the systemic response because of its dependence on internal Pi resources.

1.3.2 The local phosphate starvation response

In contrast to the systemic changes in the plant metabolism that are induced by decreased intracellular Pi levels, the local Pi starvation response is driven by alterations of extracellular phosphorus availability and mainly alters the root system architecture of *Arabidopsis* (Peret et al., 2014; Abel, 2017). These root system alterations (RSA) are independent of intracellular Pi levels and contact of the root to Pi depleted soil is crucial for their induction (Ticconi and Abel, 2004; Svistoonoff et al., 2007; Thibaud et al., 2010). The general mechanism of the local PSR of *Arabidopsis* is topsoil foraging. The primary root growth is attenuated, and the formation of secondary and lateral roots is induced to increase the root surface near the upper, P rich soil layers.

The attenuation of the primary root growth is caused by a decreased activity of the root apical meristem (RAM) and a shift to a determinate developmental program. Upon contact with low Pi medium, the cell division and cell elongation rates decrease (Reymond et al., 2006) and the differentiation of meristematic cells causes the consumption of the SCN, the loss of meristematic activity, and eventually an arrest of primary root growth (Sanchez-Calderon et al., 2005; Ticconi et al., 2009).

When it comes to Pi limitation, Pi and Fe are not only linked via the formation of Fe-P complexes in soil. Plants also hyperaccumulate Fe in Pi deprived roots and shoots. The mechanism behind this is still poorly understood and it is discussed whether this is an indirect consequence of the increased Fe-availability in Pi-depleted soils or an active measure to overcome Pi limitation. Many studies indeed showed, that Fe is crucial for the induction of the local PSR in *Arabidopsis* (Svistoonoff et al., 2007; Ticconi et al., 2009) and a debate arose whether the PSR is an effect of excess Fe toxicity rather than a controlled molecular response to a changing environmental cue (Ward et al., 2008). However, experiments where plants were grown in elevated levels of Fe in Pi-sufficient medium showed that the excess of Fe is not enough to trigger root growth inhibition and thereby rule out passive Fe-toxicity as a trigger for the PSR in *Arabidopsis* (Muller et al., 2015). Although a clear link between Fe

and Pi limitation is established, only a few important genes that orchestrate the interplay between Fe and Pi during the PSR are known and most mechanisms remain elusive.

Figure 1 summarizes some of the general molecular responses of *Arabidopsis* roots to low Pi availability and genotypes with altered PSR.

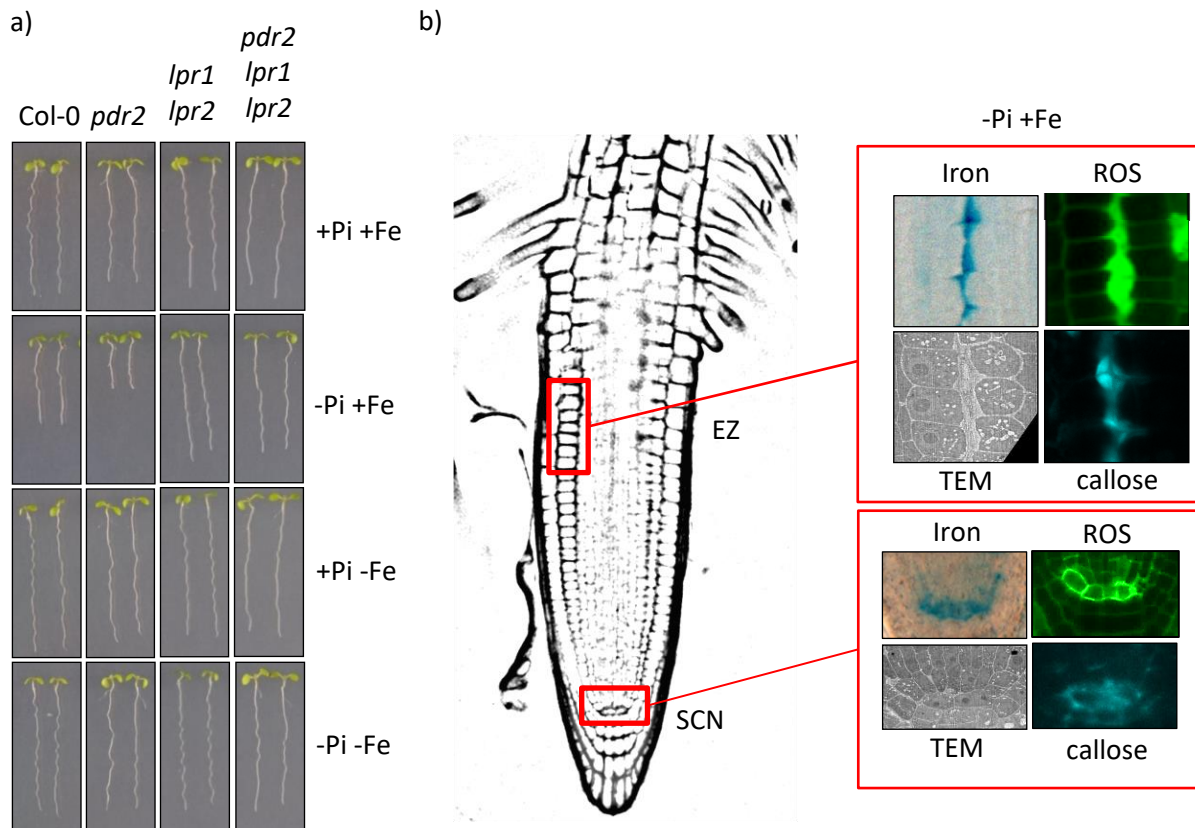


Figure 1: Molecular modifications and genes involved in the *Arabidopsis* primary root response to Pi-deprived medium. The local PSR of *Arabidopsis* depends on the availability of Fe. *PDR2* and *LPR1* & *LPR2* are main players in its regulation. a) Primary root length of different *Arabidopsis* genotypes grown for 5 days in medium containing 2.5 mM Pi and 50 μ M Fe and subsequently transferred to medium lacking Pi, Fe or both components. *pdr2* is hypersensitive to low Pi conditions whereas *lpr1 lpr2* and *pdr2 lpr1 lpr2* are insensitive to $-Pi$ conditions. The absence of Fe in the medium completely inhibits the root growth arrest during the PSR. b) Schematic picture of an *Arabidopsis* root. The depletion of Pi in the medium triggers the accumulation of apoplastic iron (Perls staining), ROS (Carboxy-H₂DCFDA) and callose (Aniline blue), and cell wall thickening (Transmission electron microscopy) in the SCN and the elongation zone (EZ) of primary roots. Images were taken by Jens Müller.

It is well established that contact of the root tip of *Arabidopsis* with low Pi medium triggers a set of changes that eventually cause an arrest of the primary root growth as a consequence of altered cell division and elongation patterns in the RAM and elongation zone (Sanchez-Calderon et al., 2005; Svistoonoff et al., 2007; Abel, 2017). Furthermore, experiments carried out in our lab showed that Pi-depletion in the medium drives the accumulation of (apoplastic) Fe in the elongation zone (EZ) and the SCN of the primary root. This Fe-accumulation is accompanied by a generation of ROS and the deposition of callose in the exact same areas. Additionally, cell walls in those regions of the roots are

thickened in –Pi conditions (Figure 1). The deposition of callose blocks cell-to-cell communication and prevents the movement of cellular compounds that are crucial for maintaining the stem cell fate of the cells of the quiescent center (QC). Most notably, blocked plasmodesmata inhibit the movement of the transcription factor SHORTROOT (SHR) from stele tissue to the QC and thereby causing a loss of the stem cell fate of the QC, eventually leading to a complete loss of meristematic activity of the RAM (Muller et al., 2015). Although many genes are involved in the regulation of the local PSR, only a few main players have been characterized so far (Chen et al., 2000; Reymond et al., 2006; Karthikeyan et al., 2014; Dong et al., 2017). Central regulators are the P5-type ATPase PDR2 (PHOSPHATE DEFICIENCY RESPONSE 2) and Multicopper oxidases (MCOs) LPR1 (LOW PHOSPHATE ROOT 1) and LPR2. Loss of function mutations of *PDR2* render the plant hypersensitive to low Pi conditions causing more severe impairment of primary root growth upon transfer to –Pi when compared with WT, whereas *lpr1*, *lpr2* and *lpr1 lpr2* show insensitivity to –Pi conditions with regards to primary root growth inhibition. *lpr1 lpr2* thereby is completely insensitive to –Pi whereas *lpr1* shows around 80 % of the primary root length on –Pi conditions compared with *lpr1 lpr2* (Svistoonoff et al., 2007). A triple mutant *pdr2 lpr1 lpr2* is also insensitive to Pi depletion. Therefore, the epistatic relationship of *LPR1/LPR2* and *PDR2* implicates a genetic interaction between them (Ticconi et al., 2009). The intensity of primary root growth inhibition in the different mutants is also mirrored by the intensity of the abovementioned accumulation of Fe, deposition of callose (Figure 2). The same is true for the generation of ROS and the cell wall thickening. So, *pdr2* plants that are severely impaired in primary root growth in –Pi conditions also show a hyper-accumulation of iron, callose and ROS in low Pi medium whereas *lpr1 lpr2* does not show any of these symptoms. However, the depletion of Fe from low Pi medium also renders the plant completely insensitive to the lack of Pi, thereby mimicking an *lpr1*-like phenotype, indicating that both, Fe and LPR1, are crucial for phosphate sensing (Figure 1).

1.3.3 Function of LPR1 during phosphate starvation response

Although LPR1 and LPR2 are known to be important players in the PSR of *Arabidopsis* for many years, their distinct function is still unknown. Since comparisons between *lpr1*, *lpr2*, and *lpr1 lpr2* regarding their primary root growth inhibition on –Pi conditions indicate that *LPR1* is most important for the PSR, this work focuses on the role of *LPR1* while putting *LPR2* aside for most of the experiments.

Studies using *pLPR1::GUS* revealed a very distinct expression domain of *LPR1* in the SCN and the EZ of the primary root which is exactly the area where many described mechanisms of the PSR are triggered (see Figure 2b). However, *LPR1* expression levels are not influenced by Pi-availability in the medium and remain unchanged upon transfer to –Pi conditions (Abel, 2017; Svistoonoff et al., 2007). *Arabidopsis* plants expressing *pLPR2::GUS* revealed expression of the gene mainly in the leaves of

seedlings whereas no expression could be detected in the roots. However, qPCR experiments conducted in our lab showed that *LPR2* is also highly expressed in roots of 6 days old seedlings (unpublished data from our lab by T. Toev).

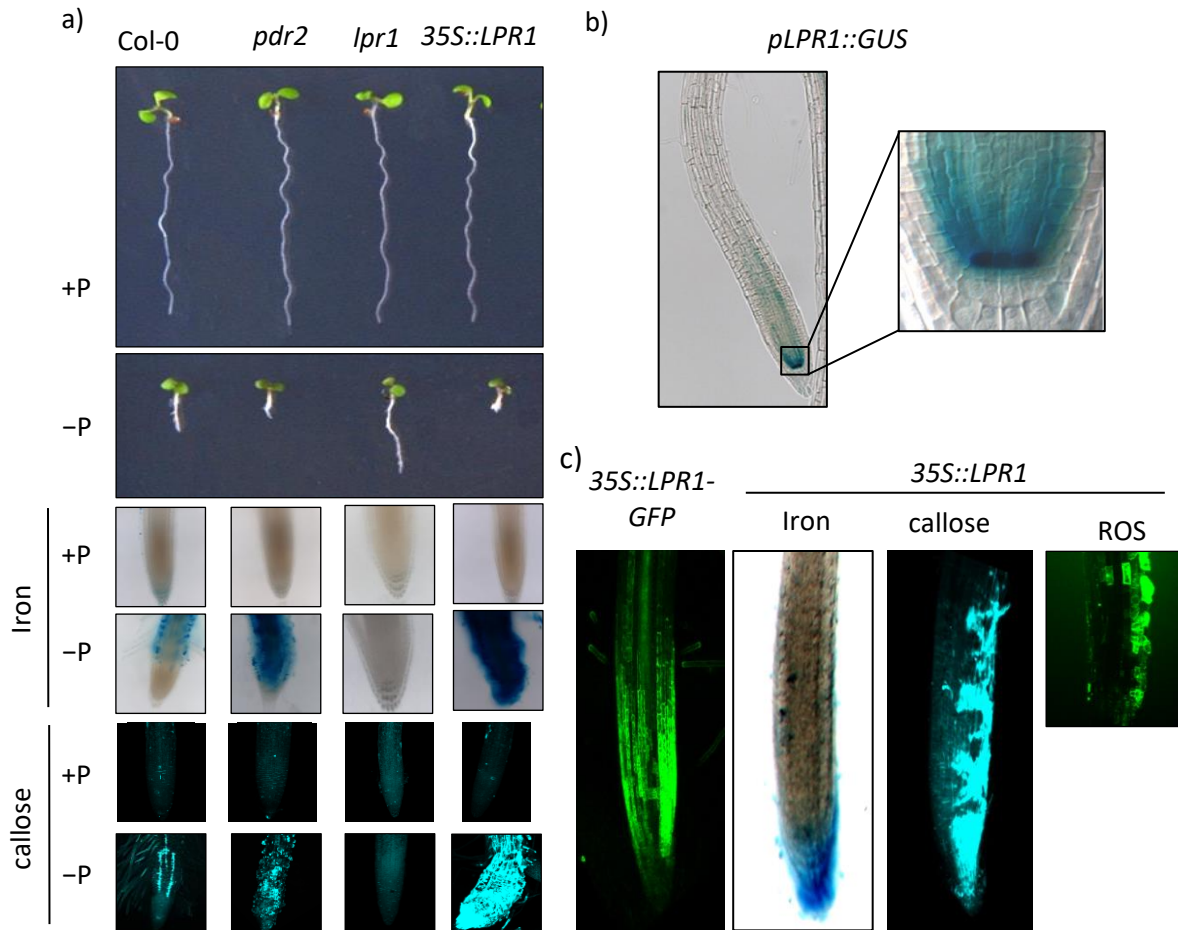


Figure 2: The ectopic overexpression of *LPR1* causes an ectopic accumulation of Fe, callose and ROS in Pi-deprived roots resembling a *pdr2*-like phenotype. Root length, Fe accumulation (Perls) and callose deposition (Aniline blue) staining of different genotypes of *Arabidopsis* were grown for 6 days on medium containing 2.5 mM (+Pi) or 0 mM (-Pi) Phosphate. b) GUS staining of a primary root of an *Arabidopsis* seedling stably transformed with *pLPR1::GUS* reveals the expression domain of *LPR1* (T. Toev). c) *Arabidopsis* seedlings stably transformed with *35S::LPR1-GFP* or *35S::LPR1* were grown on -Pi conditions. GFP-fluorescence of roots of *35S::LPR1-GFP* was determined via confocal laser scanning microscopy (cLSM700 [Zeiss]). The ectopic accumulation of Fe (Perls), callose (aniline Blue) and ROS (Carboxy-H2DCFDA) is shown in *35S::LPR1*. Pictures taken by Jens Müller.

Remarkably, a shift of the expression domain of *LPR1* from the SCN and the elongation zone in WT plants to an ectopic overexpression in the whole plant via cauliflower mosaic virus 35S promoter (Benfey et al., 1990) also alters the location of FE, callose and ROS deposition upon Pi limitation. Instead of a distinct location in the SCN and the EZ, Fe, callose, and ROS are now detectable around the whole root, indicating that *LPR1* is directly involved in these processes (Figure 2). It is also of note, that the deposition of Fe, callose and ROS at the expression sites of *LPR1* requires both, the presence of Fe and the absence of Pi in the medium. Thus, consecutive overexpression of *LPR1* is

insufficient to activate these mechanisms. Instead it requires an additional trigger that is linked to Pi-depletion, demonstrating that LPR1 function is strictly regulated.

However, besides the fact that *LPR1* is crucial for a functioning PSR in *Arabidopsis*, its distinct function remains elusive. It was shown that its expression level is directly linked to the severity of root growth inhibition in $-Pi$ conditions. LPR1s similarities to MCOs, especially to CotA of *Bacillus subtilis*, and the fact that the addition of MCO inhibitors mimic an *lpr1*-like phenotype in WT plants growing on $-Pi$ conditions, indicate that MCO activity is indeed important for its function during the PSR (Svistoonoff et al., 2007). CotA is classified as a Mn-oxidase and MCOs can have a variety of different substrates. Since LPR1 function is tightly connected to Fe availability and since Fe is also a substrate of distinct MCOs a putative function of LPR1 in Fe homeostasis is easily conceivable. A closer look on the phylogeny of MCOs indeed revealed high similarities of both LPRs of *Arabidopsis* to human ferroxidases ceruloplasmin and Hephaestin, as well as to yeast ferroxidases Fet3p and Fet5p (Figure 3).

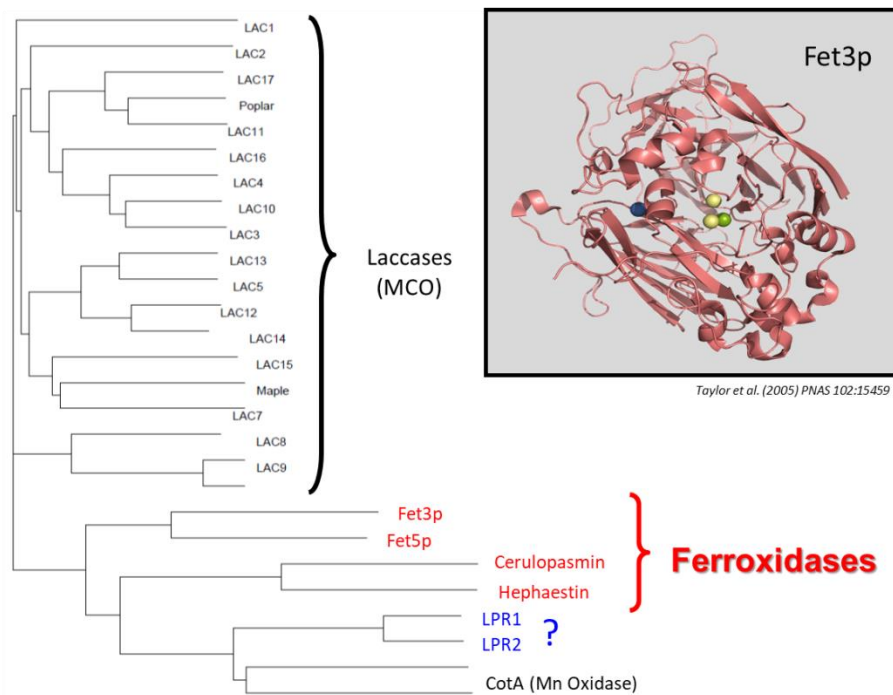


Figure 3: Phylogenetic tree of multicopper oxidases (MCOs). A phylogenetic tree of multicopper oxidases (MCOs) also known as laccases. Yeast ferroxidases Fet3p and Fet5p as well as human ferroxidases ceruloplasmin and Hephaestin are marked in red. LPR1 and LPR2 are closely related to yeast and human ferroxidases as well as to the Mn oxidase CotA of *B. subtilis*.

ferroxidases belong to the multicopper oxidases. MCOs oxidize a variety of different substrates using multiple Cu-clusters as co-factors (Krumbein and Altmann, 1973; Askwith et al., 1994; Heppner et al., 2014). Ferroxidases have been reported to be involved in numerous biological functions in organisms

throughout all kingdoms of life. In higher plants, however, only one single report was published that links the ferroxidase activity of an MCO of yellow poplar (*Liriodendron tulipifera*) to a possible function in lignification and Fe uptake in the vascular tissue (Hoopes and Dean, 2004). In contrast to that, the functions of ferroxidases in many other organisms have been elucidated. Human ferroxidase Hephaestin is crucial for the transport of Fe from the intestinal enterocytes into the circulatory system (Vulpe et al., 1999; Chen et al., 2004) whereas ceruloplasmin, another mammalian ferroxidase, is linked to the loading of Fe³⁺ to ferritin (Attieh et al., 1999; Mzhel'skaya, 2000). In yeast, Fet3 (Ferrous Transport 3) is part of cellular Fe-uptake system together with the transporter Ftr1 (Fe Transporter 1). Fe²⁺ is oxidized by Fet3 to Fe³⁺ and directly transferred to Ftr1 for uptake (Stearman et al., 1996; Radisky and Kaplan, 1999). Fet5p together with Fth1p facilitates Fe efflux from the vacuole in *S. cerevisiae* (Urbanowski and Piper, 1999).

The reaction catalyzed by ferroxidases is $4\text{Fe}^{2+} + 4\text{H}^+ + \text{O}_2 \rightarrow 4\text{Fe}^{3+} + 2\text{H}_2\text{O}$. They use Cu as cofactors to catalyze the oxidation of ferrous iron to ferric iron via the consumption of O₂ and the generation of water. Studies on Fet3 were able to map the active sites of the protein, the substrate binding sites and the amino acids that form the sites that are needed to bind the Cu-cofactors. Extensive biochemical studies elucidated the mode of function of these proteins and showed how the transport of the electron from the substrate to the electron acceptor O₂ is facilitated by the enzyme (Bonaccorsi di Patti et al., 2001; Taylor et al., 2005; Stoj et al., 2006). Multiple sequence alignments of *Arabidopsis* LPRs and Fet3 and Fet5 of yeast were able to identify all putative Cu-binding sites that are crucial for ferroxidase function in LPR1 and LPR2 (Figure 12). Furthermore, a modeling approach using PHYRE2 and 3DLigandSite servers revealed the presence of a putative iron binding site in LPR1 and LPR2 (Figure 13). Since all structural core features of ferroxidases were identified in LPR1 via *in silico* analyses, the question arose whether LPR1 might be a ferroxidase linking the Pi and Fe availability during Pi-limitation in *Arabidopsis*. The oxidation of Fe²⁺ to Fe³⁺ is a possible source for ROS via the Fenton reaction that generates hydroxyl radicals via the one electron reduction of O₂ (Aisen et al., 2001). Since ROS is also a trigger for callose deposition i.e. in plant immunity (Zipfel et al., 2004; Daudi et al., 2012; Wrzaczek et al., 2013), the enzymatic oxidation of Fe²⁺ catalyzed by the putative ferroxidase LPR1 could be the first step of a cascade of reactions eventually causing callose deposition at the plasmodesmata of the SCN. Blocked plasmodesmata prevent cell-to-cell movement of important transcription factors to the SCN and Therefore causing the loss of the stem cell identity and eventually the inhibition of primary root growth on –Pi conditions.

1.3.4 PDR2 – The great unknown

PDR2 was identified in a forward genetic screen as central player in the PSR (Chen et al., 2000; Ticconi et al., 2004). Among many pleiotropic phenotypes, plants with impaired *PDR2* function are

reduced in fertility and hypersensitive to low Pi conditions showing a more severe and faster root growth inhibition upon transfer to $-Pi$ medium. Later studies also revealed that *LPR1* and *PDR2* interact genetically (Ticconi et al., 2009). The epistatic relation of *LPR1* and *PDR2* indicates a restrictive function of *PDR2* on *LPR1* outcome (Figure 1). Currently, experiments in our lab are also investigating a possible connection between *PDR2*, Pi deficiency and autophagy.

PDR2 encodes the orphan P5-type ATPase in *Arabidopsis*, and its loss of function causes increased sensitivity towards Pi starvation, independent of Fe-availability (Ticconi et al., 2009). P-type ATPases are ubiquitously found in all kingdoms of life and characterized by a shared enzymatic mechanism that uses ATP hydrolysis to transport ions across a membrane. The name P-type ATPases originates from a phosphorylated intermediate aspartate that is formed to facilitate transmembrane transport. The superfamily can be divided into 5 major subfamilies based on their transported substrates: Heavy-metal ATPases (P1), Ca^{2+} -ATPases (P2), H^{+} -ATPases (P3), putative amino-phospholipid ATPases (P4), and ATPases with unknown substrate (P5-type ATPases) (Baxter et al., 2003). *PDR2* is the single P5-type ATPase in *Arabidopsis* and is functioning in the ER (Ticconi et al., 2009). A loss of its function results in a faster impairment of the primary root growth upon Pi-depletion because of Scarecrow (SCR) miss-expression in the root tip. SCR together with SHR is essential to maintain meristematic activity of the RAM (Sabatini et al., 2003; Cui et al., 2007). *PDR2* is required to sustain SCR during Pi-deficiency and therefore maintaining stem-cell fate in low Pi-conditions. Another study identified *pdr2* as an allele of *MIA* (*male gametogenesis impaired anthers*) that causes a defect in pollen development (Jakobsen et al., 2005). Thus, the reduced fertility of *pdr2* is attributed to a deformation of pollen grains due to altered cell wall structures and composition. The same study also used electron microscopy in combination with immunogold labeling to localize *PDR2* to the ER of anthers and pollen grains. Although qRT-PCR analysis indicated expression of *PDR2* ubiquitously in all plant organs, they failed to detect *PDR2* in roots or leaves. Moreover, *pPDR2::GUS* expression analysis indicates expression in the central and distal meristem of the primary root, independent of Pi availability (Ticconi et al., 2009). The nearly full epistasis of *lpr1 lpr2* and *pdr2*, together with overlapping expression domains of *PDR2* and *LPR1* in the RAM of the primary root, and localization to ER-derived compartments suggest a regulation of *LPR1* by *PDR2* during Pi-limitation. However, the nature of the interaction between both genes is still poorly understood. Like its yeast homologue *SPF1*, *PDR2* is linked to ER quality control and requires Ca^{2+} for functioning. However, the transported substrate remains elusive (Cronin et al., 2002; Sorensen et al., 2012). The involvement of *PDR2* in ER quality control and regulation of cell wall associated proteins indicate a possible restriction of *LPR1* trafficking or post-translational modification that alters protein function or stability. Restricting of *LPR1* substrate availability by *PDR2* is also a considerable mode of action. However, deeper knowledge about the function of *LPR1*, which seems to be a central regulator that acts rather

downstream in the PSR signaling cascade, is required to unravel the complex interplay of PDR2 and LPR1 in phosphate-deprived conditions.

Given the current status of research in our lab and from other groups, a working model of the PDR2 – LPR1 interplay as a nexus in the PSR is depicted in Figure 4.

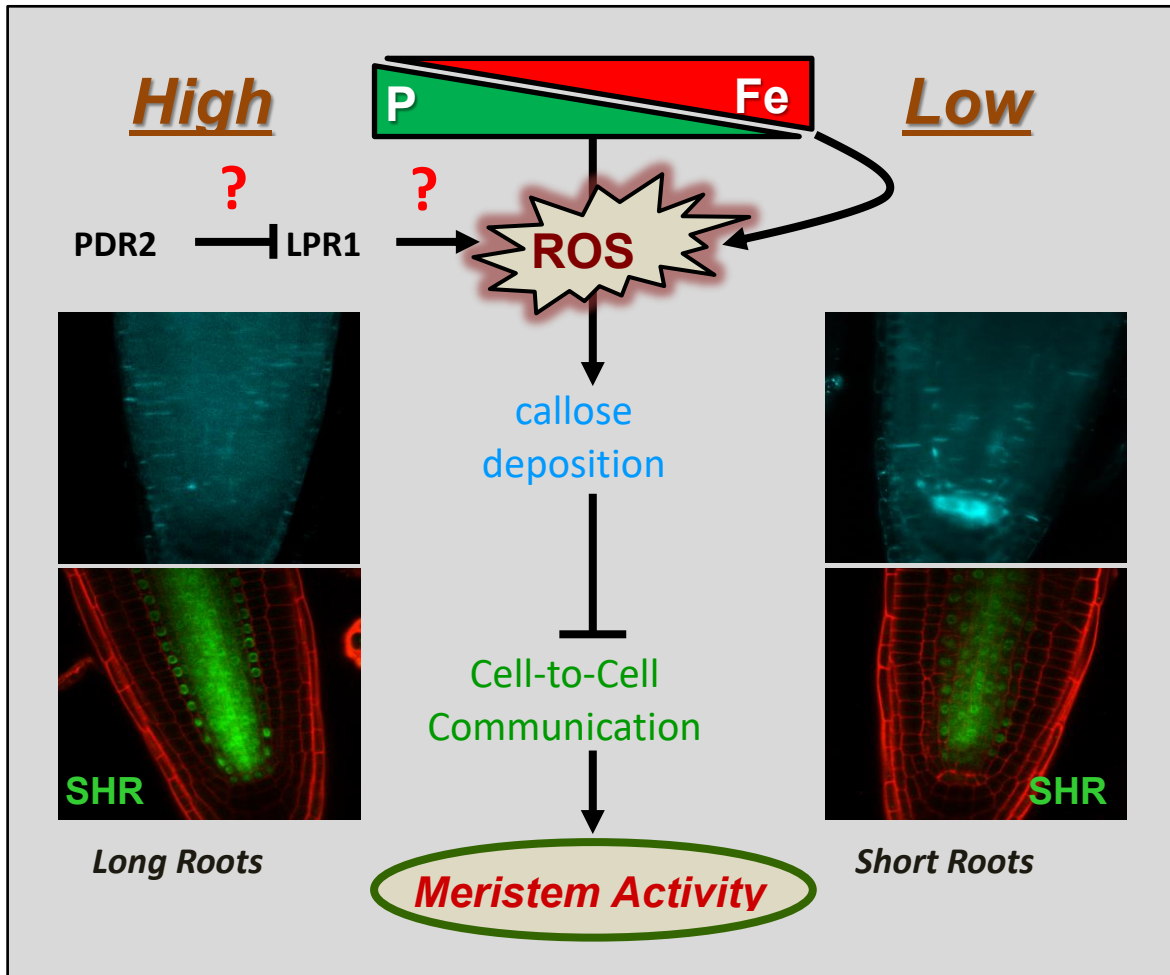


Figure 4: Working model of PDR2 and LPR1 acting together to orchestrate the local PSR. Low Pi concentrations cause elevated Fe-availability that is used as a substrate by LPR1 to generate ROS in the RAM. ROS production triggers callose deposition that blocks cell-to-cell communication that eventually leads to a loss of meristem activity upon Pi deprivation. PDR2 restricts LPR1 function by an unknown mechanism. (Muller et al., 2015)

Low Pi concentrations increase Fe availability in the surrounding of the roots. Elevated Fe concentrations and the lack of Pi result in the generation of ROS in an LPR1 dependent manner. However, PDR2 restricts the outcome of LPR1 function via an unknown mechanism. ROS generation causes callose deposition that blocks plasmodesmata of the SCN and thereby prevents diffusion of SHR to the QC resulting in loss of meristematic activity and eventually an arrest of root growth in –Pi conditions.

1.4 Aims of this work

The interplay between the P5-Type ATPase *PDR2* and the multicopper oxidase *LPR1* is a nexus in the local PSR of *Arabidopsis*. *LPR1* is closely related to ferroxidases and involved in Fe-accumulation, ROS accumulation and callose deposition. It is therefore tempting to speculate that it functions as a ferroxidase that regulates meristem activity in Pi-deprived primary roots. Since knowledge about plant ferroxidases is extremely limited, a profound characterization of protein function including subcellular localization, its regulation upon Pi starvation and structure-function studies should be carried out to elucidate its role and distinct function in the PSR. Thereby, the regulatory role of *PDR2* in *LPR1* outcome is an important aspect that will also be investigated. Besides the epistatic relationship between both genes, the general mechanism by which *PDR2* restricts *LPR1* outcome remains elusive. Therefore, transgenic *Arabidopsis* lines overexpressing *PDR2-GFP* should be established, to analyze the subcellular localization of *PDR2* and to uncover the mechanism that controls *LPR1* function. The combined results from both, *LPR1* structure-function elucidation and analyses of *PDR2* overexpression lines, will give deeper insights in the complex mechanisms that orchestrate plants adaptations to Pi-limitations in the soil.

2 Results

2.1 *LPR1* encodes a ferroxidase and acts in phosphate starvation response

In order to gain more insights into the regulation of the local phosphate starvation response in *Arabidopsis thaliana*, the first part of this work was focused on the elucidation of the function of *LPR1* and how its function is regulated during phosphate starvation response. Therefore, the localization and abundance of *LPR1* in various backgrounds under different Pi-regimes were examined. Activity assays were conducted to elucidate the function and basic biochemical properties of the enzyme. Structure-function studies including site-directed mutagenesis were used to determine the active sites of the protein and several attempts to purify the protein were undertaken to get insights in the mode of action of *LPR1*.

2.1.1 General regulation of *LPR1* protein levels

2.1.1.1 *LPR1* protein levels are elevated in *35S::LPR1* roots

To elucidate the function of *LPR1*, a set of lines that constitutively overexpress *LPR1* under the control of cauliflower mosaic virus 35S promoter (Benfey et al., 1990) was generated by T. Toev in our lab. Although higher mRNA levels of *LPR1* and conditional phenotypes had already been established in these lines (T. Toev, unpublished; Figure 2), protein levels within these lines remained to be analyzed. Moreover, direct correlation between *LPR1* promoter activity and severity of root

growth impairment during Pi-starvation has been demonstrated by several publications (Reymond et al., 2006; Svistoonoff et al., 2007). Thus, it was tempting to speculate that differences in LPR1 levels between various mutant lines are responsible for altered sensitivities towards low Pi conditions in these lines. Therefore, LPR1 levels in various transgenic *Arabidopsis* lines should be determined. The epistatic relationship of *lpr1* and *pdr2* strongly suggest a regulation of LPR1 function by PDR2. LPR1 levels in *pdr2* will provide first hints about the nature of PDR2's regulatory role on the LPR1 output. Additionally, three independent lines that express *35S::LPR1* in a Col-0 background were tested with regards to their LPR1 levels. *lpr1 lpr2* was included as a negative control. To quantify the amount of LPR1 in roots of different genetic backgrounds of *Arabidopsis*, total protein extracts from whole roots of 5–8 days old seedlings grown on SM medium (4.2.2) were generated. The protein samples were separated by SDS-PAGE and analyzed via Western Blot using an α -LPR1 antibody (Immunoglobulin [Himmelsstadt]; Figure 5)

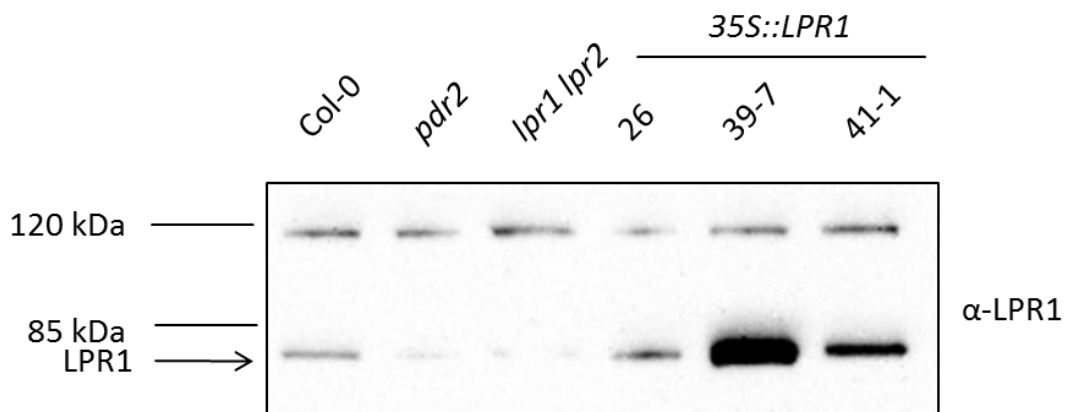


Figure 5: Protein levels of LPR1 in different genetic backgrounds. Seedlings of Col-0, *pdr2-1*, *lpr1lpr2*, and 3 different *35S::LPR1* overexpression lines were grown sterilely on +Pi agar plates for 6 days. Total protein extracts were prepared from whole roots. 70 μ g of total protein was loaded on a 10 % SDS gel. Subsequently, samples were analyzed via Western Blot using an α -LPR1 Antibody. LPR1 has a molecular weight of 66 kDa. A second, unspecific band appeared in all *Arabidopsis*-derived samples at a molecular weight of \sim 120 kDa and served as a loading control.

A specific signal could be detected at a MW of around 70 kDa (theoretical MW \sim 66 kDa). Compared to Col-0 wildtype the signal of LPR1 in *pdr2* and *lpr1lpr2* is clearly decreased. However, the reduced amount of LPR1 in *pdr2* and *lpr1 lpr2* was not observed in other experiments. Supplemental figure 5 shows a similar experiment in which LPR1 levels in *pdr2* and *lpr1 lpr2* are clearly indistinguishably of Col-0. Since *lpr1 lpr2* is generated via crossing of two T-DNA insertion lines, no LPR1 should be present. Still, semi-quantitative RT-PCR analysis revealed only slightly reduced levels of *LPR1* mRNA in *lpr1 lpr2* compared to Col-0 (Supplemental figure 6). To verify this data, *LPR1* transcript levels of another *lpr1* T-DNA insertion allele were established, showing also only a slight reduction of *LPR1* mRNA levels when compared to WT (Supplemental figure 7). However, the slight decrease in *LPR1*

mRNA seems to be enough to render plants insensitive to –Pi conditions. In contrast, all of the *35S::LPR1* lines tested showed elevated LPR1 signals compared to Col-0 with strongly increased levels in line 39-7 and 41-1 and slightly increased levels in line 26, suggesting higher protein levels of LPR1 in *35S::LPR1* lines. As a loading control an unspecific band at 120 kDa was used, which appeared in all samples derived from protein extracts of *Arabidopsis*.

Taken together, these findings suggest that the varying severity of root growth impairment in different genotypes is at least partially a consequence of altered LPR1 levels in their primary roots. A slight reduction of LPR1 levels apparently is sufficient for suppressing the local PSR in *lpr1 lpr2*, whereas increased LPR1 levels in the overexpression lines render the plant hypersensitive to Pi-depletion. However, LPR1 levels in *pdr2* are not elevated. Thus, the reason for its hypersensitivity cannot be explained by simple alterations in protein levels in comparison to WT.

2.1.1.2 Protein levels of LPR1 remain unchanged upon transfer to –Pi conditions

LPR1 is a key player in the local phosphate starvation response of *Arabidopsis*. Understanding how the abundance of LPR1 is regulated when the plant encounters low Pi conditions is crucial to gain deeper insights into the mechanisms that orchestrate the PSR in general. It was already established, that the *pLPR1::GUS* expression and *LPR1* mRNA levels are not altered in –Pi conditions in comparison to +Pi (Svistoonoff et al., 2007). However, possible changes in protein abundance after transfer to Pi-depleted medium have not yet been investigated. To address this, Col-0 seedlings were grown for 5 days on SM medium containing 2.5 mM Pi and were subsequently transferred to SM medium lacking Pi. After transfer for 2 – 48 h, whole roots were harvested, and proteins were extracted. 80 µg of total protein was loaded on a 10 % SDS gel for separation and transferred to a nitrocellulose membrane for probing with α-LPR1 antibody (Figure 6).

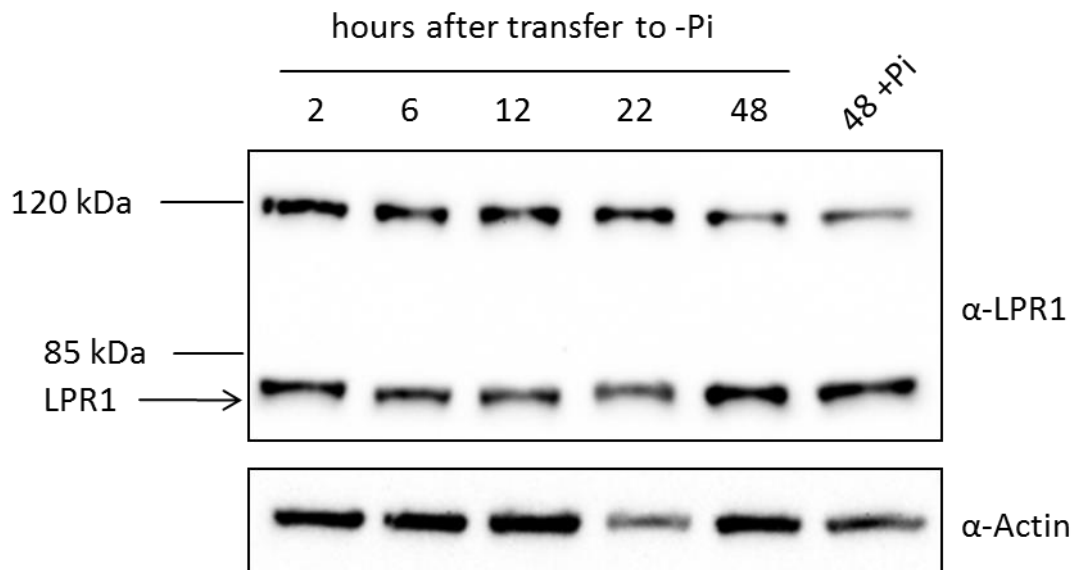


Figure 6: Levels of LPR1 in Col-0 roots after transfer to -Pi medium. Col-0 seedlings were grown 5 days on +Pi medium and were then transferred to -Pi conditions for 2, 6, 12, 22 and 48 h. As a control, seedlings were transferred to + Pi medium for 48 h. Roots were harvested and 80 μ g total protein extract was immunoblotted and probed with α -LPR1 antibody. LPR1 (66 kDa) is marked with a black arrow. actin and an unspecific band at 120 kDa served as loading controls.

Most root growth alterations as well as the Fe, ROS and callose deposition during the PSR takes place already in the first 48 h after root tip contact with low-Pi medium (Muller et al., 2015). Therefore, we assessed LPR1 levels for different time points up to 48 h after transfer. Total protein extracts of roots that were transferred for 48 h to +Pi conditions served as a control. However, no changes in the signal intensity of LPR1 (arrow at \sim 70 kDa) could be observed in the first 48 hours of growth on -Pi medium, indicating that LPR1 levels remain constant independent of Pi-availability. Similar experiments including *pdr2* plants showed that LPR1 levels remain unchanged, also in a Pi-hypersensitive mutant upon contact with -Pi medium (Supplemental figure 2). These results show that LPR1 levels are not altered when Pi availability is changed. Moreover, the hypersensitive phenotype of *pdr2* cannot be explained by a perturbed regulation of LPR1 levels after transfer to -Pi conditions pointing to a different mechanism that controls LPR1 function, which might involve protein (de)-glycosylation (Supplemental figure 8).

2.1.2 Determination of enzymatic ferroxidase activity of LPR1

2.1.2.1 Elevated ferroxidase activity in crude extracts of *35S::LPR1*

Although the specific function of LPR1 during the PSR was not clear, several hints, including its high similarity to Fet3 and ceruloplasmin as well as the ectopic deposition of iron in *35S::LPR1* lines under - Pi conditions, suggested a putative ferroxidase activity of LPR1. To test this, *Arabidopsis* seedlings

of Col-0, *pdr2*, *lpr1lpr2* and three independent *35S::LPR1* lines with slightly different levels of LPR1 were grown on agar plates for 6 – 8 days, total protein extracts from whole roots were prepared and protein levels within the samples assessed via Bradford assay. Subsequently, Ferrozine assays were carried out to determine the specific ferroxidase activity of each extract (Figure 7).

Whereas no significant differences in ferroxidase activities between Col-0, *pdr2* and *lpr1lpr2* could be detected, root extracts of all three LPR1 overexpression lines showed elevated ferroxidase activities in comparison to Col-0. The absence of differences between Col-0, *pdr2* and *lpr1lpr2* suggests the presence of other ferroxidases in root extracts of *Arabidopsis* causing constant background ferroxidase activity. Nevertheless, when comparing the ratio between the different overexpression lines and the protein levels of LPR1 in these extracts (Figure 5) a direct correlation between the amount of LPR1 and the specific ferroxidase activity of a sample becomes evident, suggesting that LPR1 indeed functions as a ferroxidase.

In the context of this experiment, *35S::LPR2* lines were also tested, but showed no elevated ferroxidase activities in comparison to Col-0 (Supplemental figure 3). However, transient overexpression of *LPR2-GFP* in tobacco seems to have at least slightly increased ferroxidase activity when compared to the GFP control (Supplemental figure 4).

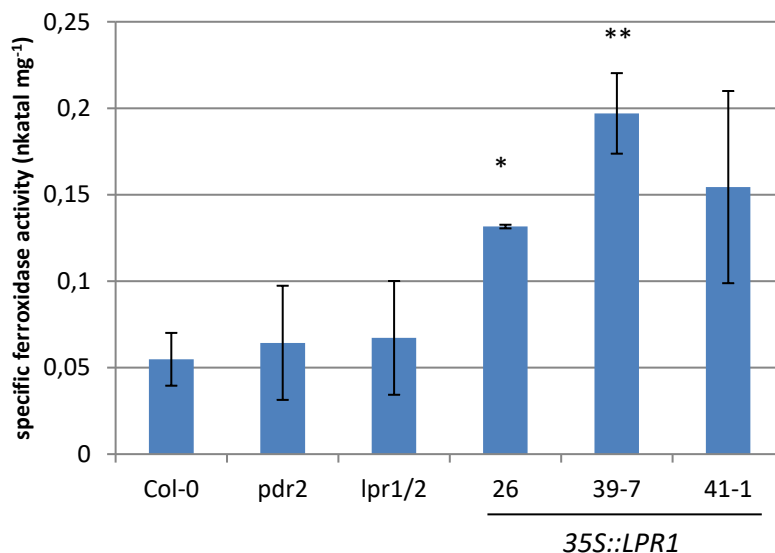


Figure 7: Specific ferroxidase activity of protein extracts from whole roots of different *Arabidopsis thaliana* genotypes. Seedlings of Col-0, *pdr2*, *lpr1lpr2* and three independent overexpression lines of *LPR1* were grown sterilely on +Pi agar plates for 5 – 8 days. The specific ferroxidase activity of protein extracts from whole roots was then determined via Ferrozine assay. 120 µg total protein and 50 µM substrate was used. Samples contained > 200 mg root material, +/- SE, * indicate $p < 0.05$ in comparison to Col-0, ** indicate $p < 0.01$ in comparison to Col-0, Student's t-test, N=3)

2.1.2.2 Ferroxidase activity of roots grown on +Pi or -Pi medium

Since LPR1 fulfills a pivotal role in the phosphate starvation response, and its function seems to be restricted to Pi-depleted conditions, it was tempting to speculate that Pi availability affects its enzymatic activity. To address this question, the specific ferroxidase activities of various *Arabidopsis* genotypes were determined after growth on + or –Pi conditions. The plants were grown for 5 days in vertical plates containing +Pi medium and were subsequently transferred to +Pi or –Pi conditions for 3 days. Total roots were harvested, and the specific ferroxidase activity of the crude extracts were determined. Figure 8 depicts the result from one representative experiment.

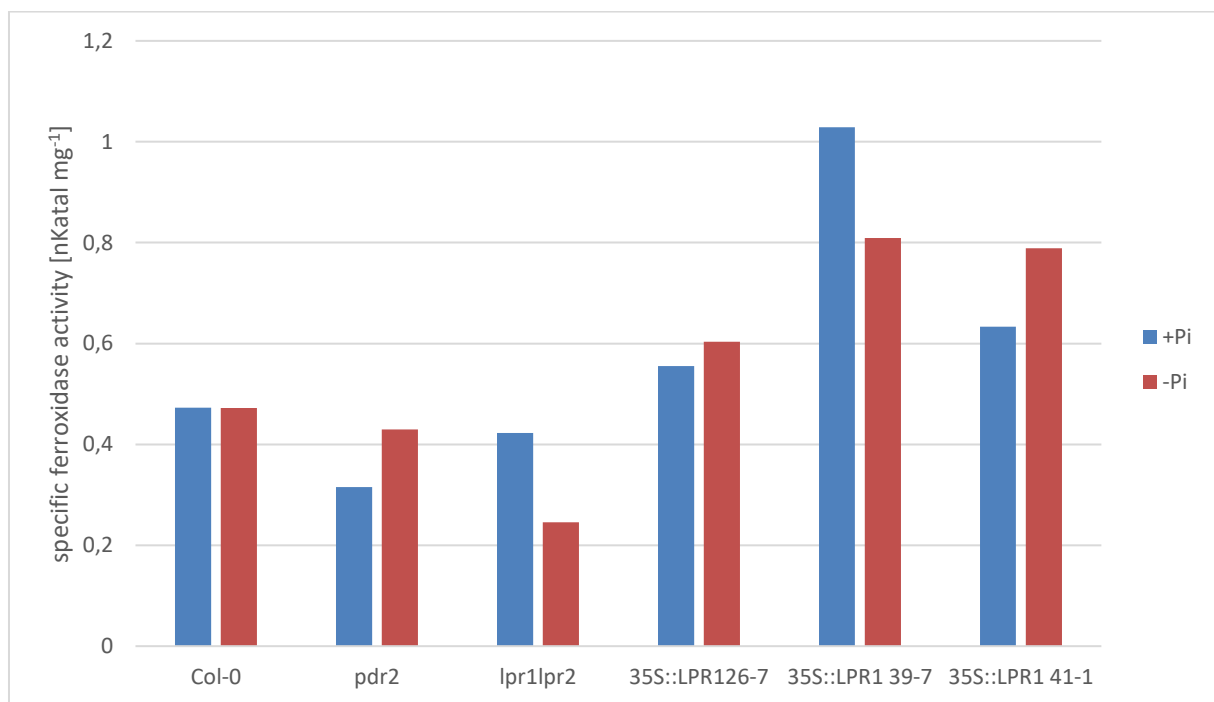


Figure 8: Specific ferroxidase activity of *Arabidopsis* roots grown on +Pi or - Pi conditions. *Arabidopsis* plants were grown in +Pi conditions for 5 days and then transferred to +Pi or – Pi conditions for 3 days. Specific ferroxidase activities of crude protein extracts from total roots were determined using Ferrozine assay. 25 µg total protein and 25 µM substrate was used for the assay. One representative experiment out of two is depicted.

When comparing the specific activities of roots grown in +Pi conditions between the different genotypes, the trend of increased ferroxidase activities of roots from plants overexpressing *LPR1* is visible, although not as in previous experiments, which is probably caused by relatively high specific activities of Col-0, *pdr2* and *lpr1lpr2* roots in comparison to previous experiments. Of all 35S::*LPR1* lines tested, line 39-7 exhibits the highest specific ferroxidase activity in both tested conditions. However, no differences could be determined between +Pi and – Pi conditions in the different genotypes. Remarkably, *lpr1lpr2* only showed around 70 % of the +Pi ferroxidase activity after transfer to –Pi conditions in both experiments. Yet, these data suggest that the total ferroxidase activity of *Arabidopsis* roots is not depending on the Pi availability in the medium. Additionally, overexpression of *LPR1* changes the total amount of LPR1 in roots. Similar specific ferroxidase

activities of *35S::LPR1* roots suggest that the overall LPR1 activity is not influenced by external Pi concentrations.

2.1.3 Confirmation of apoplastic localization of LPR1

Previous experiments using confocal laser scanning microscopy showed an apoplastic localization of GFP-tagged LPR1 in stably transformed *Arabidopsis* lines. To validate these findings cell wall proteins of *Arabidopsis* suspension cultures were extracted using sequential washing steps in high salt concentrations in order to solubilize proteins from the cell wall. Therefore, the cells were grown in 50 ml liquid SM medium and harvested 8 days after passaging via filtration through Miracloth which yielded a total of about 10 – 15 g cells. The supernatant of this step was collected, and the proteins were extracted via acetone precipitation for 1 h at -20 °C. The cells were washed sequentially in CaCl₂, DTT, NaCl and borate. All collected wash fractions were lyophilized overnight and resuspended in plant protein extraction buffer. As a total protein control (TPC), 500 mg of cells were directly dissolved in SDS sample buffer. After all the washing steps were successfully performed, 500 mg of the washed cells were dissolved in SDS sample buffer and served as a post wash control (PWC). To analyze the protein content of the medium, 10 ml of the supernatant after the 200 g centrifugation step were acetone precipitated and dissolved in SDS sample buffer. 30 µl of each sample were loaded on an SDS gel and subsequently analyzed via western blotting using α-LPR1 antibody (Figure 9). The signal of LPR1 in the TPC indicates the presence of LPR1 also in the *Arabidopsis* suspension cultures. In addition to the already described unspecific band at ~ 120 kDa, two lower MW bands appeared in some of the samples. However, LPR1 could be detected in fair amounts in the TPC, and, in lower abundances, in the DTT and borate fraction. It was not detectable in the lysed cells after the whole wash procedure. DTT and borate washing are thus capable of removing LPR1 from the cell wall, indicating that LPR1 is at least partially localized to the apoplast. This is further supported by the fact that LPR1 was not detectable in the PWC anymore, indicating that it was removed to a level below the detection limit during the numerous washing steps. To monitor cell integrity in all the samples, the blot was stripped after LPR1 detection and re-probed with α-actin antibody. Since actin is only present inside of a cell, actin signals should only be detectable in samples containing cells that were accidentally lysed during the wash procedure. Strong and weak actin signals appeared in the TPC and PWC control as well as in the borate fraction, indicating fair amounts of lysed cells in these fractions. In the TPC and PWC the cells were already lysed before analysis. Borate treatment also seems to have negative effects on the cell integrity. However, in the DTT fraction that harbors the highest amount of LPR1 of all wash steps, only a faint actin signal could be detected indicating that most of the cells survived the wash procedure intact and the majority of LPR1 is derived from the cell surface.

Taken together these results indicate that LPR1 is present at the cell wall of *Arabidopsis* suspension culture cells. This validates also the apoplastic localization of GFP-tagged LPR1 in stably transformed *Arabidopsis* lines and supports the theory that LPR1 acts in the apoplastic space.

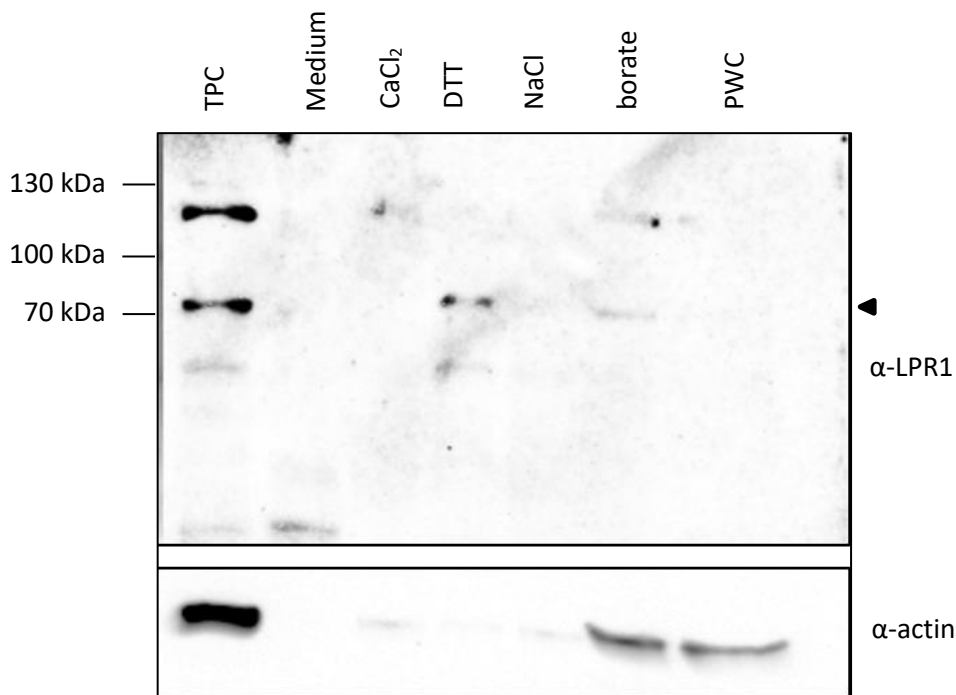


Figure 9: Determination of LPR1 levels in different fractions of *Arabidopsis* suspension cultures. 25 ml of *Arabidopsis* suspension culture was harvested 8 days after passaging. 10 – 15 g cells were then washed subsequently in CaCl₂, DTT, NaCl and borate. The collected wash fractions were concentrated via lyophilization, diluted in SDS loading buffer and analyzed via Western Blotting using an α-LPR1 AB (0.1 µg/ml). 500 mg of cells which were lysed and directly dissolved in SDS loading buffer prior and after the washing procedure served as Total Protein Control (TPC) and Post Wash Control (PWC), respectively. LPR1 (66 kDa) is indicated by ▲. As a control for cell integrity an α-actin AB (1:3000 [Sigma-Aldrich]) was used.

It had already been shown that LPR1 only acts under Pi depleted conditions and that its function is not controlled by gene expression or shifts in protein abundance (Figure 6). A common mechanism to regulate protein function during different conditions is alteration of subcellular localization. Since LPR1 was shown to localize to ER and the apoplast, it was tempting to speculate that the ratio of LPR1 in those compartments could be altered in +Pi and – Pi conditions. To test this hypothesis, *Arabidopsis* suspension culture cells were grown for 5 – 6 days in + Pi medium and transferred to medium lacking Pi for 4 h. Subsequently, the cells were harvested and the apoplastic proteins were extracted according to 2.1.3. The collected fractions were loaded on an SDS-Gel and subsequently subjected to Western Blot analysis using an α-LPR1 antibody to assess LPR1 concentrations in the different fractions (Figure 10).

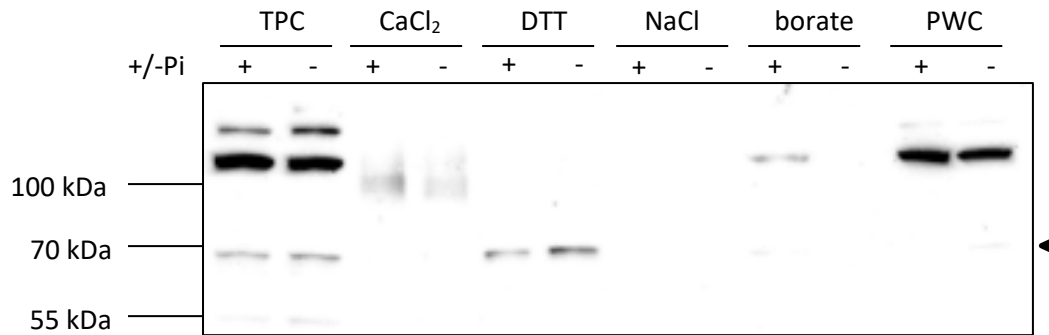


Figure 10: Determination of LPR1 levels in cell walls of *Arabidopsis* suspension cultures after transfer to +Pi and –Pi conditions. *Arabidopsis* suspension culture cells were harvested 4 h after transfer to +Pi or – Pi conditions and sequentially washed in CaCl₂, DTT, NaCl and borate. After collection, the samples were lyophilized and diluted in SDS-sample buffer. 15 µg of each sample were loaded on a 10 % SDS gel to perform western blot analysis using an α-LPR1 AB (0.1 µg/ml). 500 mg of cells which were lysed and directly dissolved in SDS loading buffer prior and after the washing procedure served as Total Protein Control (TPC) and Post Wash Control (PWC), respectively. LPR1 (66 kDa) is indicated by ▲ .

LPR1 was detectable in equal amounts in the TPC of cells grown in +Pi and – Pi conditions indicating that the overall levels of LPR1 are not altered upon transfer to – Pi conditions, which is consistent to previous experiments in *Arabidopsis* seedlings (Figure 6). A closer look at the DTT fraction revealed that there is the possibility that the LPR1 levels are slightly increased in cell walls of cells grown in – Pi conditions in comparison to +Pi. However, this minor difference could not be validated in additional experiments (data not shown). A semi-quantitative RT-PCR was carried out to ensure the expression of *LPR1* in the suspension cultures to validate that the 70 kDa signal on the Western Blots is derived from LPR1 (Supplemental figure 9).

Thus, it is therefore unlikely that subcellular localization of LPR1 is altered in response to shifting Pi concentrations of the growth medium.

2.1.4 Transient overexpression of GFP-tagged *LPR1* and *LPR2* constructs

To elucidate the function of LPR proteins in *Arabidopsis* and to verify the ferroxidase activity of LPR1, it was crucial to find a suitable system to produce sufficient amounts of protein for further experiments. Since *Nicotiana benthamiana* is widely used as a system for heterologous expression, constructs of *LPR1* and *LPR2* fused to a sequence encoding GFP-tag were used to transiently transform tobacco leaves (all constructs were provided by T. Toev). Expression of the constructs were driven by either a strong 35S promoter or a weaker *Arabidopsis thaliana* Ubiquitin10 (Ub10) promoter (Norris et al., 1993). In these constructs, the sequence encoding for the GFP was inserted between the sequence encoding the predicted N-terminal ER signal peptide (Sp) of LPR1 or LPR2 and the rest of the coding sequence to ensure a correct subcellular localization of the fusion protein without interfering with its C-terminus. Four days after infiltration, leaf discs of infected tissues were

harvested, the proteins extracted, and analyzed via Western blotting using α -LPR1 and α -GFP antibodies (Figure 11).

An α -LPR1 antibody was used for detection of LPR1 and the Sp-GFP-LPR1 fusion protein (Figure 11a). Two bands at \sim 70 kDa and 100 kDa were present in the *p35S::Sp-GFP-LPR1* sample. Given the molecular weight of LPR1 (66 kDa), GFP (26 kDa) and the respective fusion protein (92 kDa) the band at 100 kDa resembles the fusion protein Sp-GFP-LPR1. The signal at 70 kDa suggested the presence of untagged LPR1, probably caused by the cleavage of Sp-GFP-LPR1. The cleavage of GFP from fusion proteins during ER or vesicle trafficking has been described in several studies (Wirth et al., 2007).

To verify the cleavage and to evaluate the levels of Sp-GFP-LPR2 in the respective samples, another immunoblot was performed and probed with an α -GFP antibody (Sigma-Aldrich). Signals at 100 kDa were present in all samples that contain fusion proteins (Sp-GFP-LPR1 and Sp-GFP-LPR2) with the highest abundant signal for *p35S::Sp-GFP-LPR1* followed by *p35S::Sp-GFP-LPR2*. The Ub10 promoter is considered a weaker overexpression promoter in comparison to the 35S promoter which fits to the weaker signals in both, *pUb10::Sp-GFP-LPR1* and *pUb10::Sp-GFP-LPR2* in comparison to their respective *p35S* counterparts. The very weak signal in the *p35S::GFP EVC* is probably caused by a spillover from *pUb10::Sp-GFP-LPR2*. A relatively strong signal corresponding to GFP could be detected in *p35S::Sp-GFP-LPR1* underlining the hypothesis that the 70 kDa signal in this sample in Figure 11a is likely derived from the cleavage of Sp-GFP-LPR1 into GFP and LPR1. Besides this, GFP could only be detected in the samples transformed with empty vectors (EVC), indicating that in all the other samples, the GFP is not cleaved off from the fusion protein or its abundance is below detection limit.

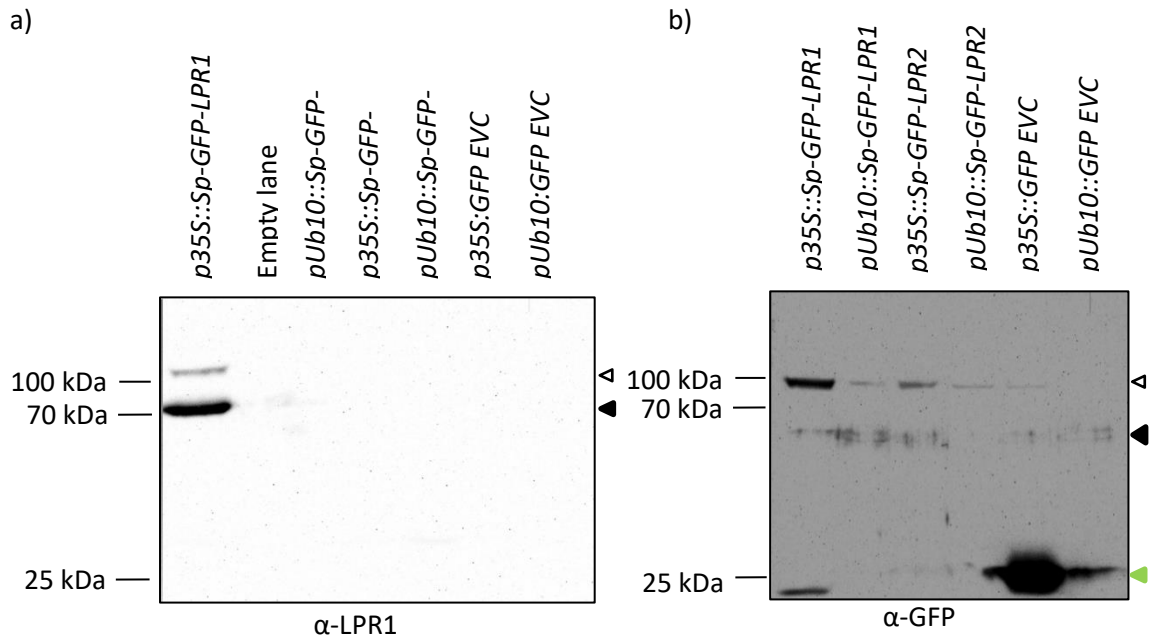


Figure 11: Transient overexpression of *Sp*[~]GFP~LPR1 and *Sp*[~]GFP~LPR2 in *N. benthamiana*. *A. tumefaciens* strains transformed with vectors carrying *p35S::Sp-GFP-LPR1*, *p35S::Sp-GFP-LPR2*, *pUb10::Sp-GFP-LPR1*, *pUb10::Sp-GFP-LPR2* and the respective EVC vectors were used to transiently transform *N. benthamiana* leaves. 4 days after transformation 8-10 leaf discs were harvested and total protein was extracted. The samples were subjected to an SDS-PAGE with subsequent immunoblotting. Two different primary AB were used. The secondary AB was goat α -rabbit Ig (Biorad; 1:10,000). Full length *Sp-GFP-LPR1/2* has a MW of \sim 92 kDa. LPR1/2 without GFP has a MW of \sim 66 kDa and GFP has a MW of \sim 26 kDa. a) Immunoblot probed with α -LPR1 AB (0.1 μ g / ml [Immunoglobulin]). LPR1-GFP is marker with \blacktriangle , LPR1 with \triangle and GFP with \blacktriangle .

Taken together, these results show that *Sp-GFP-LPR1* is likely to be cleaved into *Sp-GFP* and LPR1. This seems not to apply to *Sp-GFP-LPR2*. Furthermore, the *p35S* and *pUb10* promoters are feasible to drive the heterologous expression of LPR1 and LPR2 variants in *N. benthamiana*.

2.1.5 Identification of putative iron and copper binding sites in LPR1

A phylogenetic tree of MCOs showed that LPR1 and LPR2 are highly similar to ferroxidases such as Fet3p and Fet5p from yeast. Fet3p has been studied extensively in the last 25 years. Its mode of action has been elucidated on the molecular level and important amino acid residues for the protein function have been identified (de Silva et al., 1997; Taylor et al., 2005; Stoj et al., 2006). It was shown in previous sections of this work that LPR1 exhibits ferroxidase activity (Figure 7). Although ferroxidases have been a subject of many studies throughout all other kingdoms of life, no plant ferroxidase has yet been characterized in detail. To get a first hint whether the mode of function of LPR1 is similar to Fet3p or Fet5p, a multiple sequence alignment of the amino acid sequence of LPR1, LPR2, Fet3p and Fet5p was generated to see if the amino acids which are important for the function of Fet3p and Fet5p are also conserved among LPR1 and LPR2. Therefore the conservation of the amino acids forming the copper and iron binding sites in the Fet proteins was examined throughout LPRs and Fet proteins using the MUSCLE multiple sequence alignment tool (Edgar, 2004). The result is

depicted in Figure 12. Conserved amino acids of the T1 copper cluster are highlighted in dark blue, T2/T3 forming amino acids in light blue, and the amino acids responsible for iron binding in red.



Figure 12: Multiple sequence alignment of LPR1, LPR2, Fet3p and Fet5p. The amino acid sequences of LPR1, LPR2, Fet3p and Fet5p were analyzed with the MUSCLE multiple sequence alignment algorithm regarding to their sequence similarities and conserved amino acids. Amino acids forming the T1 copper cluster are highlighted in ■, amino acids forming the T2/T3 copper cluster in ■, and amino acids forming the iron binding site in ■. For graphical illustration, Jalview was used (Waterhouse et al., 2009).

On sequence level, all important amino acids forming the copper and iron binding sites in the Fet proteins are at least partially conserved in the LPRs. In Fet3p the T1 copper binding site is formed by two histidine (H489 and H413) and one cysteine (C484) residues. H413 and C484 are equivalent to H464 and C484, respectively, in LPR1 and are fully conserved. H489 of Fet3p is represented by H568 in LPR1 and displaced by three positions within the sequence. The trinuclear T2/T3 copper cluster of Fet3p is composed of six histidine residues, binds three copper atoms, and is completely conserved in Fet3p and LPR1. The iron binding site of Fet3p is formed by two aspartic acid residues (D283 and D409) and on glutamic acid (E185). Whereas E185 of Fet3p is equivalent to E269 in LPR1 and found exactly at the same position, D283 and D409 of Fet3p are replaced by D370 and D462, respectively, in LPR1 and their position is slightly shifted within the amino acid sequence of the protein.

This conservation of the copper and iron binding sites within Fet proteins and the LPRs strongly indicate that also in LPR1 the formation of the metal binding sites is accomplished by the same amino acids like in Fet3p, indicating a similar mode of action of both proteins.

To get a better understanding of the structural similarities and differences between Fet3p and LPR1 the putative structure of LPR1 has been modeled based on the known structure of Fet3p. Therefore the amino acid sequence of LPR1 was subjected to the Protein Homology/AnalogY Recognition

Engine, version 2.0 (Phyre2) (Brachmann et al., 1998). Subsequently the 3DLigandSite server was used to identify putative ligand binding sites (Wass et al., 2010). The algorithm identified the T2/T3 trinuclear copper cluster in LPR1. The T1 copper cluster as well as the amino acid triad that forms the Fe^{2+} -binding site could be detected via manual analysis also including the information from the multiple sequence alignment (Figure 12). They show a similar formation like in Fet3p. The modeling and analysis of the ligand binding sites have been carried out by Dhurvas Chandrasekaran Dinesh in our lab.

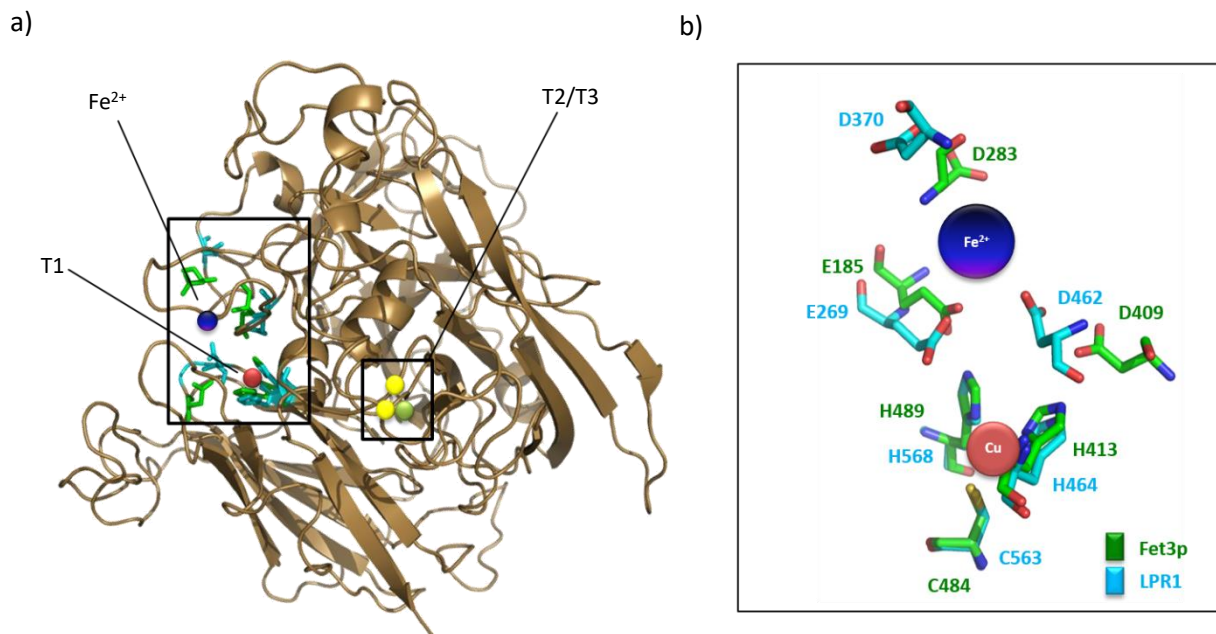


Figure 13: Predicted structure of LPR1 including putative ligand binding sites based on Fet3p modeled with the PHYRE2 and 3DLigandSite servers. The putative structure of LPR1 was modeled using the PHYRE2 algorithm. The 3D structure was subsequently subjected to the 3DLigandSite server to identify putative metal binding sites. a) The model of LPR1 including the predicted iron and copper binding sites. The T2/T3 trinuclear copper cluster has been identified by 3DLigandSite. The T1 copper cluster and the Fe^{2+} -binding site were identified via manual analysis including the data from the multiple sequence alignment (Figure 12). b) A more detailed view on the amino acids of LPR1 that form the Fe^{2+} -binding site and the T1 copper cluster superimposed with those of Fet3p. Modeling by Dhurvas Chandrasekaran Dinesh.

2.1.5.1 Site directed mutagenesis to inhibit the formation of the Fe^{2+} -binding site and the T1 copper cluster of LPR1

Numerous amino acids putatively important for the formation of the active sites of LPR1 have been identified (Figure 12 & Figure 13). The next steps aimed to verify these *in silico* analyses using *in vitro* and *in vivo* approaches. Therefore, site directed mutagenesis was carried out to generate single amino acid exchanges of the amino acids forming the Fe^{2+} -binding site as well as those forming the putative T1 copper cluster. Additionally, a point mutation in LPR1 (P365L) was included in these studies, which has been identified in a screen conducted in the lab of Prof. Laurent Nussaume (CEA

Cadarache). Although P365 is not located directly in a predicted active center of the protein, the underlying mutation causes the same insensitive root growth phenotype on $-P_i$ conditions like an *lpr1* KO. Since the generation of *LPR1* (P365L) was not successful, *LPR1* (P365A) was used as a substitution. In subsequent steps the effect of these mutations on protein activity and the ability to complement an *lpr1* mutant should be examined. All amino acid substitutions that have been carried out changed the coding triplet of the original amino acid to GCC which codes for an alanine. An overview of all single amino acid exchanges carried out within the framework of this thesis is depicted in Table 3. The primers which have been used for site directed mutagenesis are shown in Supplemental table 2.

Table 3: Overview of all amino acid exchange variants of LPR1 generated.

Mutation	putative Fe ²⁺ -binding-sites	Position CDS	Triplet of original amino acid
#1	E269A	805-807	GAA
#2	D370A	1108-1110	GAT
#3	D462A	1384-1386	GAT
#1#3	E269A; D462A		
#1#2#3	E269A; D370A; D462A		
	putative T1 copper cluster		
#4	H464A	1390-1392	CAT
#5	H568A	1702-1704	CAT
#6	C563A	1687-1689	TGT
	Loop adjacent to D370		
#7	P365A	1093-1095	CCT

The generation, cloning and subsequent biological and biochemical analysis of different mutated variants of *LPR1* is very time consuming. Since the binding of iron and the initial transfer of the electron to the T1 copper cluster are crucial steps for the activity of ferroxidases, it was decided to concentrate the experimental efforts on generating mutants affecting the putative Fe²⁺-binding site and the T1 copper cluster leaving the characterization of the T2/T3 copper cluster aside.

To generate the different site-directed mutations (SDMs), PCRs were carried out according to 4.5.1.7. *LPR1_pENTR* vector served as a template for all single amino acid exchanges. SDM#1#3 was generated by introducing SDM#1 in SDM#3_pENTR. For the generation of SDM#1#2#3, SDM#1#3 served as template. All generated mutated variants of *LPR1* were cloned in the vector pB7WG2 were they are fused to a 35S promoter. The same protocol was also used to generate the *35S::LPR1* constructs, already described in Figure 5. Subsequently, all generated *LPR1* variants were transformed into *A. tumefaciens*.

2.1.5.2 Overexpression of mutated *LPR1* variants in *Nicotiana benthamiana*

To examine the effects of the exchanged amino acids in the putative active sites of LPR1 on protein function, all variants were expressed transiently in *N. benthamiana* for 3 – 5 days under the control of the 35S promoter. Crude protein extracts were prepared, and the specific ferroxidase activity of each extract was determined via Ferrozine assays, using a substrate concentration of 25 μ M and protein amounts between 25 – 70 μ g per reaction. In Figure 14 the mean values of three independent experiments are depicted. To establish LPR1 protein levels in the samples, western blots using an α -LPR1 antibody were carried out. Since protein amounts of each variant differed in all three experiments, a representative blot for one experiment is shown in Supplemental figure 10.

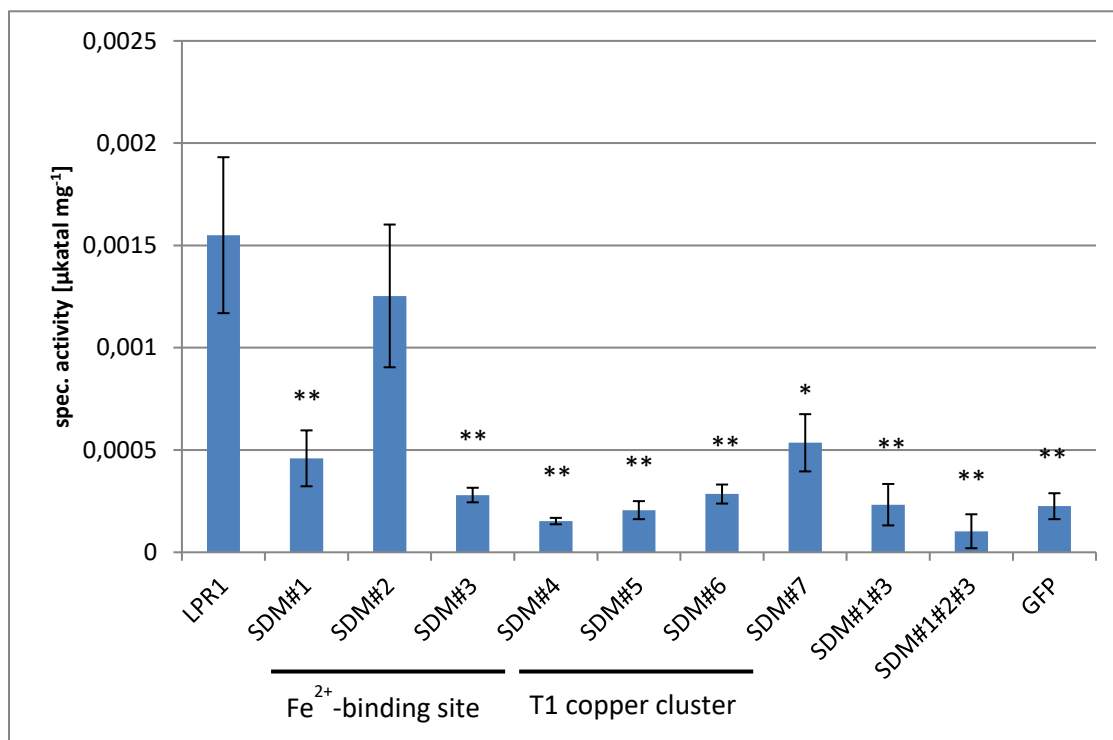


Figure 14: Specific ferroxidase activity of crude extracts of *N. benthamiana* transiently expressing different LPR1 variants. Different 35S::LPR1 variants were transiently expressed in *N. benthamiana* and the specific ferroxidase activities of the respective crude protein extracts were determined via Ferrozine assays. 50 – 90 μ g of total protein was used in the different experiments. 25 μ M substrate solution was used in each experiment. 35S::LPR1 WT served as a reference whereas 35S::GFP was used as a negative control. The mean values of 3 independent experiments are shown here. All activities were compared to LPR1 via two-tailed student's t-test. Error bars indicate SD; * indicate $p < 0.05$; ** indicate $p < 0.01$; N=3

Expression of *LPR1* in tobacco resulted in the highest specific ferroxidase activity of all tested crude extracts. Exchanges in amino acids contributing to the active sites of the protein were expected to affect the ferroxidase activity of the protein resulting in decreased specific ferroxidase activity of the respective crude extracts. That was the case for all but one of the generated variants of LPR1. Only crude extracts of SDM#2 (D370A) showed a specific ferroxidase activity comparable to LPR1. The expression of all other generated LPR1 variants including the double mutant SDM#1#3 and the triple

mutant SDM#1#2#3 resulted in a significantly decreased specific ferroxidase activity of their respective crude extracts.

The expression of the different variants of LPR1 resulted in different protein levels in the samples as shown in Supplemental figure 10. Although the amounts of LPR1 for the same variant differed between the three experiments, it became clear that the overexpression of SDM#4, SDM#5 and SDM#6 in tobacco always yielded very low amounts of protein in comparison to all the other variants. Since the putative T1 copper cluster is affected in SDM#4, #5 and #6 and copper is an important co-factor for ferroxidases, it was tempting to speculate that the protein stability is compromised in those variants. To examine this, qPCR analysis was carried out using primers P071 & P072 (Supplemental table 1) to determine the amount of *LPR1* mRNA after transient expression of all variants in tobacco. All expression levels were normalized to *PP2A* using primers MH93 + MH94 and their relative amount to *LPR1* was calculated (Figure 15).

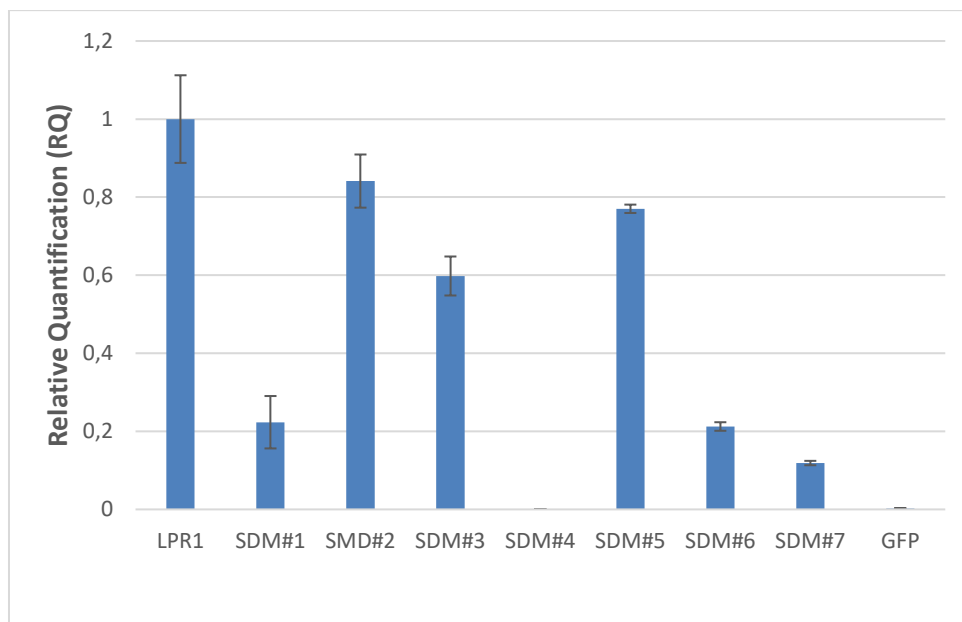


Figure 15: Analysis of mRNA levels of different *LPR1* variants after transient expression in *N. benthamiana*. Different *LPR1* variants were transiently expressed in tobacco under the control of the 35S promoter. 4 days after infiltration leaf discs were harvested, total RNA was extracted, and cDNA was generated from 5 µg of the extracted RNA. 1 µl of cDNA served as a template for qPCR analysis to determine relative expression levels of the different *LPR1* variants. The expression levels were normalized to *PP2A* expression and the relative expression to *LPR1* was assigned.

The amount of *LPR1* mRNA was the highest in LPR1. The relative expression of all other variants in comparison to LPR1 differed from 10 % (SDM#1 and SDM#7) to 90 % expression (SDM#2). No transcript could be detected for SDM#4. However, the levels of mRNA cannot be directly correlated with the amounts of protein detected within the samples (Supplemental figure 10), indicating that the protein levels in the samples are rather determined by protein stability than by protein production *per se*.

In summary, these results suggest that all applied amino acid exchanges in the different variants of LPR1 except of SDM#2 severely impact the ferroxidase activity of LPR1. Thus, confirming the *in silico* predicted active sites via *in vitro* assays. A comparison of the relative expression levels, the protein amount and the specific ferroxidase activity of the different variants also hint to the importance of the T1 copper cluster for the stability of the protein, because all variants with defects in the T1 copper cluster show reduced LPR1 levels regardless of their respective *LPR1* mRNA levels.

2.1.5.3 Complementation of *lpr1* with generated variants of 35S::*LPR1*

In silico analysis predicted Fe and Cu-binding sites within LPR1. Since the importance of the Fe²⁺-binding site and the T1 copper cluster had been demonstrated by measuring the ferroxidase activities of different *LPR1* variants after transient expression in tobacco and numerous amino acids crucial for the formation of the Fe and Cu-binding sites had been identified, the next step was to examine the effect of single amino acids exchanges on the function of LPR1 in the PSR of *Arabidopsis*. To do so, all generated variants of LPR1 should be tested with regards to their ability to complement the *lpr1* root growth phenotype on –Pi conditions. Therefore, *lpr1-2* plants expressing the constructs described in 2.1.5.1 were generated via *A. tumefaciens* facilitated stable transformation of *Arabidopsis lpr1* plants using the floral dip method. Due to time limitations, homozygous T₃ plants could only be identified for plants expressing *LPR1*, SDM#1, SDM#2 and SDM#3. For plants transformed with variants compromised in the T₁ copper cluster T₂ seeds are available for segregation analysis.

Homozygous lines of *lpr1-2* plants overexpressing either *LPR1*, SDM#1, SDM#2 or SDM#3 were grown 5 days on +Pi medium, transferred for 2 days on +Pi or –Pi plates. The primary root growth after transfer was measured and depicted in Figure 16. Col-0 and *lpr1* plants served as controls. In addition, LPR1 39-7 which expresses LPR1 under the 35S promoter in the background of Col-0 was implemented as another control.

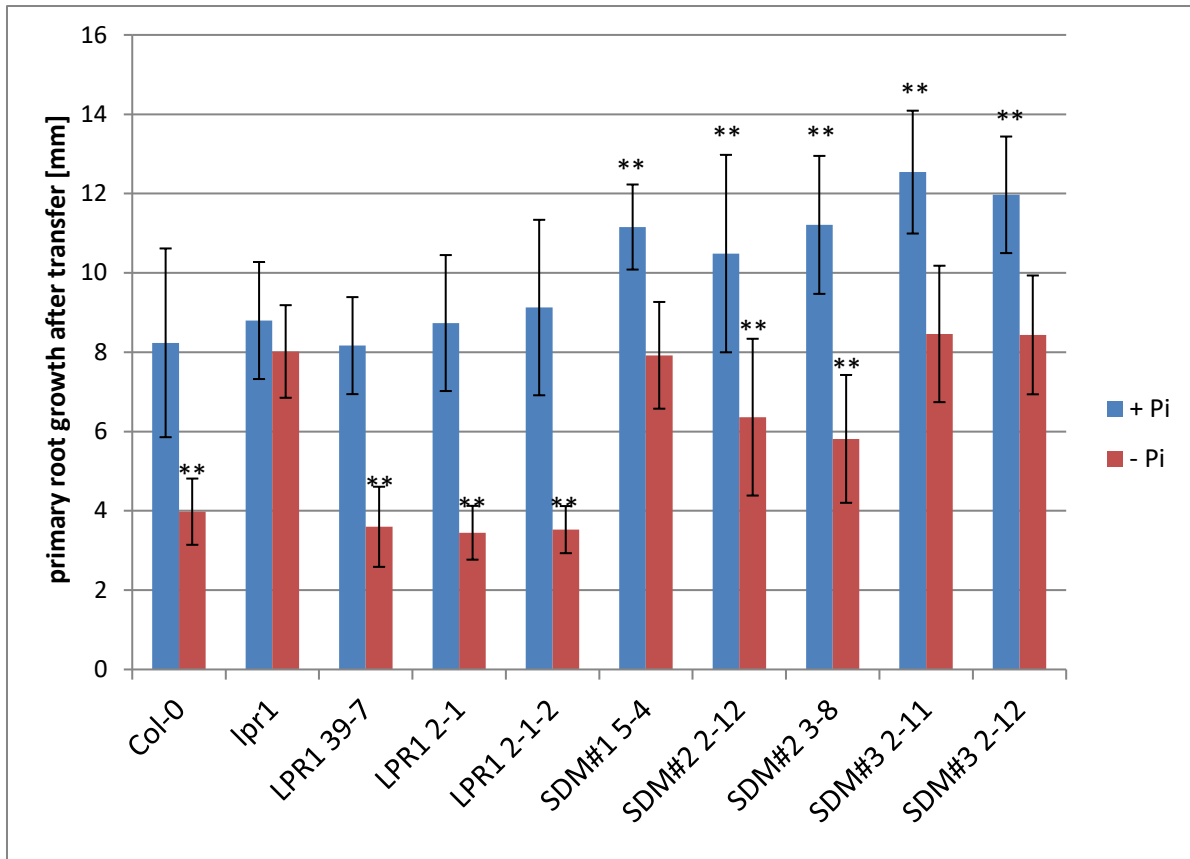


Figure 16: Primary root growth of *lpr1* plants transformed with different variants of *LPR1*. *lpr1* plants expressing different variants of *LPR1* under the control of the 35S promoter were grown for 5 days on +Pi medium and subsequently transferred to +Pi or –Pi plates. Primary root growth was measured 2 days after transfer. $n > 15$, two tailed student's t-test compared all lines to *lpr1* +/-Pi conditions, respectively. * indicated $p < 0.05$; ** indicate $p < 0.01$

Col-0 shows inhibited primary root growth after transfer to –Pi conditions when compared to +Pi. In contrast, the primary root growth of *lpr1* is insensitive to low Pi conditions showing no difference in root growth between +Pi and –Pi conditions. To test if the overexpression of the different *LPR1* variants can restore the sensitivity of *lpr1* to low Pi conditions, the primary root growth after transfer of all lines was compared to *lpr1* in +Pi and –Pi conditions. All *35S::LPR1* lines showed a WT-like root growth in both, +Pi and Pi depleted conditions. The presence or absence of the original genomic *LPR1* locus also did not alter the primary root growth in any conditions. After transfer to –Pi conditions, the primary root growth of all three *35S::LPR1* lines showed an impaired root growth like Col-0 and in contrast to insensitive *lpr1* seedlings. This indicates that the introduction of intact *LPR1* in an *lpr1* background is capable of restoring a WT like primary root growth in –Pi conditions. The overexpression of all SDMs used in this experiment lead to an increased root length already in +Pi conditions in comparison to *lpr1*. In –Pi conditions, the root lengths of SDM#1 & SDM#3 were similar to *lpr1*. Both *SDM#2* lines showed slightly, but significantly shorter roots than *lpr1* on – Pi medium indicating only a partial rescue of the *lpr1* phenotype.

These data indicate that the overexpression of LPR1 in an *lpr1* background is completely sufficient to restore the sensitivity of the plants primary root growth to $-Pi$ conditions. This, however, is not the case for the overexpression of SDM #1 and SDM#3, that still show *lpr1* like root growth under Pi depletion. Compared to that, *35S::SDM#2* lines showed slightly longer roots than Col-0, but still significantly shorter than *lpr1*, indicating only a partial restoration of the Pi sensitivity in these plants. Taken together, these results imply that the function of LPR1 in SDM#1 and SDM#3 is completely impaired and therefore lead to an absence of root growth inhibition on low Pi conditions. The amino acid exchange in SDM#2 seems to have only minor effects on the protein function and so, the primary root growth is only slightly inhibited under these conditions.

All in all, the results from this section clearly show that the function of LPR1 is tightly connected to the presence of at least two important active sites within the protein. Firstly, the binding of the substrate Fe^{2+} , which is very likely facilitated by E269A, D370A & D462A. Second, an intact T1 copper cluster that is crucial for the stability of the protein. The formation of both abovementioned active sites is crucial for the ferroxidase activity of the protein and also for the *in vivo* function of the protein and its function in controlling the PSR of *Arabidopsis*.

2.1.6 Various approaches to obtain active, purified LPR1 protein for subsequent biochemical analyses

It has been shown that LPR1 is a ferroxidase and two active sites of the protein were already identified using *in vitro* and *in vivo* approaches within the context of this work. Since the knowledge of ferroxidases in plants is very limited, especially with regards to their functionality, the biochemical properties of LPR1 should be investigated. Detailed biochemical studies, however, require substantial amounts of purified protein. Therefore, numerous attempts to purify LPR1 from plants, bacteria and yeast, using different approaches, were undertaken.

2.1.6.1 Purification via the GFP-tag

In a first attempt, *p35S::Sp-GFP-LPR1* constructs transiently expressed in tobacco as described in 2.1.4 were used to produce GFP-tagged LPR1 for subsequent affinity purification using the GFP-Trap system (Chromotek).

400 mg leaf material was harvested and diluted in 600 μ l of GFP-Trap Extraction buffer. The crude extract (CE) was incubated with 25 μ l of the beads for 90 min at 4 $^{\circ}$ C. After centrifugation, the supernatant was transferred to a new reaction tube and hereafter referred to as the flow-through (FT). The bound protein was eluted from the beads via incubation in 100 μ l 0.2 M Glycine pH 2.2 and subsequently neutralized using 10 μ l Tris-HCl pH 10.4. As a negative control, leaf material from

uninfected plants (control) was treated in the same way. To evaluate the efficiency of the purification process, 25 μ l of each sample were loaded on an SDS gel and subsequently analyzed via Western Blotting using antibodies against GFP and LPR1 (Figure 17 a & b). GFP-LPR1 has a MW of \sim 95 kDa and could be identified in the elution fraction of GFP-LPR1 with α -LPR1 as well as with an antibody recognizing GFP. Remarkably, both antibodies failed to detect GFP-LPR1 in the CE, indicating that the total amount of GFP-tagged LPR1 within the sample is rather low. On the other hand, this shows that the purification process itself is quite efficient in concentrating GFP-LPR1 in the elution fraction. The α -LPR1 antibody reveals the presence of untagged LPR1 in the CE and the FT fraction of GFP-LPR1. As the cleavage of GFP-LPR1 had already been shown in Figure 11 this result was not surprising. However, the ratio between GFP-LPR1 and LPR1 was shifted even more to LPR1 in this experiment in comparison to Figure 11. Since there was still a fair amount of GFP-LPR1 present in the concentrated elution fraction of GFP-LPR1, the ferroxidase activities of all the samples were assessed (Figure 17 c & d).

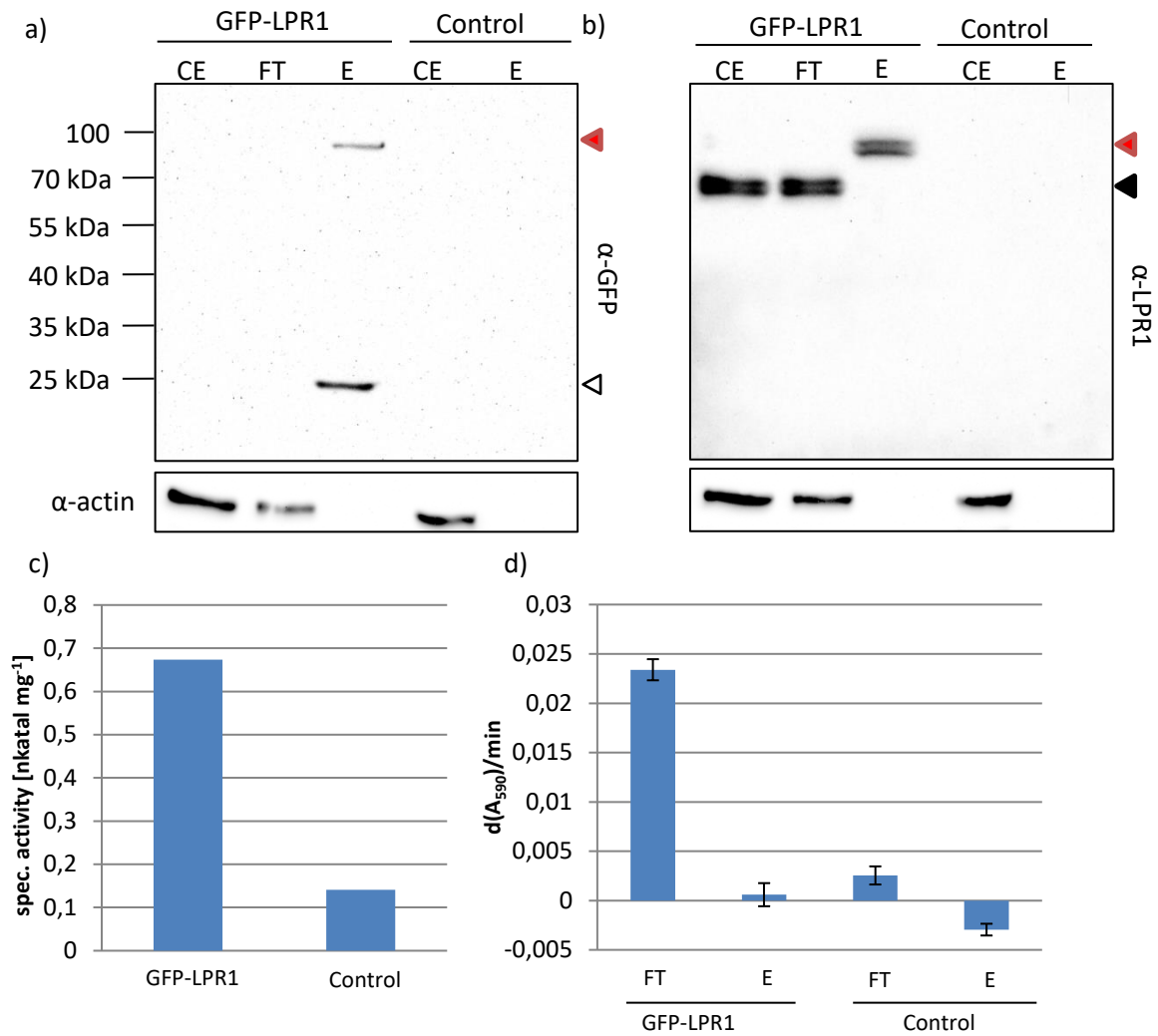


Figure 17: Protein levels and ferroxidase activities of GFP-LPR1 prior and after purification via GFP-Trap. GFP-LPR1 was expressed transiently in *N. benthamiana* and the proteins were extracted from leaf discs 4 days after infiltration. Leaf discs from uninfected plants served as a negative control. GFP-tagged LPR1 was then purified using GFP-Trap agarose beads. 25 μ l of each fraction was loaded to a 10 % SDS gel and the abundance of GFP-LPR1 in every fraction was assessed via WB using α -LPR1 AB (a) or α -GFP AB (b). GFP-LPR1 (~ 95 kDa) is marked by \blacktriangle whereas \blacktriangleleft and \triangleleft indicate LPR1 and GFP, respectively. actin served as a control for loading and purification efficiency. c) The specific ferroxidase activity of the crude extracts of GFP-LPR1 and the control sample was determined via Ferrozine assay. d) To estimate the relative ferroxidase activity of the FT and elution fraction of GFP-LPR1 and control, a Ferrozine assay was carried out and the decrease of the absorption at 540 nm / min of 25 μ l of each fraction was measured and used as a proxy for the relative ferroxidase activity of the samples.

A comparison between the specific ferroxidase activity of GFP-LPR1 and the control showed that the former is much higher (0.6 nKatal mg⁻¹) than the not infected control which exhibits only 0.13 nKatal mg⁻¹ prior to purification. Since the total protein concentrations of the elution fractions could not be determined, the specific ferroxidase activities of these samples could not be calculated. To estimate the relative differences between the FT and the elution of GFP-LPR1 and the control samples, Ferrozine assays were carried out and the decrease of the absorbance at 540 nm over time was used as a proxy to determine the ratio of the ferroxidase activities of the samples after the purification. Therefore, 20 μ l of FT and elution from GFP-LPR1 and control subjected to a Ferrozine assay with 25

μM of Fe^{2+} substrate. The only sample which caused a significant decrease of the absorbance at 540 nm over time was the FT of GFP-LPR1. Addition of any other sample did not alter the amount of Fe^{2+} in the reaction tube indicating a lack of inherent ferroxidase activity of these samples.

These findings suggest that the increased ferroxidase activity of GFP-LPR1 CE is not caused by GFP-LPR1, but by untagged LPR1. The cleavage of GFP-LPR1 to LPR1 and GFP in the CE results in high amounts of LPR1 within this sample which in the end causes increased ferroxidase activities. However, since untagged LPR1 is not bound by the GFP-Trap beads, the elution of GFP-LPR1 only harbors GFP-LPR1 and GFP but lacks LPR1. Therefore, it is quite tempting to speculate that the fusion of a GFP-tag to the n-terminus of LPR1 inhibits the enzymatic activity of the protein.

Additional experiments with various tags of different sizes (3xHA, Flag-tag and Myc-tag) fused to the N- or C-terminus of LPR1 yielded the same results indicating that the termini of the protein must not be changed to preserve its ferroxidase activity.

2.1.6.2 Purification via antibody-coupled beads

To circumvent the problem that the addition of tags to LPR1 seems to inhibit its ferroxidase activity, a purification of native LPR1 via antibody-coupled agarose beads were carried out. Therefore, LPR1 was expressed transiently in *N. benthamiana* under the control of the 35S promoter. As a control 35S::GFP was used. Leaf discs were harvested 4 days after transformation and the proteins were extracted (CE). 2 μg of α -LPR1 AB were added and the reaction was incubated while rotating slowly for 2 h at 4 °C. After addition of Protein A beads and a 2 hours incubation step, the beads were separated from the sample via centrifugation. To prevent denaturation of the target protein, the antigen-antibody complexes were eluted from the beads via incubation at pH 2.2. The elution was then neutralized using 1 M Tris-HCl pH 7.5. The supernatant was referred to as Flow-through (FT). The separated beads were then incubated in SDS sample buffer at 95 °C to elute possible remnants of the target protein (Beads). To analyze the efficiency of the purification process, all samples were boiled in SDS sample buffer, loaded on an SDS gel and subsequently analyzed via Western blotting

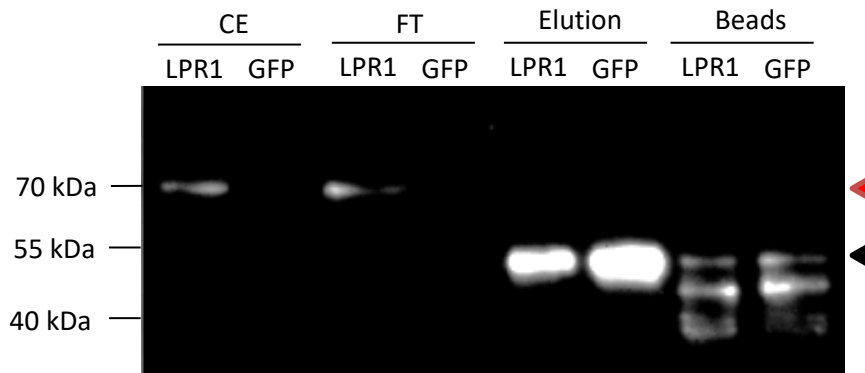


Figure 18: Purification of untagged LPR1 using LPR1 antibody coupled to Protein A beads. LPR1 and a GFP control was expressed transiently in *N. benthamiana* and purified via incubation with 2 μg α -LPR1 AB. The antigen-antibody complexes were subsequently bound to Protein A agarose beads (Pierce) and separated from the rest of the sample (FT) via centrifugation. The antigen-antibody complexes were eluted via pH 2.2 (Elution) and the beads were boiled in SDS sample buffer (Beads). 60 μg of CE and FT and 20 μl of Elution and Beads fraction was loaded to a 10 % SDS gel. After Western Blot, α -LPR1 AB (0.1 μg / ml) was used to analyze the purification efficiency. LPR1 has a MW of \sim 66 kDa and is indicated via \blacktriangleleft and was detectable in the CE and the FT of LPR1. No signal of LPR1 was detectable in the elution or beads fraction indicating no binding of native LPR1 to the Antibody. The IgG heavy chain has a MW of \sim 50 kDa (indicated via \blacktriangleleft) and is detectable in all elution and beads fractions.

LPR1 has a MW of 66 kDa and could be detected in the CE and the FT clearly showing the presence of LPR1 in the sample after extraction. However, a comparison of the signal intensities reveals the same amount of LPR1 present in both fractions, indicating a poor binding of LPR1 to the AB. This is further supported by the complete absence of LPR1 in the elution or the beads fraction. Yet, the IgG heavy chain derived from the LPR1 antibody is present in all elution fractions indicating that the binding of the AB to the beads works well. Thus, the absence of LPR1 in elution and beads fraction is probably caused by an impaired binding of native LPR1 to the peptide AB. This is further supported by the inability of the antibody to detect LPR1 after Western Blots of native gels and on histological samples (Data not shown).

2.1.6.3 Native purification from yeast

Because of the findings that the purification of active LPR1 can neither be achieved by using tagged variants of the protein nor by using the available antibody, we tried to purify native LPR1 via a combination of different classical purification approaches i.e. size exclusion and ion exchange chromatography. However, these approaches require large amounts of starting material. Since the extraction of proteins in high quantities from plant material is inconvenient and labor intensive, it was decided that heterologous expression of *LPR1* in yeast could be used to produce substantial amounts of LPR1 for subsequent purification via classical approaches. *S. cerevisiae* transformed with a plasmid containing *LPR1* under the control of a galactose-inducible promoter was grown in SD-U medium with raffinose as carbon source to an $\text{OD}_{600} \sim 0.6$. *S. cerevisiae* transformed with a plasmid

harboring *Fet3* under the control of the same promoter was used as a control. 2 % Galactose was added to induce gene expression and cells were harvested 12 h after induction via centrifugation. Cells were lysed via Zymolase digestion, sonicated and then analyzed via Western Blotting using an α -LPR1 antibody (Figure 19).

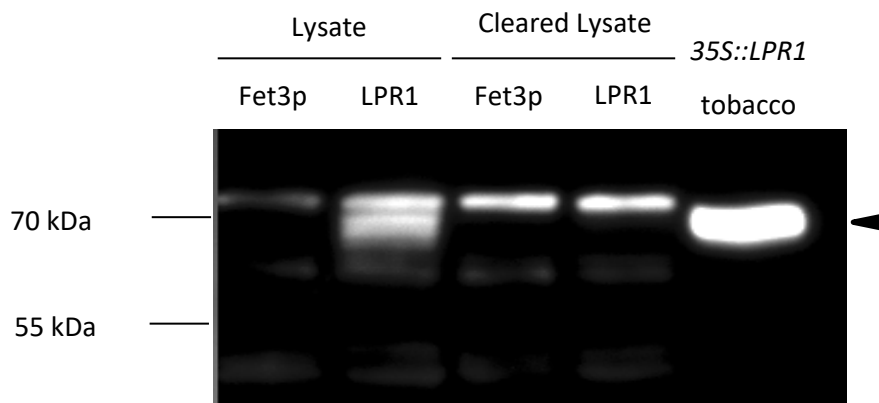


Figure 19: Detection of LPR1 in different fractions of *S. cerevisiae* overexpressing LPR1 or Fet3. *LPR1* or *Fet3* were expressed in *S. cerevisiae* under the control of a Galactose-inducible promoter. 12 h after the induction with Galactose the cells were harvested via centrifugation. The cells were lysed, a sample was taken (Lysate) and the remaining sample was centrifuged to retrieve the Cleared Lysate. 20 μ l of each fraction were loaded on an 8 % SDS gel and analyzed via Western blotting using an α -LPR1 (0.1 μ g / ml) AB. As a control 20 μ l of a CE of tobacco leaves transiently expressing *35S::LPR1* were used. LPR1 has a MW of \sim 66 kDa and is indicated via \blacktriangleleft .

Previous experiments demonstrated that our α -LPR1 antibody is producing unspecific bands at \sim 120 kDa in crude extracts of *Arabidopsis*. Here, a band appeared above a MW of 70 kDa in all yeast-derived fractions, too. However, the MW of this band is lower than of those visible in *Arabidopsis*-derived samples (Figure 5 & Figure 6). To distinguish LPR1 from the unspecific signals, crude extract of tobacco leaves that transiently overexpress LPR1 was used as a positive control. A comparison between the MW of LPR1 produced in tobacco and the signals detected in the yeast samples indeed reveals a slightly higher MW for the unspecific signal than for LPR1. Thus, LPR1 could only be identified in the lysate fraction of *S. cerevisiae* expressing *LPR1*. The absence of this signal in the cleared lysate of *LPR1* indicates that LPR1, when expressed in yeast, is also localized to the cell wall. This result also drastically lowered the chances for a successful classical purification of LPR1 from yeast extracts, since the protein must be separated from the rest of the cell wall fraction prior to downstream purification steps.

Taken together, all attempts that were undertaken to use commonly established methods for protein purification failed to enrich active LPR1 from various organisms. Since no plant ferroxidase had been extensively characterized until then and the biochemical characterization of the LPR1 was one of the main goals of this work, it was decided that the crude characterization of the enzymatic function of LPR1 should be carried out using Crude Extracts instead of pure protein.

2.1.7 Determination of basic biochemical properties of LPR1 with crude extracts of transiently transformed tobacco leaves

LPR1 was successfully identified as a ferroxidase. The knowledge of this class of enzymes in plants is very limited and therefore, the basic biochemical properties of the enzyme should be elucidated. Since all attempts to obtain purified, active LPR1 within the framework of this thesis failed, it was decided that the determination of the basic biochemical properties of the protein should be carried out using crude extracts to reveal if the general functionality of ferroxidases in plants is at least in general, comparable to other organisms i.e. yeast. Furthermore, the enzymatic character of the reaction should be verified. Therefore, total protein extracts from transiently transformed tobacco leaves should be used. Crude protein extracts (CE) of tobacco leaves transiently expressing *LPR1* under the control of the 35S promoter were subjected to Ferrozine assays in various conditions to determine some basic enzymatic properties, like temperature dependence of the activity, optimal pH and enzymatic activity of LPR1 depending on the concentration of available Fe^{2+} concentrations. One out of two representative experiments that showed the same relative values is shown in (Figure 20). Different crude extracts were used for different experiments. For comparability reasons, each figure shows data obtained from one crude extract.

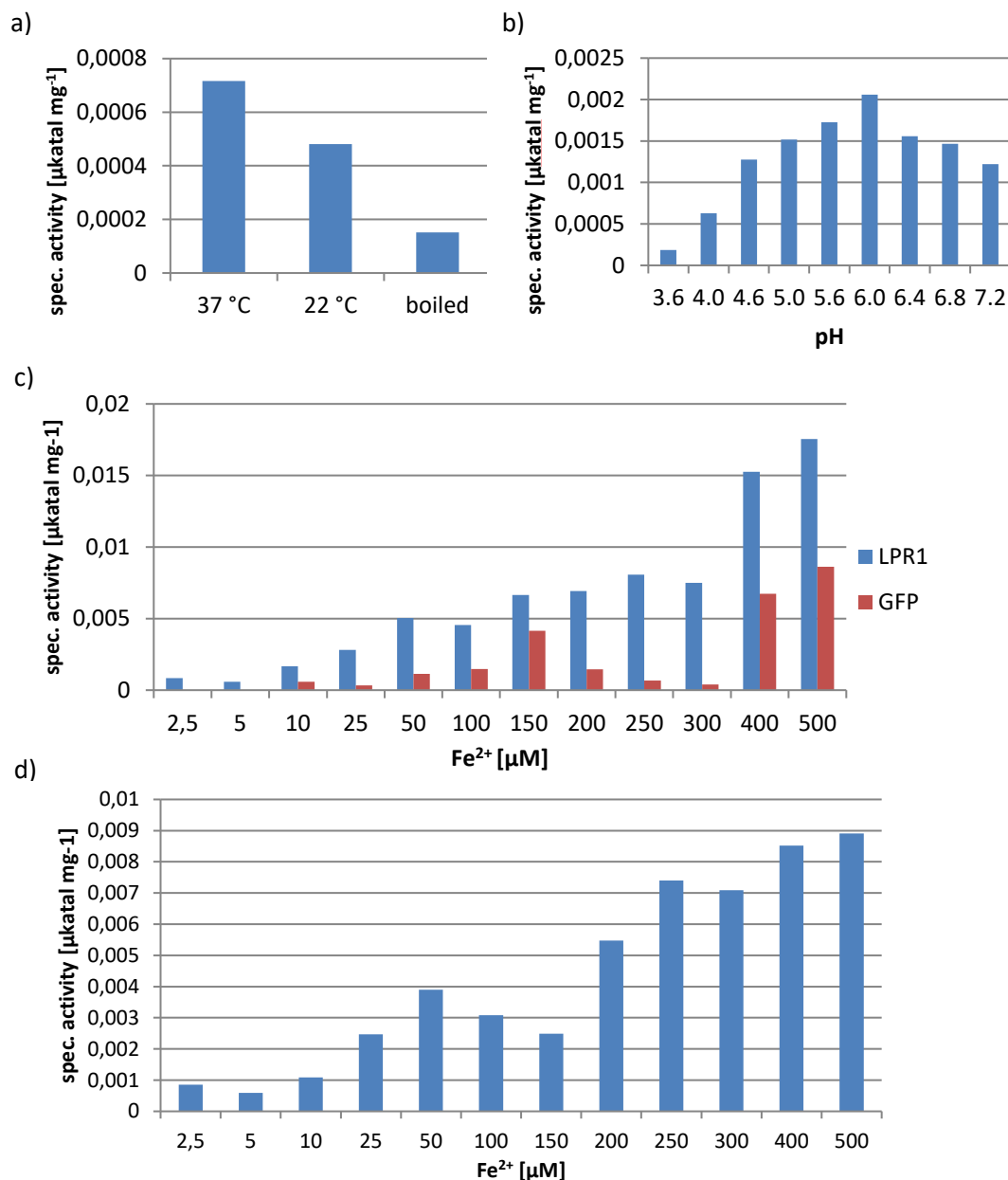


Figure 20: Determination of basic biochemical properties of LPR1 using crude extracts of transiently transformed tobacco leaves. Crude protein extracts from tobacco leaves transiently express *35S::LPR1* were harvested and the specific ferroxidase activity of the samples was determined in various conditions: a) Specific ferroxidase activity *35S::LPR1* was determined at 22 °C and 37 °C as well as after boiling the sample for 10 min at 95 °C (boiled). 50 μg total protein was used, the substrate concentration was 25 μM and the pH was set to 5.6. b) The specific ferroxidase activity of LPR1 was measured at a range from pH 3.2 to 7.2 at 22 °C with a substrate concentration of 25 μM and 25 μg total protein. c) Establishing the specific ferroxidase activity of *35S::LPR1* and *35S::GFP* at different substrate concentrations at 22 °C and pH 5.6. d) Specific ferroxidase activities of *35S::LPR1* and *35S::GFP* at the indicated substrate concentrations.

Temperature and pH are two important factors for the functionality of enzymes. To establish how LPR1 is affected by different temperatures, the reaction was carried out at 22 °C, 37 °C and after pre-incubating the protein for 10 min at 95 °C (Figure 20a). The specific ferroxidase activity of LPR1 is slightly increased at 37 °C compared to 22 °C. A pre-incubation of the CE at 95 °C for 10 min significantly decreases the activity of the protein to a level, comparable to the background activity

seen in all experiments when using CE. To examine the influence of the pH on the function of LPR1, the specific ferroxidase activity of LPR1 CEs was measured under different conditions, ranging from pH 3.6 to 7.2 (Figure 20b). This showed that LPR1 exhibits the highest ferroxidase activity at a pH between 5.6 and 6. The activity drops decreases slowly until pH 4 and is completely abolished at pH 3.6. On the other hand, an increase of the pH up to 7.2 has only a mild negative effect on the protein's ferroxidase activity. Increasing pH values higher than 7.2 lead to significantly increased oxidation of Fe^{2+} even without the addition of any protein and were therefore excluded from further analyses.

A general feature of enzymatic reactions is the dependency of the reaction velocity v on the substrate concentration $[S]$ when the amount of enzyme is constant. However, a maximum velocity v_{max} is reached at a certain $[S]$ where the addition of more substrate does not lead to higher reaction velocities. Since the spec. activity is directly proportional to v_{max} , it can be used as a proxy to determine the concentration of substrate at which v_{max} is reached. To determine v_{max} for Fe^{2+} oxidation of LPR1 the specific ferroxidase activities of Crude extracts of tobacco leaves transiently overexpressing LPR1 were determined using increasing substrate concentrations. To distinguish LPR1 specific activity from background activity, Crude extracts from plants expressing GFP were also subjected to the assay (Figure 20c). The specific ferroxidase activity of LPR1 increases with increasing substrate concentrations rather linear until $50 \mu\text{M Fe}^{2+}$. Addition of higher substrate concentrations only marginally increase spec. activities. Crude extracts of GFP, however, exhibit much lower activities at every measured substrate concentration when compared to LPR1. The activity of GFP CEs peaked at first at $150 \mu\text{M Fe}^{2+}$. Above $300 \mu\text{M}$, spec. activities of LPR1 and GFP samples are increasing drastically indicating unspecific, enzyme independent oxidation of the substrate. To exclude the activity of other ferroxidases in the CE of tobacco leaves, the values of the specific activities of GFP were subtracted from the ones of LPR1 (Figure 20d). The subtracted activities revealed a first peak for the activity at $50 \mu\text{M Fe}^{2+}$, a subsequent plateau until $200 \mu\text{M}$ and a maximum activity of $400 - 500 \mu\text{M}$. When comparing the subtracted values of LPR1 and GFP, a shift of the first peak from $150 \mu\text{M}$ to $50 \mu\text{M}$ in GFP and LPR1, respectively, becomes evident. Thus, overexpression of LPR1, causes increased ferroxidase activities at Fe^{2+} concentrations until $50 \mu\text{M}$ in comparison to GFP.

Although the determination of biochemical properties of LPR1 in crude extracts is not as accurate as it would be for purified protein, a general insight into the functionality could be obtained. The activity of the protein depends on the temperature with slightly higher activity at 37°C than at 22°C . An incubation at 95°C , the addition of the detergent SDS and of the known MCO inhibitor sodium azide cause a complete inactivation of the protein function. The optimal pH for the ferroxidase

activity of LPR1 is in the range between 5.6 and 6.0. Furthermore, the availability of substrate affects the ferroxidase activity of LPR1 in a way, typically for enzymatic reactions.

Taken together, these findings validate the enzymatic features of the ferroxidase activity of LPR1 confirming its function as a ferroxidase.

2.1.8 Complementation of a yeast *fet3*-KO mutant with LPR1

The putative ferroxidase activity of LPR1 was originally proposed based on its similarities to Fet3p of *S. cerevisiae*. Further analyses in the framework of this study indeed revealed *in vitro* ferroxidase activity of LPR1. It was also shown that structural core features of LPR1 are shared with Fet3p (Figure 14). It was therefore tempting to test whether LPR1 can complement a $\Delta fet3$ mutant, which shows a severe growth inhibition when challenged with low iron availability (Askwith et al., 1994). To investigate this, growth of various strains of *S. cerevisiae* BY4741 WT and *S. cerevisiae* BY4741 $\Delta fet3$ containing different plasmids that encode for LPR1 and Fet3 were generated. Subsequently, their ability to grow on medium lacking iron was determined. Despite all similarities of LPR1 and Fet3p, there are still some significant differences in the general structure of both proteins. To take the slightly different predicted signal peptides of LPR1 and Fet3p and the additional C-terminal membrane anchor of Fet3p into account, an additional plasmid was constructed that codes for a chimeric variant of LPR1 and Fet3p (SpF-LPR1-cF). In this chimera the original ER signal peptide of LPR1 was exchanged with the one of Fet3p. Also, the short C-terminal membrane anchor of Fet3p was added at the C-terminus of this construct to maintain a localization of the chimera to the cell membrane. In all plasmids, the expression of the constructs was controlled by a galactose-inducible promoter. As controls, strains that were transformed with empty p426Gal1 vectors were used (Empty Vector Control). From two individual experiments, one is depicted in (Figure 21).

Since the first attempts using agar plates to monitor complementation efficiency turned out to be difficult to analyze, we decided to perform a more detailed analysis of yeast growth in liquid cultures.

Yeast expression medium, containing 2 % Galactose to induce gene expression and lacking Fe, was inoculated to a percentage of 0.5 % (v/v) with precultures of various *S. cerevisiae* strains containing the abovementioned plasmids. Subsequently, the cultures were grown for 52 h at 160 RPM in 28 °C. Samples were taken at the indicated time points and the OD₆₀₀ of every culture was determined to assess their ability to cope with low iron availability (Figure 21).

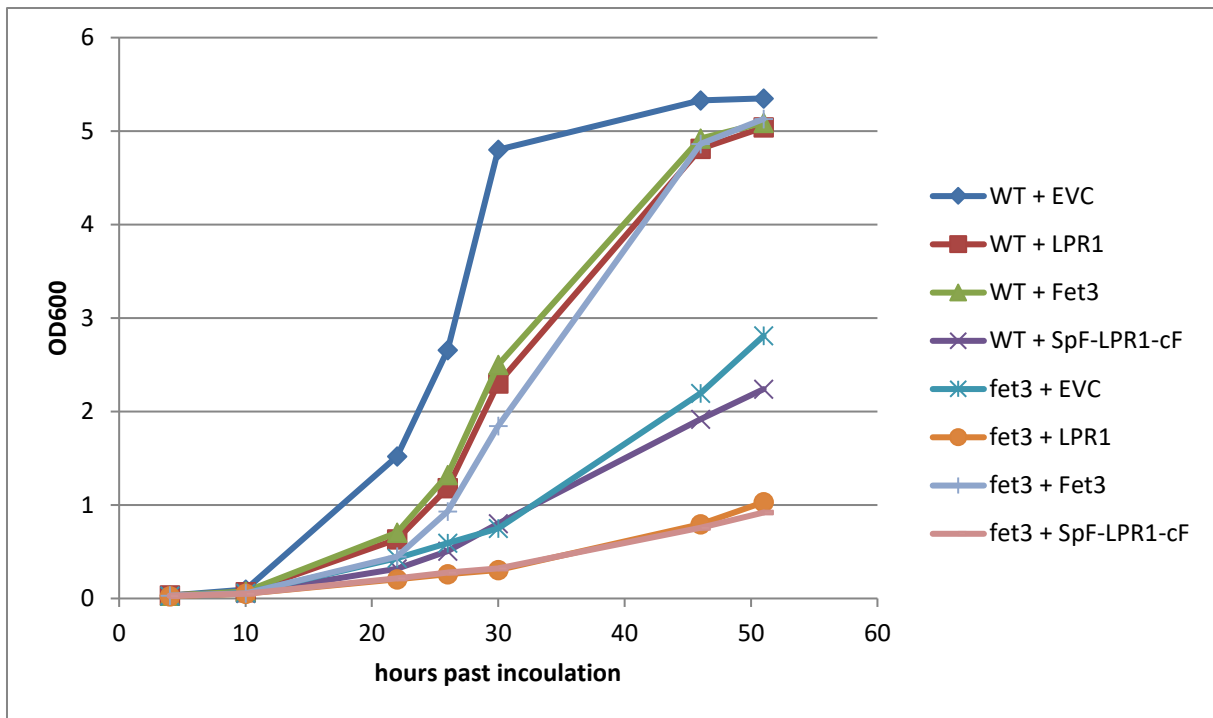


Figure 21: Complementation of $\Delta fet3$ with *LPR1*, *Fet3* and a chimeric variant of both. *S. cerevisiae* WT and $\Delta fet3$ transformed with the indicated plasmids were grown for 52 h in liquid SD-U medium containing 2 % Galactose for induction of gene expression and lacking Fe. OD₆₀₀ was measured at the indicated time points up to 52 h.

When comparing the growth of all strains, WT + EVC shows the fastest growth by reaching an OD₆₀₀ of around 5 already after 30 h. WT + LPR1 and WT + Fet3 both showed an OD₆₀₀ of 2.4 after this time and reached an OD₆₀₀ of 5 after 46 h. WT + SpF-LPR1-cF surprisingly was impaired in growth compared to all other WT strains and showed an OD₆₀₀ of 2.2 after 52 h of growth. An analysis of the growth of all strains with a deleted *fet3* gene revealed that only $\Delta fet3$ + Fet3 showed a growth comparable to WT + LPR1 and WT + Fet3 with an OD₆₀₀ of 1.9 after 30 h and 4.9 after 46 h, respectively. All other strains with a deletion of *Fet3* were severely impaired in terms of growth in low Fe medium. In summary, all strains with a functional chromosomal *Fet3* exhibited normal growth under iron limiting conditions, whereas the $\Delta fet3$ strains showed impaired growth in the same conditions. The induced expression of *Fet3* is sufficient to complement a $\Delta fet3$ mutant in terms of growth under low iron conditions. In contrast, the expression of *LPR1* in a $\Delta fet3$ background did not lead to enhanced growth. Thus, *LPR1* cannot complement the growth defect of $\Delta fet3$ under iron deficiency.

In summary, LPR1 has been identified as a ferroxidase that localizes to the apoplast. Important amino acids could be identified by homology modelling, based on the yeast ferroxidase Fet3p. The significance of these active sites could further be confirmed by *in vivo* complementation assays of *Arabidopsis lpr1* mutants. Although many attempts have been undertaken, the purification of active LPR1 from different organisms could not be carried out successfully. Thus, the basic biochemical

properties of the enzyme were determined via crude extracts from plants overexpressing LPR1. Therefore, an in-depth analysis biochemical and structural analysis remains elusive. The results, however, suggest that the LPR1 functionality is quite similar to Fet3p. Yet, the inability of LPR1 to complement a $\Delta fet3$ mutant in yeast also indicates that there are various aspects that distinguish LPR1 and Fet3p as ferroxidases in plants and yeast, respectively.

2.2 PDR2 encodes a P5-Type ATPase and acts in the phosphate starvations response

The local phosphate starvation response in *Arabidopsis* is orchestrated by various proteins and among those, the interaction of the ferroxidase LPR1 with PDR2 is an important module (Ticconi et al., 2004; Jakobsen et al., 2005; Ticconi et al., 2009). PDR2 has been subject of many studies and was identified as a P5-Type ATPase with unknown substrate specificity, which is localized to the ER membrane. However, a distinct role of PDR2 in the phosphate starvation response and its influence on LPR1 still remains unclear. One reason for this is the intricate handling of *PDR2* when it comes to cloning. It turned out that transformation of *E. coli* with a CDS that codes for a functional PDR2 protein inhibits further growth of the cells. Thus, the amplification and transformation of full-length *Arabidopsis PDR2* turned out to be challenging and the generation of transgenic plants for gene expression and localization studies is therefore very difficult.

One goal of this work therefore was to successfully clone *PDR2* in a Gateway compatible pENTR vector as a tool for various upcoming experiments. Once constructed, PDR2_pENTR can easily facilitate the subcloning of *PDR2* in various expression vectors for a variety of different applications to unravel the functioning of *PDR2* in the phosphate starvation response and its interplay with *LPR1*.

2.2.1 Cloning of the PDR2-locus into the gateway compatible pENTR vector

The construction of expression vectors that carry a gene of interest controlled by different promoters and facilitate translational fusions to fluorescent tags is a prerequisite for a variety of experiments to uncover the function of genes and their products. However, subcloning of DNA sequences into different expression vectors is time consuming and often labor-intensive. Additionally, previous studies, including experiments carried out in our lab, showed, that amplification and cloning of the *Arabidopsis PDR2* cDNA is quite problematic since it is long and encodes for a membrane protein (Sorensen et al., 2012). To circumvent these problems, the full-length genomic sequence of *PDR2* should be amplified and cloned into a pENTR/D-TOPO vector to use Gateway Cloning System (Thermo Fisher Scientific) for further subcloning. Usage of the Gateway system facilitates subcloning of a sequence between different expression vectors without additional amplification steps and Therefore prevents the introduction of unwanted mutations during subcloning. To amplify the genomic sequence of *PDR2*, Phusion High-Fidelity Polymerase (Thermo Fisher Scientific) was used.

Primers were chosen to amplify the whole genomic sequence, including all introns, from ATG to the last base before the stop codon. This allowed the generation of variants carrying c-terminal tags, which would be important for upcoming experiments.

To amplify the genomic sequence of *PDR2* without stop codon from genomic *Arabidopsis* DNA, a PCR reaction was carried out according to the following parameters.

PCR mix:

5 x Phusion buffer	10 μ l
dNTPs (2.5 mM each)	1 μ l
Primer for (MH 84)	2.5 μ l
Primer rev (MH 85)	2.5 μ l
Col DNA	1 μ l (240 ng)
Phusion DNA Polymerase	0.5 μ l
H ₂ O	ad 50 μ l

PCR setup:

Temperature	Time	
98 °C	30 s	
98 °C	10 s	} X 36
72 °C	4 min	
72 °C	5 min	

The genomic sequence of *PDR2-stop* has a size of 6890 bp. After successful amplification of *PDR2-stop* (Figure 22a), the PCR fragment was extracted from an agarose gel and ligated into a pENTR/D-TOPO vector. The ligation mix was subsequently transformed into *E. coli* Top10 cells and plasmids from single colonies were extracted. Analysis of the restriction pattern after digestions with PstI identified several clones that contained *PDR2-pENTR* (Figure 22b).

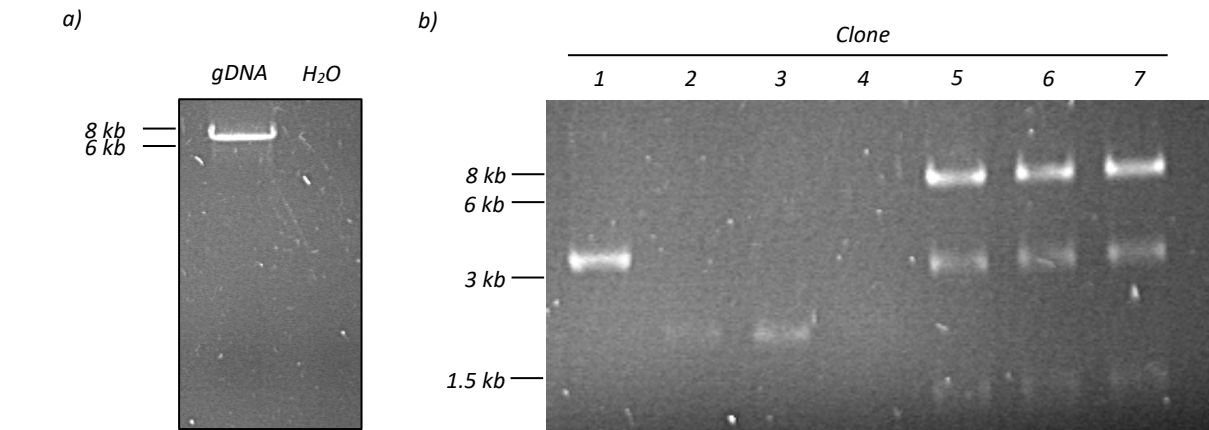


Figure 22: Amplification and test digestion of genomic *PDR2* from *Arabidopsis* in pENTR/D-TOPO. a) The genomic sequence of *PDR2-stop* (6890 bp) was amplified from genomic *Arabidopsis* DNA. The PCR mix was subsequently loaded to a 0.8 % Agarose gel and the PCR product was extracted from the gel for further cloning into the pENTR/D-TOPO Vector. b) Plasmid DNA was isolated from 7 different *E. coli* clones after transformation generated *PDR2_pENTR* and the restriction pattern after digestion with PstI was analyzed using a 0.8 % Agarose gel. Transformation with the correct *PDR2_pENTR* should result three PCR fragments (1218 bp, 2595 bp, 5686 bp) which is true for clones 5, 6 & 7.

Sequencing of isolated plasmids of clone 5 and 6 validated the correct vector sequence of *PDR2-pENTR*. Clone 5 was stored at -80 °C and used for subcloning *PDR2-stop* into other Gateway-compatible vectors.

2.2.2 Subcellular localization of PDR2-GFP

Results from previous studies already indicated ER localization of PDR2 in anthers, using immunohistochemistry and electron microscopy (Jakobsen et al., 2005). However, despite the ubiquitous presence of *PDR2* transcript, a (subcellular) localization of PDR2 in other organelles failed. Since the local phosphate starvation response is taking place in roots, localization of PDR2 in root tissues should be carried out to reveal PDR2's potential function in phosphate sensing. For this purpose, vectors expressing *PDR2-GFP* controlled by the 35S promoter (*PDR2_PB7FWG2*) were generated (Karimi et al., 2002) and transformed into *N. benthamiana* and the *Arabidopsis pdr2-2* mutant to perform *in vivo* localization studies using confocal laser scanning microscopy (cLSM).

2.2.2.1 Localization of PDR2-GFP after transient overexpression in *N. benthamiana*

Leaves of *N. benthamiana* were transiently transformed with PDR2_pB7FWG2 (35S::PDR2-GFP). After 24 h and 48 h, leaf discs were cut out and the GFP fluorescence was analyzed using confocal laser scanning microscopy (Figure 23a). Since PDR2 was previously reported to be localized to the ER, *N. benthamiana* leaves were co-transformed with PDR2-mCherry and GFP-HDEL to confirm its ER localization. The C-terminal HDEL sequence serves as ER retention signal and Therefore can be used as a marker for ER structures (Brandizzi et al., 2003). Co-transformed leaves were subsequently analyzed via confocal laser scanning microscopy (Figure 23)

GFP-signals are detectable 24 h after the transformation and reside at least for 48 h. However, the localization pattern of PDR2-GFP resembles a typical ER-localization, forming a dense net throughout the cell that is also covering structures that are most likely nuclear envelopes and ER bodies (Figure 23a). The latter ones are moving, bright dots at the net-like ER structures. Co-localization of PDR2-mCherry with GFP-HDEL validates the ER-localization of PDR2 (Figure 23b). PDR2 is localized to ER membranes throughout cell. Additionally, a more detailed view on the nucleus also reveals a co-localization of PDR2-mCherry and GFP-HDEL at nuclear envelopes and tonoplasts (Figure 23c).

Localization studies of PDR2 in *N. benthamiana* therefore confirm the predicted ER localization of PDR2 in plant leaves *in vivo*. They also reveal an accumulation of PDR2-GFP to moving ER bodies and most likely localization to the nuclear envelope after the transient overexpression of PDR2-GFP.

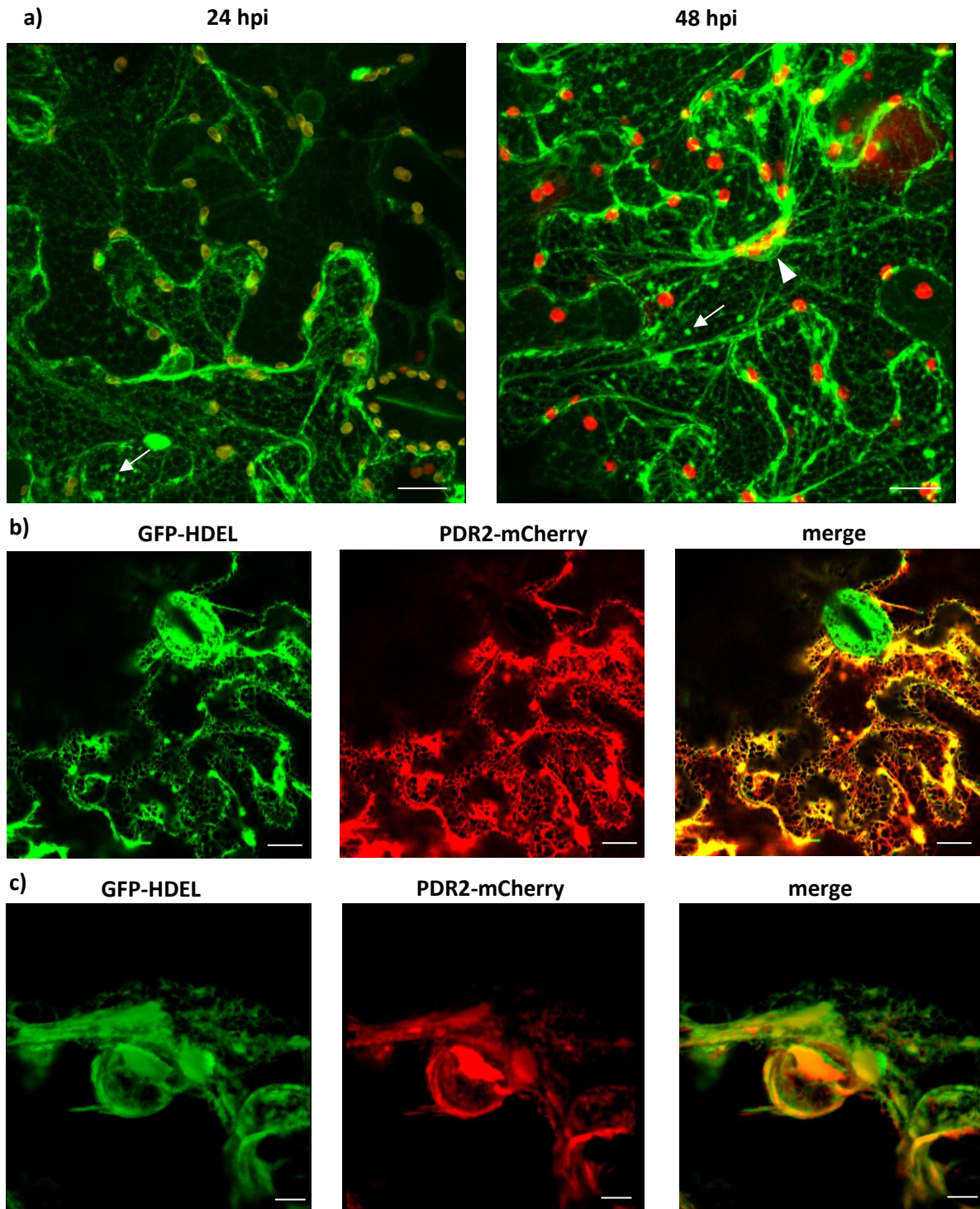


Figure 23: Subcellular localization of PDR2-GFP in *N. benthamiana*. a) Leaf discs of tobacco transformed with *35S::PDR2-GFP* were analyzed via confocal laser scanning microscopy 24 and 48 h after transformation. PDR2-GFP signal is depicted in green. PDR2-GFP shows a typical net-like ER-localization pattern. White triangles indicate localization to nuclear envelope. Bright, dot-like structures (white arrows) are most likely ER-bodies. The auto-fluorescing plastids are marked as red. White bars indicate distances of 20 μm . Excitation/Emission of GFP was 488nm / 523nm. For detection of mCherry, 555nm / 585 nm was used. b) *N. benthamiana* leaves were co-transformed with *35S::GFP-HDEL* (green) and *35S::PDR2-mCherry* (red) and analyzed via confocal laser scanning microscopy. Merged picture of GFP (green) and mCherry (red) confirms co-localization of PDR2-mCherry and ER-marker GFP-HDEL. 20-fold magnification, bars indicate distances of 20 μm . c) Co-localization of PDR2-mCherry (red) and GFP-HDEL (green) indicates a localization of PDR2-mCherry to the nuclear envelope and tonoplast. 40-fold magnification, white bars indicate distances of 5 μm .

2.2.2.2 Localization of PDR2-GFP in stably transformed *Arabidopsis* plants

The transient overexpression of PDR2-GFP and PDR2-mCherry confirmed the localization of PDR2 to ER and nuclear envelopes in tobacco leaves. To find out more about the possible function of PDR2 in the local phosphate starvation response of *Arabidopsis*, subcellular localization of PDR2-GFP in stably transformed *Arabidopsis* roots was investigated using confocal laser scanning microscopy. Therefore, *Arabidopsis pdr2-2* plants were stably transformed with PDR2_PB7FWG2. Homozygous *pdr2-2* lines carrying genomic *35S::PDR2-GFP* were grown on +Pi medium for 6 – 8 days. Roots were analyzed using confocal laser scanning microscopy (Figure 24).

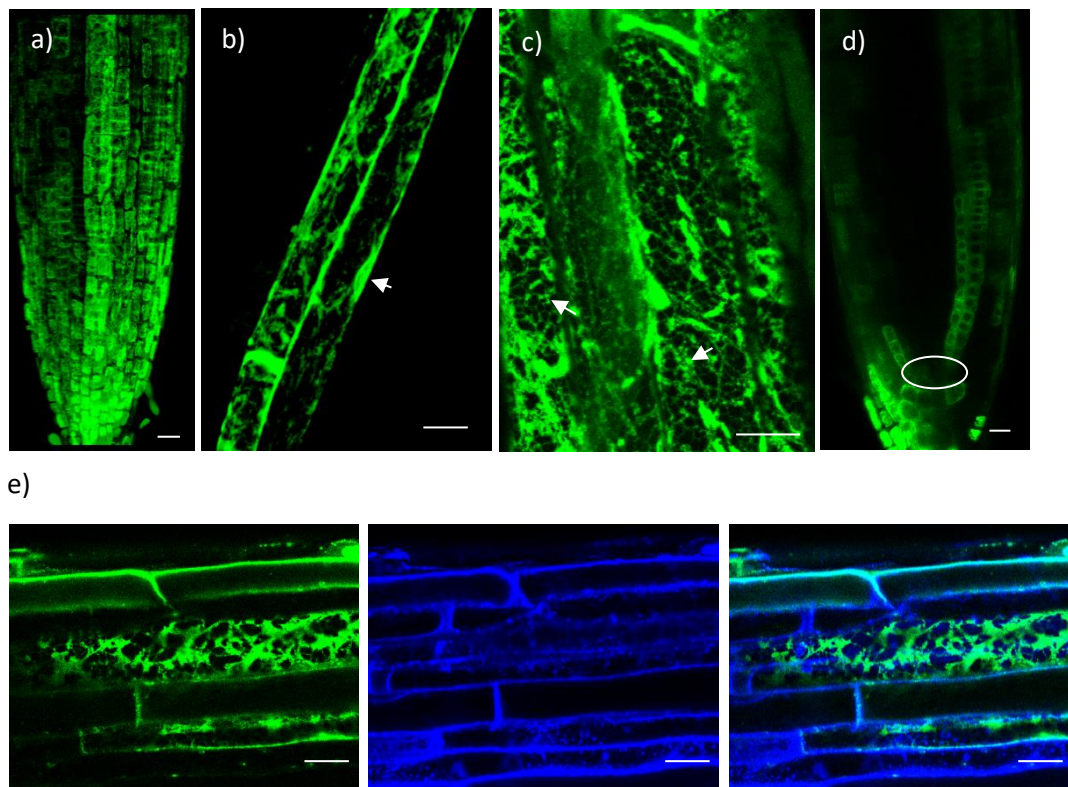


Figure 24: Localization of PDR2-GFP in roots of *Arabidopsis*. PDR2_pB7FWG2 encoding for *35S::PDR2-GFP* was stably transformed into *Arabidopsis pdr2-2* plants and the localization of PDR2-GFP was investigated using confocal laser scanning microscopy. White bars indicate a distance of 20 μm . Excitation/Emission of GFP was 488nm and 523nm, respectively. FM4-64 was excited and detected at 555 and 585, respectively. a) PDR2-GFP is detectable throughout the whole root tip. b) PDR2-GFP is localized in ER-like patterns in root cells and shows localization to the nuclear envelope (white arrow). c) Moving ER bodies are formed upon the expression of *35S::PDR2-GFP* in *Arabidopsis*. d) Although *35S::PDR2-GFP* is ubiquitously expressed in the whole root, PDR2-GFP could never be detected in the stem cell niche (white oval) of *Arabidopsis* primary roots. e) Plants expressing *35S::PDR2-GFP* were stained with FM4-64 that decorates the cell membrane and early endosomes to investigate a possible localization of PDR2-GFP to the cell membrane. No co-localization of PDR2-GFP (green) and FM4-64 (blue) could be observed indicating that PDR2 is not localized to plasma membranes of *Arabidopsis* cells.

Expression of *35S::PDR2-GFP* causes strong GFP signals throughout the whole root and root tip (Figure 24a). A more detailed view of single cells of the elongation zone revealed that GFP is organized in a net-like structure reminiscing to ER-localization (Figure 24b). Similar to transient overexpression of *35S::PDR2-GFP* in *N. benthamiana*, PDR2-GFP is localized to structures that are

most likely nuclear envelopes (white arrow). Figure 24c also reveals the formation of GFP decorated, moving ER-bodies in *Arabidopsis* roots. Although *35S::PDR2-GFP* seems to be expressed ubiquitously throughout the whole root, PDR2-GFP has never been detectable in the stem cell niche and the QC of *Arabidopsis* roots (Figure 24d). Localization of PDR2-mCherry to ER in tobacco was verified via Co-expression with ER-marker GFP-HDEL. Since GFP-HDEL was the only available ER in our lab at that time and the generation of plants expressing PDR2 with any other fluorescing tag than GFP was not finished, a repetition of the co-localization experiment from tobacco was not possible. However, roots of *Arabidopsis pdr2-2* plants expressing *35S::PDR2-GFP* were stained with FM4-64, a dye that decorates cellular membranes and early endosomes. No co-localization of PDR2-GFP and FM4-64 could be observed indicating that PDR2-GFP is not localized to the plasma membranes of *Arabidopsis* root cells (Figure 24e) and that the observed GFP localization pattern is most likely due to ER localization of PDR2-GFP.

To investigate whether the availability of external phosphate affects the localization of PDR2-GFP, the same set of analyses was carried out with seedlings transferred to – Pi conditions for 2 days after 5 days of growth on +Pi medium. However, the localization pattern of PDR2-GFP was similar to +Pi conditions.

In summary, localization studies of PDR2-GFP in primary roots of *pdr2-2* showed that PDR2-GFP is ubiquitously present in nearly all cells throughout the whole root. Like PDR2-GFP in tobacco, it shows ER-like expression patterns with additional localization to nuclear envelopes and ER bodies. However, PDR2-GFP was never detected in the QC and the stem cell niche of *Arabidopsis* roots. Transfer experiments to –Pi conditions also revealed that localization and amount of PDR2-GFP remain unchanged upon Pi limitation, at least when constitutively expressed via 35S promoter.

2.2.3 Complementation of *pdr2* with *35S::PDR2-GFP*

Like its homologue, the P5-type ATPase Spf1 of yeast, PDR2 is linked to ER stress responses. It is therefore not surprising that *PDR2* mutants exhibit pleiotropic phenotypes (Cronin et al., 2002). The most important phenotype with regards to the phosphate starvation response is a hypersensitivity of *pdr2* to low Pi conditions in terms of primary root growth. Besides this, *pdr2* also displays defects in pollen and silique development (Jakobsen et al., 2005). Since lines constitutively expressing *PDR2-GFP* on a *pdr2* background were generated within the framework of this thesis, complementation analyses should be carried out to test the functionality of PDR2-GFP. Therefore, it should be investigated whether *35S::PDR2-GFP* is able to rescue the phenotypes of *pdr2*.

2.2.3.1 No complementation of short root growth phenotype on low Pi

Our working hypothesis predicts that absent restriction of LPR1 function by PDR2 results in a hypersensitive, short root phenotype of *pdr2* in –Pi conditions. However, the expression domain of LPR1 is limited to the stem cell niche of roots. Yet, *35S::PDR-GFP* expression does not produce detectable amounts of PDR2-GFP in the SCN. Silencing of the 35S promoter in the SCN has been observed in many cases. Thus, it was questionable if the generated construct would affect the function of LPR1 in *pdr2*. To address this, root growth assays were carried out to determine whether the introduction of *35S::PDR2-GFP* is able to complement the hypersensitive root growth phenotype of *pdr2* on –Pi conditions.

Arabidopsis pdr2-2 plants stably transformed with *35S::PDR2-GFP* were grown + Pi agar plates for 5 days and subsequently transferred to –Pi plates. Primary root growth after transfer was determined 3 and 4 days after transfer (Figure 25).

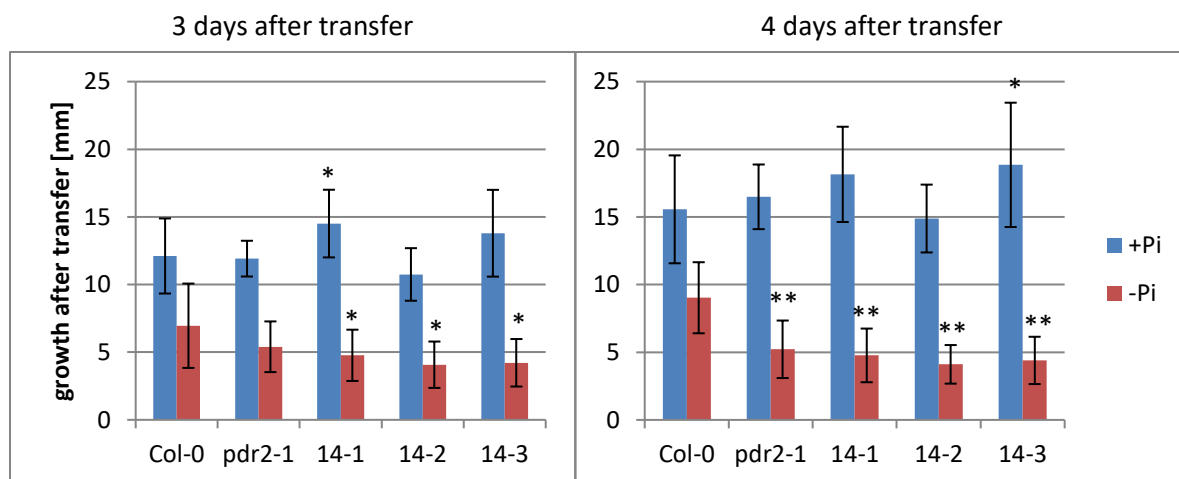


Figure 25: Primary root growth of *pdr2-2* lines overexpressing PDR2-GFP. Seedlings of *pdr2-2* stably transformed with *35S::PDR2-GFP* were grown on +Pi medium for 6 days and subsequently transferred to +Pi or –Pi medium. The primary root growth after transfer was measured 3 and 4 days after transfer. $n > 15$, two tailed student's t-test compared all lines to Col-0 +/-Pi conditions, respectively. * indicated $p < 0.05$; ** indicate $p < 0.01$

When transferred to + Pi conditions, differences between WT, *pdr2-2* and complementation lines 14-1, 14-2 & 14-3 are very subtle. Only lines 14-1 and 14-3 show slightly longer roots than WT after 3 and 4 days, respectively. However, differences in –Pi conditions between WT and all other lines are more obvious. Although primary root growth of *pdr2* is not significantly inhibited 3 days after transfer, the growth of all complementation lines was slightly, but significantly, reduced at the same time. Roots of Col-0 still elongate between 3 and 4 days after transfer on –Pi conditions, resulting in longer roots after 4 days, when compared to 3 days after transfer. Root growth of *pdr2-2* and complementation lines arrests between 6 day 3 and 4 after transfer, causing a significant inhibition of the root length 4 days after transfer when compared to Col-0.

Complementation analyses revealed that expression of *35S::PDR2-GFP* in *pdr2-2* is not able to enhance root growth of *pdr2-2* on –Pi conditions to a level comparable to WT. In fact, no difference between *pdr2-2* and the complementation lines could be observed. These results suggest that overexpression of *PDR2-GFP* is not able to rescue the *pdr2*-derived hypersensitivity of the primary root growth on low Pi conditions. The likeliest explanation for this is the absence of PDR2-GFP in the expression domain of *LPR1*. However, this cannot exclude that PDR2-GFP is not functional at all.

2.2.3.2 Complementation of silique phenotype

Vectors expressing *35S::PDR2-GFP* were not only generated to investigate the phosphate starvation response of *Arabidopsis*, but also as a tool for upcoming experiments to investigate the still unknown functionality of the P5-type ATPase in *Arabidopsis*. The generated *35S::PDR2-GFP* constructs can be used to produce fair amounts of tagged PDR2 from tobacco or *Arabidopsis* that can help to characterize the protein function. Still, it had to be verified that the addition of the GFP tag to PDR2 does not interfere with its function within the plant. It was shown that *35S::PDR2-GFP* is not able to complement a *pdr2-2* mutant regarding to its hypersensitivity on low Pi conditions. This is likely caused by a lack of PDR2-GFP in the SCN of primary roots (Figure 24). However, an interference of the GFP tag with PDR2 function cannot be excluded. A mutation in *PDR2* causes impaired development of siliques that is visible by the naked eye. Eventually, this causes the formation of very small, crippled siliques that produce less seeds. To determine the functionality of PDR2-GFP, a possible complementation of the silique development phenotype of *pdr2* by *35S::PDR2-GFP* was investigated.

Col-0, *pdr2-2* and plants from three different *pdr2-2* lines transformed with *35S::PDR2-GFP* were grown on soil for 8 – 10 weeks until siliques developed. Subsequently, silique appearance and development were analyzed (Figure 26).

In comparison to Col-0, most of the siliques of *pdr2* plants are much shorter and crippled. The siliques of *pdr2* plants that were transformed with *35S::PDR2-GFP* show wildtype-like, healthy, big siliques. A normal silique development in the complementation lines shows that PDR2-GFP can rescue the *pdr2* phenotype in siliques indicating that PDR2-GFP is indeed functional.

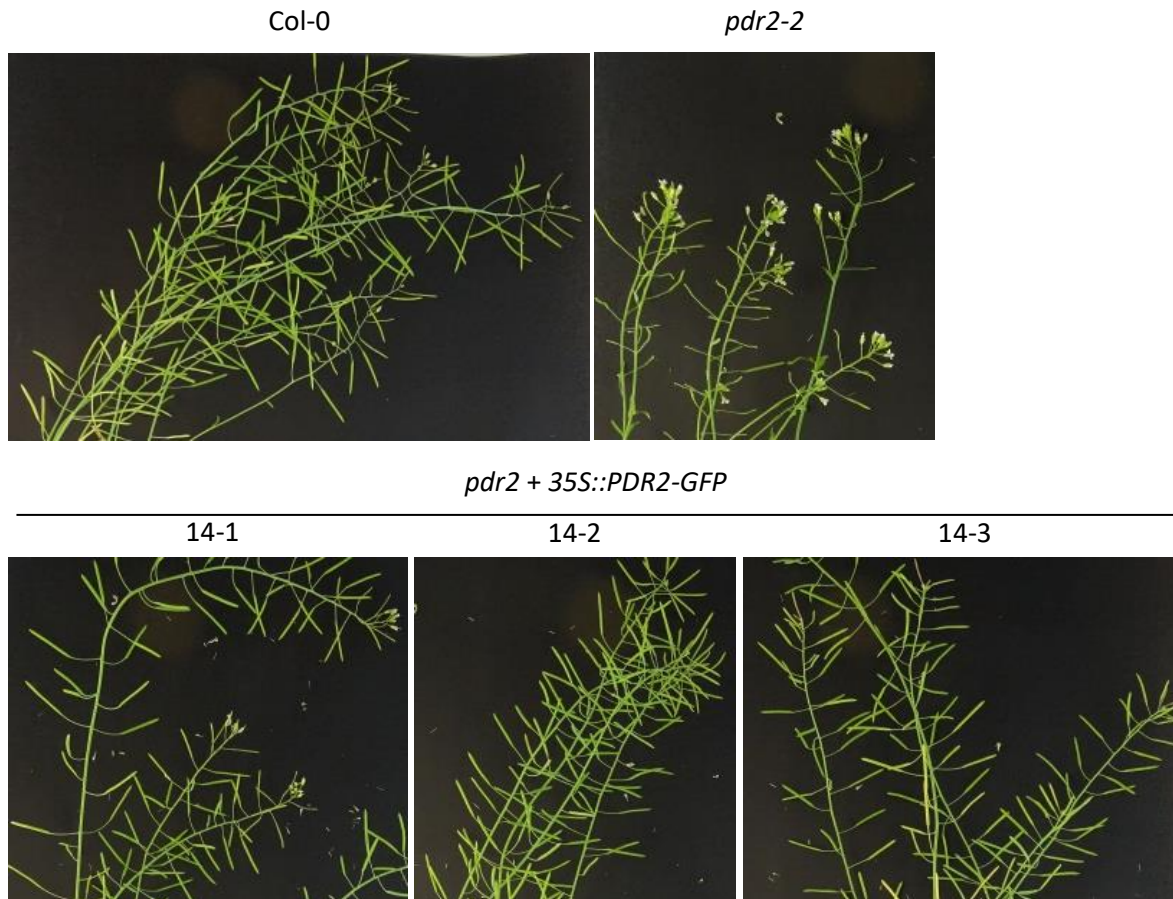


Figure 26: Siliques of *Col-0*, *pdr2* and three different *pdr2* lines transformed with *35S::PDR2-GFP*. *Arabidopsis Col-0*, *pdr2* and complementation lines 14-1, 14-2 & 14-3 were grown on soil. Pictures of plants were taken ~ 8 – 10 weeks after germination, when siliques development was finished. *pdr2-2* shows mostly impaired silique development with very small, crippled siliques. In comparison to that, all complementation lines developed normal sized siliques comparable to *Col-0*.

In summary, *35S::PDR2-GFP* is not able to complement the hypersensitivity of *pdr2* primary roots to low Pi conditions, most likely due to a lack of expression of *PDR2-GFP* because of silencing of the 35S promoter in the SCN. It is, however, capable to rescue the silique phenotype of *pdr2*.

Taken together, the subcellular localization of *PDR2-GFP* confirms the already proposed ER-localization of the protein. Additionally, the overexpression of *PDR2-GFP* causes the formation of moving ER bodies, decorated with *PDR2-GFP*. *35S::PDR2-GFP* is expressed in nearly all cells within the *Arabidopsis* root except of the SCN, which is most likely the reason for the unavailability of *PDR2-GFP* to complement a *pdr2* mutant's hypersensitivity towards $-Pi$ conditions. However, the functionality of *PDR2-GFP* itself could be verified by the rescue of the silique development phenotype of *pdr2* by *35S::PDR2-GFP* and Therefore makes the generated vectors and transgenic lines valuable resources for upcoming experiments.

3 Discussion

3.1 The outcome of LPR1 function is limited to –Pi conditions

Severity of root growth inhibition due to Pi-depletion is in direct proportion to *LPR1* promoter activity in different *Arabidopsis* accessions. However, *LPR1* promoter activity and *LPR1* mRNA levels are not altered due to transfer of plants to –Pi conditions, suggesting other regulatory mechanisms beyond mRNA abundance (Svistoonoff et al., 2007; Abel, 2017). Therefore, the first part of this work focused on the putative differences in LPR1 abundance in various genotypes and Pi regimes, to explain links between LPR1 levels and sensitivity of primary root growth to –Pi conditions. At first, LPR1 levels in various genetic backgrounds were established (Figure 5). Decreased LPR1 levels *pdr2* and *lpr1 lpr2* compared to WT were detected in the first place. As both genotypes have opposing phenotypes after transfer to –Pi conditions, this was quite unexpected. Several experiments and controls revealed, that the antibody we were using for LPR1 detection also recognized an unspecific protein in *Arabidopsis* with nearly at the same size of LPR1 in around 70 % of the experiments. Since there was no other antibody available at that time, we had no choice but to keep using it for the rest of the experiments. A repetition of the experiments showed that the levels of LPR1 are indistinguishable in Col-0, *pdr2* and *lpr1 lpr2*. Only *35S::LPR1* lines showed increased levels of LPR1 in all three overexpression lines (Supplemental figure 5). This was surprising since *lpr1 lpr2* carries a T-DNA insertion in *LPR1* that is supposed to disrupt the gene and eventually prevent formation of a functional LPR1 protein. This pointed again to unspecific signals caused by our LPR1 antibody. However, mRNA analyses of three different T-DNA insertion lines for *LPR1* revealed only partial knockdowns for all tested lines, thereby explaining still detectable levels of LPR1 protein in those lines (Supplemental figure 7). However, a very subtle decrease of LPR1 abundance in *lpr1 lpr2* seems to be enough to completely abolish root growth impairment on –Pi conditions. In contrast, transgenic *Arabidopsis* plants, that constitutively overexpress *LPR1* and thereby have substantially increased levels of LPR1 in roots, show conditional hypersensitivity when grown on –Pi conditions. Nevertheless, similar levels of LPR1 in WT and *pdr2* suggest that the hypersensitivity of *pdr2* is not a consequence of a simple alteration of LPR1 abundance. Moreover, LPR1 levels in WT and *pdr2* roots remain unchanged after transfer to –Pi conditions (Figure 6; Supplemental figure 2) and increased LPR1 levels in *35S::LPR1* roots only affect the root growth in –Pi conditions. Taken together, these findings indicate, that a threshold amount of LPR1 is required to trigger an appropriate phosphate starvation response in *Arabidopsis*. However, its function is restricted to –Pi conditions by more sophisticated mechanisms than regulation of protein abundance in different Pi-concentrations.

Very often posttranslational modifications (PTMs) like (de-) phosphorylation are used to regulate protein functions upon certain triggers. Indeed, various putative phosphorylation sites could be

identified in the sequence of LPR1 (data not shown). However, to date, no experimental evidence for the phosphorylation of LPR1 could be found. Besides phosphorylation, glycosylation is a common mechanism that many proteins of the secretory pathway undergo. Alterations of protein glycosylation patterns due to different stimuli can affect their function, localization, or stability (Varki, 1993; Marino et al., 2010; Liebminger et al., 2013). The yeast ferroxidase requires its interaction partner Ftr1 to be correctly glycosylated in the ER before it is transported to the cellular membrane as its final destination. However, incorrect glycosylation of Fet3p only interferes with its correct localization to the plasma membrane, but does not affect its ferroxidase function (Askwith and Kaplan, 1997; Ziegler et al., 2010). A direct prove for LPR1 glycosylation remains elusive and deglycosylation assays of protein extracts of *Arabidopsis* roots do not show conclusive data for LPR1 glycosylation (Supplemental figure 8). Still, regulation of LPR1 function via the manipulation of its glycosylation pattern cannot be excluded and should be subject of future studies. Particularly, using enriched or purified LPR1, instead of crude protein extracts that might contain molecules that prevent appropriate deglycosylation of target proteins, could improve the experimental outcome.

In yeast, Fet3p activity requires the presence of Ftr1, a membrane-bound permease, to be transported to the plasma membrane (Stearman et al., 1996; Askwith and Kaplan, 1997; Radisky and Kaplan, 1999). Given the high similarity of LPR1 and Fet3p, a to date unknown putative interaction partner could be required for LPR1 function. Since the oxidation of Fe^{2+} is coupled to the reduction of another substrate, the putative interaction partner could be a receptor for electrons to minimize the risk of generating unwanted ROS species via leaky reduction of O_2 . Abundance or activity of this putative protein could be regulated to restrict LPR1 outcome and thereby ROS generation to $-\text{Pi}$ conditions. However, potential interaction partners of LPR1 have not been identified, yet.

Another explanation why LPR1-dependent oxidation of Fe^{2+} only takes place in $-\text{Pi}$ conditions is the formation of P-Fe complexes in Pi-sufficient medium, that decrease Fe availability and, thereby preventing the binding of Fe^{2+} to LPR1. However, experiments carried out in our lab using Pi-sufficient medium supplied with Fe concentrations up to 1 mM do not show an induction of the PSR or signs of LPR1 activity like increased Fe accumulation, ROS production and callose deposition in the primary root. Since LPR1 is localized to the ER and the apoplast in *Arabidopsis* (Figure 9 & Figure 10), but most likely functions in the apoplast, translocation of LPR1 from ER to apoplast upon a Pi-dependent trigger is another option to restrict its function during Pi-sufficient conditions. Yet, localization studies of 35S::LPR1-GFP lines did not reveal obvious changes in the ratio of ER-localized and apoplastic GFP signals when plants are grown on +Pi or -Pi conditions (Muller et al., 2015). Furthermore, apoplastic LPR1 levels of *Arabidopsis* suspension cultures grown in medium containing low Pi concentrations were indistinguishable of those from cells, grown in Pi-sufficient medium

(Figure 10) indicating that LPR1 localization is not altered upon transfer to $-Pi$ conditions. Nevertheless, transgenic lines expressing $pLPR1::LPR1-GFP$ could shed light on potential LPR1 re-localization upon Pi-starvation, provided that native *LPR1* expression levels are above the detection limit.

In summary, there is no evidence of a regulation of LPR1 in mRNA or protein levels and LPR1 localization seems to be unaffected by the Pi-concentrations of the surrounding medium. However, *Arabidopsis* needs a certain amount of LPR1 to maintain a proper response to low Pi conditions. All these findings suggest that LPR1 is always present at its target location, the apoplast of the QC of the RAM. However, if it requires activation upon a certain trigger or is just restricted by Fe-unavailability in Pi-sufficiency, remains an open question.

3.2 Identification of LPR1 as an apoplastic ferroxidase

LPR1 was identified as a key component in the PSR of *Arabidopsis* that directly affects the accumulation of apoplastic Fe and ROS, and the deposition of callose upon phosphate starvation (Figure 2). It was also already classified as a multicopper oxidase (Svistoonoff et al., 2007) with high similarities to Fet3p, a part of the system that takes up extracellular Fe via an oxidase-permease complex (Stearman et al., 1996; Askwith and Kaplan, 1997). Since a structural modeling of LPR1 identified putative Fe- and Cu-binding sites in the protein, it was tempting to speculate that LPR1 indeed is a ferroxidase. A first indication for this are significantly increased specific ferroxidase activities of root extracts of *35S::LPR1* lines (Figure 7). Moreover, there is a direct proportionality of the specific ferroxidase activity and the levels of LPR1 of a sample. However, no significant difference of the ferroxidase activities of Col-0, *pdr2* and *lpr1 lpr2* could be detected, although they show sensitivities to $-Pi$ conditions (Figure 1). Nevertheless, this could be explained by similar LPR1 levels in Col-0, *pdr2* and *lpr1 lpr2*. Thus, LPR1 function *in planta* may be controlled by a mechanism that not only restricts its function to $-Pi$ conditions, but also balances its function during the PSR to prevent the over-accumulation of Fe and potentially dangerous ROS in Col-0 roots. In *pdr2*, this mechanism is absent or inactivated, causing hypersensitivity of *pdr2* to low Pi conditions. However, upon protein extraction from the roots, this mechanism is abolished, and the specific ferroxidase activity measured is directly dependent on the LPR1 levels in the samples. This model provides further indications, that LPR1 function is restricted to $-Pi$ conditions by the mandatory presence of another protein that facilitates LPR1 function. The interaction of both proteins could be inhibited on $+Pi$ conditions by spatial separation in different compartments. When the roots sense low Pi conditions, the interaction partner is translocated to the apoplast and LPR1 function is activated. Similar specific ferroxidase activities of roots grown on $+Pi$ and $-Pi$ conditions also support the model, that all components that facilitate the *in vitro* ferroxidase activity are present in the roots, independent of

the Pi status of the medium. However, during Pi-sufficient conditions, LPR1 function is, at least *in vivo*, constantly repressed to be rapidly activated during –Pi conditions. This is also supported by the fact that LPR1 levels in the apoplast of *Arabidopsis* suspension cultures seem to be constant and not altered because of Pi starvation (Figure 10).

Increased ferroxidase activities in tobacco leaves that were infiltrated with *35S::LPR1* or *35S::LPR1-GFP* validate these results. In summary, Ferrozine assays of total protein extracts of *Arabidopsis* and *N. benthamiana* show that specific ferroxidase activity of a sample depends on LPR1 amounts in the sample, thereby indicating that LPR1, like its yeast homologue Fet3p, is a ferroxidase and that its function is repressed during +Pi conditions (Figure 11 & Figure 14).

However, since the natural substrate of LPR1 is not known yet and the Ferrozine assay is based on substrate consumption, there is still the possibility that LPR1 may have ferroxidase activity, but the actual *in vivo* substrate is something different.

Still, the identification of LPR1 as an apoplastic ferroxidase is in agreement with previous findings of the *LPR1*-dependent accumulation of Fe³⁺ in the apoplast of Pi-deprived *Arabidopsis* roots (Muller et al., 2015; Balzergue et al., 2017; Singh et al., 2018).

3.3 Structure-function studies and biochemical properties of LPR1

Identification of LPR1 as a ferroxidase in the phosphate starvation response of *Arabidopsis* gave rise to numerous questions since ferroxidases are an enzyme class that has not been subjected to in-depth studies in plants, yet. The high similarity of LPR1 to Fet3p could result in reaction mechanisms similar to Fet3p and other ferroxidases like ceruloplasmin. To address this question, the general mode of action of LPR1 had to be elucidated.

In general, ferroxidases are characterized by the oxidation of Fe²⁺ and the reduction of O₂. Therefore, some core structural features are needed to catalyze this reaction: That is the presence of an Fe²⁺-binding site and several copper clusters to transfer the electron from Fe²⁺ to the acceptor O₂ and to prevent premature release of partially reduced O₂ that potentially causes the unwanted generation ROS. In Fet3p, Cu is incorporated in a mononuclear T1-Cu cluster, formed by two histidine residues and one cysteine residue (Figure 12 & Figure 13). The T1-Cu site is the primary acceptor of the substrate electron. Another T2/T3 trinuclear Cu-cluster is formed by a mononuclear T2 and a dinuclear T3 Cu-cluster and functions as the site where O₂ is bound and reduced (di Patti et al., 1999). Analyses of the amino acid sequence of LPR1 revealed that two out of three amino acid that form the Fe-binding site in Fet3p and Fet5p, are also present in LPR1 (Figure 12). The third one, E185 in Fet3p,

could be identified as E269 in LPR1 via structural modeling (Figure 13). The amino acids of the T1 Cu-site and the T2/T3 Cu-cluster are conserved on a sequence level.

The identification of the putative Fe and Cu-binding sites of LPR1 via modeling of the protein structure was a first step towards elucidation of its mode of action. Different mutations of *LPR1* were produced via site-directed mutagenesis to disrupt the putative Fe binding site and to compromise the proteins T1 copper cluster. In Fet3p, the Fe binding site is formed by one aspartic acid and two glutamic acid residues. E185 and D409 are involved in the transport of the electron from Fe²⁺ to the T1 Cu site whereas D283 is important for the positioning of Fe²⁺ in the substrate binding site and (Stoj et al., 2006). E185 and D409 also contribute to specificity of Fet3p towards ferrous iron as substrate. In consistence with that, mutations in *LPR1* that alter the amino acids corresponding to Fet3p E185 and D409 (SDM#1 and SDM#3, respectively) to an alanine exhibit significantly decreased ferroxidase activity, when compared to WT (Figure 14). The same is true for the double mutant variant SDM#1#3 and the triple mutant variant SDM#1#2#3. Like in Fet3p, the exchange of the third amino acid of the Fe-binding site - D283 in Fet3p and D370 in LPR1 – to alanine has only a subtle effect on the ferroxidase activity of the protein. However, the synergistic effect of Fet3p double mutant E185A/D409A on the K_m towards Fe²⁺ is not measurable in the specific ferroxidase activities of SDM#1#3 when compared to single mutants SDM#1 and SDM#3. Reasons for this could be a fully compromised LPR1 activity by either one of these mutations or, that our reaction setup, using specific ferroxidase activities of crude extracts, is not sensitive enough to distinguish between very low activities. In summary, these results indicate that the Fe-binding site of LPR1 is comprised of E269, D370 and D462, validating the *in silico* predictions and thereby pointing towards a reaction mechanism comparable to Fet3p.

Stable transformation of *lpr1* plants using *35S::LPR1* and the generated LPR1 variants with a compromised Fe binding site under the same promoter support these findings. Overexpression of *LPR1* in *lpr1* plants complements the *lpr1* phenotype by reducing the primary root growth on –Pi conditions to WT levels without affecting the root length on Pi-sufficient conditions (Figure 16). The production of a functional LPR1 protein is therefore sufficient to restore the plants ability to respond to –Pi conditions. However, *lpr1* plants stably transformed with *35S::SDM#1* and *35S::SDM#3* that encode for protein variants with impaired ferroxidase activity (Figure 14), are still insensitive to –Pi conditions, indicated by an *lpr1*-like long root phenotype. Remarkably, the introduction of SDM#2 - a variant of LPR1 that is only slightly impaired in ferroxidase activity - causes an intermediate phenotype with roots marginally longer than the WT but not shorter than *lpr1*. This strongly suggests, that primary root growth inhibition of *Arabidopsis*, as an outcome of the local phosphate starvation response, is directly depending on LPR1s ferroxidase activity. Inactive LPR1 variants are

not able to trigger the PSR. Slight inhibitions of LPR1 activity like in SDM#2 cause intermediate root length on $-P_i$ conditions, indicating a direct proportionality of severity of local PSR and LPR1 activity. Since all LPR1 variants are overproduced due to the usage of 35S promoter, LPR1 levels in all tested variants including 35S::LPR1, are much higher than in WT. Still, roots of 35S::LPR1 lines on $-P_i$ conditions are not shorter than WT roots, suggesting that LPR1 activity is limited to a certain level, even when protein abundance is increased. These facts support the idea that a certain threshold of LPR1 abundance is needed to execute a proper PSR. If LPR1 levels are decreased below this threshold or ferroxidase activity is inhibited, the plant does not react to P_i -deficiency anymore. This is the case for *lpr1* and *lpr1 lpr2*, in which slightly decreased LPR1 levels cause total insensitivity towards P_i -depletion. However, an increase of LPR1 levels above this threshold does not increase the root growth impairing effect of LPR1 on $-P_i$ conditions. This is most likely due to a, still unknown, mechanism that restricts LPR1 activity to a certain extent on $-P_i$ conditions and completely inhibits it on $+P_i$ conditions.

After validating the substrate binding site of LPR1 and evaluating how altered iron binding availability of LPR1 affects protein function, we wanted to find out if the structural similarity of LPR1 and Fet3p are also true for the putative Cu binding site of LPR1. In Fet3p, the T1 copper binding site is comprised of H413, H489 and C484 and it facilitates the transfer of the electron from the substrate binding site to the T2/T3 trinuclear copper cluster, where the reduction of O_2 takes place. To avoid the formation of ROS, the bound O_2 is reduced with two electrons from the T3 coppers causing the formation of peroxide intermediate which is then rapidly reduced by two electrons of the T1 and T2 coppers. The product is then released and the resting enzyme is restored (Shin et al., 1996). Since the T1 copper site seems to be most important in terms of stability and it is the center of the electron transfer chain, we decided to concentrate our efforts on the investigation of this Cu binding site. The respective AAs that form the putative T1 copper site in LPR1 are H464, H568 and C563 (Figure 13).

Extracts of tobacco leaves transiently expressing different variants of LPR1 showed total inhibition of LPR1 ferroxidase activity by a disruption of the putative T1 Cu binding site (Figure 14). Yet, in contrast to variants with a compromised Fe binding site that exhibit very high protein levels, variants with alterations in T1 copper binding site are rarely detectable by western blotting after transient expression in tobacco leaves (Supplemental figure 10). qRT-PCR experiments revealed that LPR1 mRNA is present in tobacco leaves after transient expression with the exception of 35S::SDM#4 (Figure 15), suggesting that either translation efficiency or protein stability is severely decreased for SDM#5 and SDM#6. It has already been described that the Cu-binding sites contribute to correct folding and therefore to protein stability of MCOs. The substitution of C484 to serine causes the loss of the T1 copper ion that eventually destabilizes Fet3p (Sedlak et al., 2018). Moreover, the T1 copper

binding site is allosterically coupled to the T2/T3 trinuclear copper cluster causing a nonlinear increase of overall protein stability after incorporation of all Cu ions (Augustine et al., 2008). It is therefore tempting to speculate that the introduced mutations SDM#5 (H563A) and SDM#6 (C563A) inhibit the Cu incorporation into the T1 copper site causing the production of misfolded, instable LPR1 variants. However, the Cu incorporation, folding state and protein stability must be tested with purified LPR1 and the respective variants to verify these findings. The Cu loading of the protein could be tested via electron paramagnetic resonance spectra (Augustine et al., 2008), whereas the folding state could be determined via measuring the partial unfolded states of the protein after Urea treatment using circular dichroism or the intrinsic tryptophan fluorescence (Sedlak et al., 2018). Also, complementation assays in *lpr1* plants should be carried out to verify the effects of a perturbed T1 copper site *in vivo*.

In summary, site directed mutagenesis revealed that LPR1 Fe binding site is highly similar to Fet3p with E269 and D462 most likely to facilitate electron transfer from Fe to T1 Cu and with D370 having only minor effects on the ferroxidase activity. Moreover, perturbations of the T1 copper binding site negatively affect LPR1 stability, most likely because of impaired Cu incorporation into the active site.

Analyses of the general biochemical features of LPR1 and its ferroxidase activity using crude extracts of *N. benthamiana* leaves transiently expressing *35S::LPR1* reveal typical characteristics of an enzymatic reaction (Figure 20). It is temperature-dependent and can be inhibited by boiling or addition of chemical detergents like SDS. The pH optimum for LPR1's ferroxidase activity is between 5.6 and 6.0 which is also true for Fet3p (de Silva et al., 1997). Increasing pH further decreases its ferroxidase activity, which is also in agreement to findings that *lpr1* roots are not longer than WT at pH 6.5 (Svistoonoff et al., 2007). Remarkably, there was no sign of activity towards ABTS oxidation that is commonly used as an indicator substrate that can be oxidized by the vast majority of MCOs. However, the lack of ABTS oxidation ability of the crude extracts could be due to remaining reductases within the sample that prevent the formation of oxidation products.

Altogether, LPR1 shows high similarities to Fet3p with regards to its structure and mode of action. Besides that, LPR1 is up to now the only plant ferroxidase whose structural features and functionality have been investigated so far.

3.4 Purification of LPR1

After the basic biochemical characterization of LPR1 was carried out, using crude extracts of transiently transformed tobacco leaves, we aimed for more in-depth analyses of LPR1 to gain

detailed knowledge about its enzymatical properties. Therefore, establishing K_M values for LPR1 and the generated mutated variants was our first goal. Additionally, other putative substrates could be tested to determine putative side reactions that might occur *in planta*. However, decent amounts of purified protein were required for these experiments. Additionally, using purified protein prevents unwanted side reactions catalyzed by putative counteracting enzymes that could be present in the crude extracts and side effects caused by the overexpression of LPR1 in *N. benthamiana*. Since many constructs were already available in our lab, including tagged variants of LPR1, we first tried affinity purification using different tags and methods. It turned out that tagged variants of LPR1 are inactive after purification. Since it is reported for Fet3p, that its C-terminus is involved in forming the T2/T3 Cu cluster, it is not unlikely, that tags induce misfolding and therefore, eventually inhibit the formation of the Cu cluster. This also is supported by the fact that neither for Fet3p nor for ceruloplasmin or haephaestin, other well-studied ferroxidases, purification protocols using tagged protein variants have been reported. According to the literature, purification of native protein is the most promising method. However, using α -LPR1 antibody coupled to agarose beads to purify LPR1 from crude extracts remained unsuccessful. Because the antibody was generated using a short peptide, comprised only of 9 amino acids, it is quite likely that LPR1 in its native fold state is not recognized by it and need to be unfolded prior to binding. This is also supported by the fact that the antibody did not bind to any proteins in any immuno-histological experiments, using *Arabidopsis* root sections, carried out in our lab (data not shown).

Initially, the purification of Fet3p has been done with 40 – 70 l of *S. cerevisiae* cells that were grown overnight in iron limiting medium to induce the Fet3p production. The purification itself was achieved by a sequence of size exclusion, anion exchange and a final metal affinity purification step yielding relatively low amounts of protein (de Silva et al., 1997). Later studies used *S. cerevisiae* transformed with a plasmid encoding for a Fet3p variant that lacks the C-terminal membrane anchor to directly produce and harvest Fet3p from the medium after gene expression (Stoj et al., 2006). However, the purification procedure itself remained unchanged from the original publication. This suggests that for Fet3p, purification via size exclusion and anion exchange is quite likely the best option to get hands on the protein. We Therefore decided to go for a similar approach to purify LPR1 from yeast. However, although it was possible to express LPR1 in *S. cerevisiae*, the amounts were still not satisfying. Moreover, most of the protein ended up in the cell wall fraction (Figure 19). On the one hand, this validates our previously described findings, that LPR1 is localized to the apoplast. Still, cell wall association of LPR1 in yeast makes it more difficult to purify since it must be separated from the rest of the cell wall components prior to the next purification steps. To circumvent this problem, transformation of *S. cerevisiae* with a plasmid containing *LPR1* lacking the ER signal peptide could be used. This would prevent the transport of LPR1 to the ER and Therefore the final association to the

CW. However, possible PTMs that very likely contribute to LPR1 function and are carried out in the ER will also be hampered which, in consequence, rendering this strategy not suitable for our purpose.

In summary, many attempts to purify LPR1 from various sources failed and this part of the project had to be put aside due to time constraints. However, plant material from *35S::LPR1* plants is currently used as a starting material for the aforementioned sequence for classical purification including size exclusion and ion exchange chromatography. A successful purification could pave the way for numerous experiments including detailed structure-function studies, crystal structures and interaction studies and would thereby be a big leap for our understanding of this enzyme class and its function in plants.

3.5 Complementation of a Δ fet3 *S. cerevisiae* strain by LPR1

In the course of the characterization of LPR1, numerous experiments were performed to elucidate its *in vivo* function. All data suggest that LPR1, like its yeast analogue Fet3p, is a ferroxidase. However, all experiments including *in vitro* ferroxidase assays with crude extracts as well as the previously published LPR1-dependent iron deposition in the SCN of *Arabidopsis* roots provide only indirect evidence for Fe³⁺ generation. The Ferrozine assay used to assess *in vitro* activity of LPR1 in crude extracts is a measure for Fe²⁺ depletion in the samples, used as a proxy for Fe³⁺ generation. Yet, no generation of Fe³⁺ by LPR1 has been measured to date. The microscopic pictures of Pi-deprived roots that show Fe accumulation in the SCN are not suitable to distinguish between ferrous and ferric iron completely and Therefore, both species are detected.

To validate the *in vivo* Fe oxidation capability of LPR1, a yeast Δ fet3 mutant should be complemented by LPR1 (Figure 21). Structurally, LPR1 shares a lot of similarities with Fet3p. Still, an important difference of both proteins is the presence of a short C-terminal transmembrane helix in Fet3p, that is absent in LPR1. Thus, Fet3p is anchored to the membrane and its active sites are oriented to the apoplast. In contrast, LPR1 is localized to the apoplast in *Arabidopsis* without membrane anchorage. This might influence the ability of LPR1 to complement the function of Fet3 in the Fe uptake system of yeast drastically. To circumvent this problem, we generated a variant of LPR1 in which the predicted ER signal peptide is substituted by the signal peptide of Fet3p. Additionally, the C-terminus of Fet3p including its transmembrane domain was added to the protein to anchor the core protein with its active sites to the membrane (Supplemental figure 11). Another key feature of the high affinity Fe uptake system in yeast is the interaction of Fet3p with Ftr1. After translation of both proteins, they are translocated to the ER where Fet3p is loaded with its Cu cofactors by CCC2 (Cross-Complements Ca²⁺ phenotype of *csg1*). Proper folding and binding of Fet3p to Ftr1 is required for a

proper Fet3p function afterwards. The protein complex is subsequently transported to the PM. Fet3 facilitates the oxidation of Fe^{2+} and the generated Fe^{3+} is directly transported by Ftr1 from the apoplast to the cytoplasm (Figure 27).

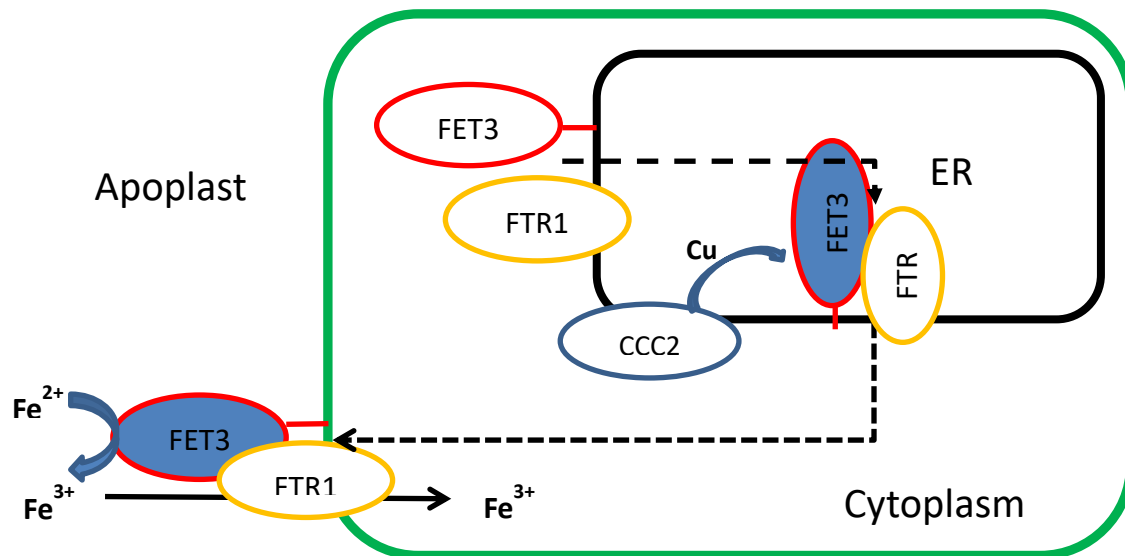


Figure 27: Assembly and function of the Fet3p-Ftr1 Fe uptake system in *S. cerevisiae*. The plasma membrane and ER membrane are depicted as a green and black line, respectively. Fet3p and Ftr1 are transcribed and concomitantly assembled in the ER. CCC2 (Cross-Complements Ca^{2+} phenotype of *csg1*) facilitates the loading of Fet3 with Cu at the same time. The Fet3p Ftr1-complex is translocated to the membrane where Fet3p is anchored with its transmembrane domain and the active site facing the apoplast. Ftr1 is spanning the membrane. Fet3p oxidizes Fe^{2+} to Fe^{3+} which is then transported via Ftr1 to the cytoplasm (Fu et al., 1995; Stearman et al., 1996). — Plasma membrane; — ER membrane

As expected, the growth rate of Δfet3 strains was severely impaired on Fe-deficient medium in comparison to WT *S. cerevisiae* in general. The transformation with a plasmid encoding for Fet3p could restore the growth to levels comparable to WT + LPR1 and WT + Fet3, indicating that the expression is working fine. Expression of *LPR1* and *Fet3* in WT yeast caused a slight growth inhibition when compared to WT + EVC, most likely due to induction of gene expression via addition of galactose. However, WT yeast expressing the chimeric construct SpF-LPR1-cF showed severely reduced growth rates similar to a Fet3 deletion mutant. Thus, expression of the chimeric construct, but not LPR1 or Fet3, inhibited the growth of WT yeast in Fe-deficient medium. Numerous possible reasons for this exist. The yeast ER signal peptide that was fused to the chimeric construct could cause ER stress due to overload of ER with the chimeric protein. It could also prevent proper ER translocation of the chimera because addition of the signal peptide to a non-yeast protein inhibits the translocation by an unknown mechanism. Moreover, due to the high similarities of LPR1 and Fet3p, it is tempting to speculate that chimeric LPR1 can bind Ftr1 like Fet3p. Still, existent structural differences between Fet3p and LPR1 inhibit proper function of the protein-protein complex. Induction of chimeric gene expression therefore induces the formation of non-functional chimera-

Ftr1 protein complexes and eventually slowing down the growth rate due to partially impaired Fe^{3+} uptake by the Fet3p-Ftr1 complex.

Anyway, LPR1, despite being highly similar to Fet3p, is not able to complement the impaired growth of a Fet3 deletion strain. One reason could indeed be, that LPR1 is not a ferroxidase *per se* and therefore fails to oxidize Fe^{2+} in the apoplast. So, since the transport capability of Ftr1 is limited to Fet3p-derived Fe^{3+} the high affinity Fe uptake system is disturbed, and the growth is therefore inhibited. However, we found many indications that LPR1 is capable of oxidizing Fe^{2+} to Fe^{3+} . Since Fet3p and Ftr1 function very closely together, the aforementioned small structural differences in LPR1 and Fet3p might prevent a proper formation of the permease-oxidase complex formed by both proteins. High-affinity iron uptake in yeast depends on functional Fet3p-Ftr1 complex due to a direct translocation of Fet3p-originated Fe^{3+} to Ftr1. Thus, insufficient binding of LPR1 to Ftr1 could inhibit the Fe uptake and therefore prevent the complementation of ΔFet3 by LPR1. It would therefore be of great interest to test, if Fe^{2+} is indeed oxidized by LPR1 in yeast to see if LPR1 is still functioning as a ferroxidase in these conditions. Additionally, the formation of protein-protein complexes including LPR1 and Ftr1 should be tested to verify that LPR1 can bind to the permease to serve as a ferroxidase in the Fe uptake system.

Taken together, the expression of *LPR1* in a yeast strain lacking *Fet3* was not able to complement the impaired growth phenotype caused by Fe depletion in the medium. Therefore, direct proof of *in vivo* ferroxidase activity of LPR1 still remains elusive.

3.6 The regulatory function of PDR2 in the phosphate starvation response

Although genetic interactions between *LPR1* and *PDR2* have been described many years ago (Ticconi et al., 2009), the function of *PDR2* remains elusive, partly because of its intricate handling in the lab. Cloning of full length *PDR2* is rather difficult to achieve and therefore only very few experiments have been carried out to unravel its function (Jakobsen et al., 2005; Ticconi et al., 2009; Sorensen et al., 2012). After several failed attempts to clone the coding sequence, we speculated that transformation of *PDR2* CDS into bacteria might prevent their growth, since *PDR2* is a large transmembrane ATPase. To overcome the bottleneck of missing expression vectors, we first generated a pENTR/D-TOPO vector containing the genomic sequence of *PDR2* ranging from the starting ATG until the last codon before the “stop”. This should be used as a base for subcloning the construct into various expression vectors to tackle numerous questions.

Previous studies localized *PDR2* to the ER in anthers (Jakobsen et al., 2005). Since our focus is the PSR in roots, we aimed for an in-depth localization of *PDR2*-GFP in this part of the plant. Because we used the genomic sequence of *PDR2* for cloning, accurate splicing of the generated mRNA is necessary for

translation of the desired gene product. First indications that the system was working as intended were the transient transformed tobacco leaves that express *PDR2-GFP*. Incorrect splicing most likely would have caused frame shifts and therefore prevented the formation of the C-terminal GFP tag. Nevertheless, localization studies confirmed GFP signals in the ER of transformed leaves, which was also true for stably transformed *Arabidopsis pdr2-2* seedlings. This validates the findings from previous publications that PDR2 is indeed ER localized. The formation of moving ER bodies (Figure 23a) is also in agreement with previous findings, that retention of GFP in the ER often causes formation of fusiform bodies with unknown function (Hawes et al., 2001; Nelson et al., 2007). Still, as a membrane protein containing 12 transmembrane helices, the gene product of *PDR2* is rather difficult to handle, too. Numerous attempts to detect PDR2-GFP translational fusions via Western Blotting failed. To validate functionality of the translational fusion proteins, we intended to functionally complement the root growth phenotype of *pdr2-2* on $-Pi$ conditions. However, no difference in root growth of *pdr2-2* and three independent *pdr2-2* lines transformed with *35S::PDR2-GFP* was measurable (Figure 25) indicating inhibited function of GFP-tagged PDR2. However, the expression domain of *LPR1* and also Fe deposition, ROS and callose production as its main outcome in the PSR, are mostly limited to the SCN of primary roots (Muller et al., 2015). Therefore, a co-localization of *LPR1* and PDR2 in this area of the root is required for direct interaction between both proteins. Yet, we were unable to detect PDR2-GFP in the SCN of any primary root, regardless of supplied Pi. Since silencing of transgenic constructs or other transformed elements is a common mechanism of plants - most likely as a defense strategy against plant viruses - it is quite possible that *35S::PDR2-GFP* is unable to rescue the *pdr2-2* root growth phenotype because its expression is silenced in the SCN (Voinnet, 2001; Martin-Hernandez and Baulcombe, 2008).

Disrupting *PDR2* function causes – besides hypersensitivity of primary root growth to $-Pi$ conditions – pleiotropic phenotypes. Many of them are linked to ER stress and putatively connected to autophagy. A major phenotype, however, is partially impaired seed development of *pdr2*, causing it to develop short, crippled siliques that contain significantly less seeds than WT siliques (Jakobsen et al., 2005). Complementation assays in the *pdr2-2 + 35S::PDR2-GFP* lines revealed that PDR2-GFP is indeed capable of rescuing the seed development phenotype of *pdr2-2* (Figure 26). Complementation lines showed WT-like healthy siliques in comparison to *pdr2-2*. We therefore concluded that at least in silique development, PDR2-GFP is functionally redundant to PDR2.

Although PDR2-GFP is thereby not able to regulate *LPR1* function during the PSR as native PDR2 does, it is at least partially functional with regards to its role in silique development. Therefore, the constructed GFP tagged variant can be used for further experiment to uncover other functions of PDR2 in *Arabidopsis*. As a short-term goal, a purification of GFP-tagged PDR2 from *Arabidopsis* roots

could be used to find possible interaction partners of the P5-type ATPase. Purified PDR2 could also be subjected to various *in vitro* assays to find out its still unknown substrate.

Additionally, the overexpression lines can be used to check for altered PSR parameters like Fe-accumulation, ROS production and callose deposition to gain new insights in the way how PDR2 affects the plants response to low Pi conditions.

3.7 Working model

The identification of LPR1 as a ferroxidase has improved our understanding of its function in phosphate starvation response and thereby gave rise to a new working model to explain the mechanisms that control the biochemical and developmental processes that orchestrate the complex adaptations of *Arabidopsis* roots to Pi deficiency (Figure 28).

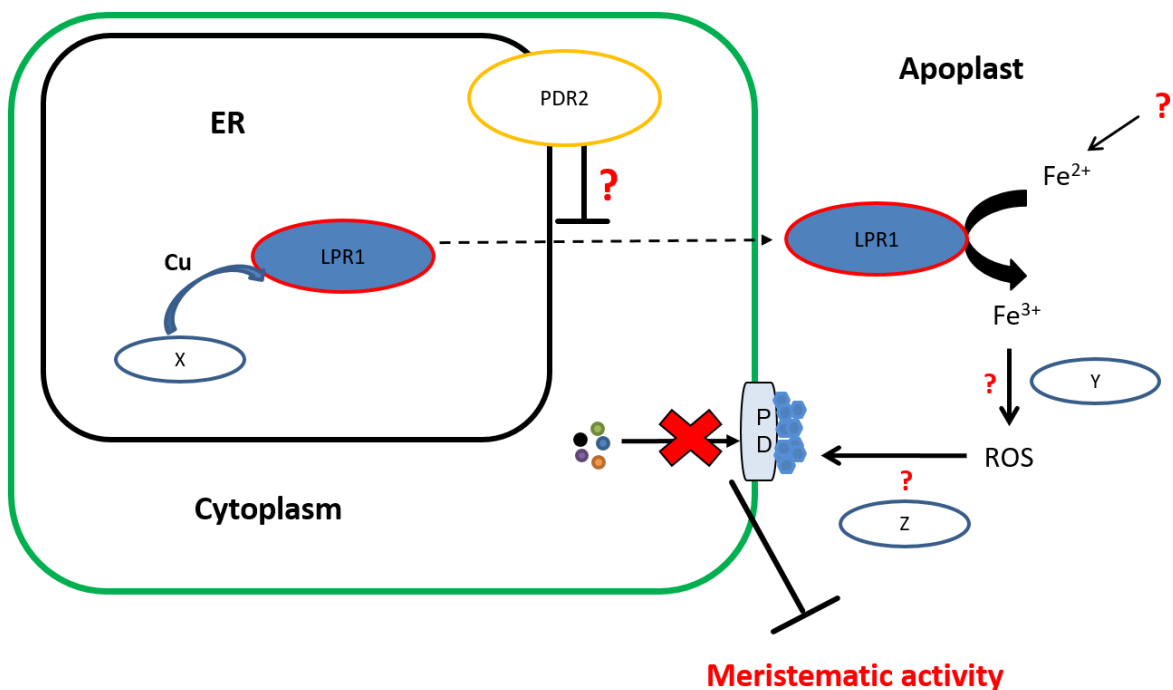


Figure 28: Working model of the interplay between PDR2 and LPR1 during the phosphate deficiency response in the SCN of *Arabidopsis* primary roots. A cell in the SCN of *Arabidopsis* primary root is depicted. Plasma membrane. — ER membrane. PD=Plasmodesmata; ● = callose plaques; Small, colored circles = various cellular components

LPR1 requires copper-loading – most likely facilitated by a yet unknown chaperone – to ensure proper folding prior to translocation to its apoplastic destination. PDR2 restricts LPR1 outcome directly or in an indirect fashion, maybe by preventing its translocation to secretory vesicles. Upon Pi-starvation, Fe^{2+} is liberated from phosphate-iron complexes at the apoplast and becomes available for LPR1-catalyzed oxidation. The thereby generated labile Fe^{3+} is used for ROS generation via Fenton reaction or enzymatic reactions. Increased ROS levels trigger callose formation and thereby block plasmodesmata. This prevents movement from cellular components, i.e. transcription factors to

neighboring cells. Since meristematic activity in primary roots depends on unrestricted movement of several transcription factors between various cell layers, blocked cell-to-cell communication eventually inhibits meristematic activity by inducing stem cell differentiation and thereby causing root growth arrest of the primary root. Although containing many yet elusive aspects, this model provides a simple and elegant way for the plant to maintain a shallow, broadly branched root system to efficiently mine Pi when its concentrations are rather low in the environment soil.

3.8 Very recent findings

A recent study managed to uncouple the mechanisms that cause root growth inhibition on $-Pi$ conditions in the EZ and the SCN of the primary root (Balzergue et al., 2017). Mutations in *ALMT1* (*ALUMINUM ACTIVATED MALATE TRANSPORTER 1*) and in its regulating transcription factor *STOP1* (*SENSITIVE TO PROTON TOXICITY1*) do not accumulate Fe and still show $+Pi$ -like cell elongation in the EZ upon transfer to $-Pi$ conditions. However, Fe accumulation and inhibition of cell proliferation in the SCN in $-Pi$ conditions are not affected in these mutants. Since *lpr1lpr2* plants do not show any Fe accumulation in the EZ or SCN, it is therefore speculated that root growth inhibition in $-Pi$ conditions is caused by a bipartite mechanism formed by the rapid inhibition of cell elongation in the EZ and inhibition of cell division in the SCN. The latter mechanisms are independent of *ALMT1* and only depend on *LPR1* whereas both, *ALMT1* and *LPR1*, are crucial for inhibition of cell elongation in the EZ. Atomic force microscopy also identified Pi deficiency-induced, *LPR1*-dependent cell wall stiffening as a probable reason for inhibited cell wall elongation. This is furthermore supported by the fact that Pi deprivation causes altered expression of cell wall related genes, accumulation of callose and non-esterified pectins in *Arabidopsis* WT roots, but not in *lpr1lpr2* (Hoehenwarter et al., 2016). Since the incorporation of ions in CW networks is known to affect crosslinking of CW components, *LPR1* might also influence the integration of Fe ions to manipulate CW integrity. Therefore, *LPR1* might not only affect Fe accumulation and callose deposition, but also cell wall composition in general by facilitating the incorporation of additional compounds that impact cell wall stiffness in roots.

Additionally, with *ALS3/STAR1* an ABC transporter has been identified that, when mutated, hyper-accumulates Fe^{3+} in roots and shows hypersensitivity to Pi deprivation. However, this phenotype can be rescued by introducing *lpr1* in these plants, suggesting a crosstalk between these pathways (Dong et al., 2017). This publication also shows that *als3/star1* mutants are likely to have altered cell wall compositions supporting the importance of cell wall composition in the PSR. Furthermore, *ALS3* also plays a role in aluminum toxicity. Experiments from our own lab already indicated a possible interplay between Pi-deficiency, Fe-availability and Al-toxicity. With validated interplays between aluminum affected proteins like *ALS3* and *ALMT1* and *LPR1*, a central player in the PSR, interactions

between those and LPR1 as a pivotal integrator of different pathways will become more and more important for upcoming research.

Another study was able to elucidate a role of brassinosteroid (BR) signaling in the PSR of *Arabidopsis* (Singh *et al.*, 2018). The enhanced root growth on –Fe conditions – independently of Pi levels – is partially explained by elevated brassinosteroid signaling. They show that *LPR1* is repressed in the EZ by the BR dependent TF BZR1, causing decreased Fe accumulation and therefore, enhanced cell elongation. They also show that low Fe promotes root growth by stimulating the BR pathway in dependency of BRI1, the BR receptor. However, receptor-ligand binding is not required for triggering root growth enhancement. In summary, *LPR1*-affected Fe levels seem to counteract the BRI1-dependent root growth enhancement and *vice versa*.

3.9 Outlook

To further improve our understanding how LPR1 catalyzes the oxidation of Fe²⁺, purified enzyme can be used to determine the biochemical features of the ferroxidase reaction in more detail in a controlled environment with specified components. To validate its mode of action, those assays should also be carried out in anoxic conditions to verify the forecast need of oxygen for this specific reaction. Although several allegedly Fe³⁺-specific dyes were tested in our lab, until now, none of them proved to be specific at all. Therefore, the identification of additional Fe³⁺-specific dyes could be useful for future activity assays. Determining product formation instead of substrate consumption is a more precise way to assess the specific ferroxidase activity of LPR1 and its generated variants. Furthermore, these dyes could be used for microscopic analyses of roots grown in various Pi regimes to elucidate the exact sites of iron deposition during Pi-deprivation. Co-localization studies using fluorescing Fe³⁺-dyes together with markers for specific subcellular compartments and structures would provide important hints on the specific functions of Fe and the ferroxidase LPR1 in the PSR of *Arabidopsis*.

Uncovering similarities and differences of regulation and mode of action of LPR1 in comparison to its yeast homologue Fet3p will provide important knowledge to elucidate its distinct function in *Arabidopsis*. To find out why *LPR1* cannot complement a yeast Δ Fet3 strain is an important step towards this goal. Therefore, ICP-MS (inductively-coupled plasma mass spectrometry) measurements could be used to determine if LPR1 produces Fe³⁺ in yeast. Additionally, pulldown experiments could be carried out to analyze the putative protein-protein interaction between LPR1 and the transporter Ftr1 to validate a correct assembly of the yeast Fe uptake system in the complementation strain.

To elucidate the mechanism by which *PDR2* controls the outcome *LPR1* function is still a major task. The knowledge about Fet3p in yeast and how it is regulated can be used as a basis for designing

upcoming experiments. Since Fet3p folding and translocation to the PM requires a chaperone that facilitates proper incorporation of Cu into the molecule, a similar mechanism might exist in *Arabidopsis*. A search for deregulated chaperones or genes that are involved in Cu translocation in *pdr2* plants could yield promising candidates. The comparative transcriptomics/proteomics dataset that has been published in 2016 including work from our lab could be a valuable resource for that (Hoehenwarter et al., 2016). A more detailed investigation of LPR1 localization comparing WT and *pdr2* roots in different Pi regimes could be used to identify subtle changes in localization of protein amounts. However, since specific antibodies for immunohistochemistry or high-resolution microscopy are lacking, this will be difficult to accomplish. Since recent results from our lab (not published) indicate (in-)direct involvement of PDR2 in translocation of Fe, the search for feasible Fe-marking dyes that could be used to identify exact subcellular sites for Fe distribution in roots should be a high priority goal for the near future.

However, in the medium-run, the integration of various stresses and responses to nutrient deficiencies will become more and more important to deeply understand the plants adaptations to varying environmental conditions and the mechanisms that orchestrate concomitant developmental changes.

3.10 Summary

The interplay of the multicopper oxidase LPR1 and the P5-type ATPase PDR2 orchestrates the phosphate starvation response in *Arabidopsis* in an antagonistic fashion. LPR1 is thereby crucial for initiating a cascade that triggers Fe deposition, ROS production, and callose deposition to eventually inhibit primary root growth by meristem differentiation when the plant encounters Pi-depleted conditions. Mutations in *PDR2* render the plant hypersensitive to $-Pi$ conditions causing hyperaccumulation of Fe, ROS and callose indicating that *PDR2* contains the severity of the PSR by balancing LPR1 activity to prevent premature differentiation of the primary root meristem.

Here, we show that LPR1 is a ferroxidase, located at the apoplast of *Arabidopsis* root meristems. Although its functionality is restricted to $-Pi$ conditions, no differences of mRNA or protein levels could be observed after transfer to different Pi conditions. Even in hypersensitive *pdr2* plants, *LPR1* levels and corresponding protein abundances are similar to WT, indicating that LPR1 function is not regulated via tweaked transcription or translation in response to low Pi availability. Also, its apoplastic translocation seems not to be affected by external Pi concentrations indicating a totally different way of controlling its function than influencing protein availability. Although no evidence

phosphorylation or glycosylation of LPR1 have been identified, a regulation via post translational modification cannot be excluded, yet.

However, according to structure-function analyses LPR1 shows high similarities to its close homologue Fet3p. It uses conserved amino acids to bind its substrate. Most likely, the electron from Fe^{2+} is transported via a T1 Cu cluster to O_2 that is bound in a T2/T3 trinuclear Cu cluster and serves as the terminal acceptor. Perturbing the Fe binding site, especially amino acid residues E269 and D462 significantly diminishes *in vitro* ferroxidase activity whereas substitution of any amino acid of the T1 Cu site results in drastically decreased protein levels, probably due to misfolding and subsequent degradation of the protein. Notably, mutated versions of *LPR1* encoding for inactive or only partially active enzymes are not, or only to some extent, able to complement the *lpr1* root growth phenotype on $-\text{Pi}$ conditions, emphasizing the relevance of LPR1 activity for the PSR. In the future, a detailed characterization of its enzymatic properties using purified enzyme could be used to elucidate distinct characteristics of this plant ferroxidase. To verify its specific function in the PSR, *in vivo* ferroxidase activity should be assessed using Fe^{3+} -specific dyes.

The successful construction of expression vectors for *PDR2-GFP* allowed us to nail down the localization of the P5-type ATPase to ER membranes in *Arabidopsis* roots. Complementation of the hypersensitivity of *pdr2* towards low Pi-conditions using *35S::PDR2-GFP* was not successful, most likely due to silencing of the 35S promoter in the RAM. Regardless, GFP-tagged PDR2 was able to complement silique developmental phenotype of *pdr2* showing that PDR2-GFP is, at least partially, active. As the orphan P5-Type ATPase in *Arabidopsis* with a variety of postulated functions, PDR2 is of particular importance for many processes in plants. Moreover, since P5-Type ATPases are still poorly understood in all kingdoms of life, insights into PDR2 functioning could be relevant beyond the field of plant research. Thus, elucidating its distinct function is of great interest and the lines generated in the framework of this thesis can contribute as a promising resource for upcoming experiments.

Taken together, LPR1 and PDR2 are part of a complex signaling hub that uses Fe as a proxy to determine Pi levels in the medium. The interplay between both enzymes has a determining influence on the readjustment of the root system architecture when plants adapt to changing external Pi availability. By now, researchers just start to address the complex interplay between different nutrients in the soil. However, understanding the relatively simple network that is regulated by LPR1 and PDR2 will help to understand the multifaceted networks that are used to integrate all the different environmental cues that affect plant growth in a complex environment.

3.11 Zusammenfassung

Die Interaktion der *multicopper oxidase* LPR1 und der P5-typ ATPase PDR2 regulieren die Phosphatmangelantwort in *Arabidopsis* in einer antagonistischen Art und Weise. LPR1 ist dabei entscheidend an der Einleitung der Kaskade beteiligt, die zur Akkumulation von Eisen, Produktion von reaktiven Sauerstoffspezies sowie der Einlagerung von Callose. Dadurch wird das Wachstum der Primärwurzel inhibiert, sobald diese mit Phosphatmangel im umgebenden Boden konfrontiert wird. Mutationen in *PDR2* führen zu einer Hypersensibilisierung der Pflanze gegenüber Phosphatmangel was sich in einer Hyperakkumulation von Eisen, ROS und Callose unter Phosphatmangelbedingungen äußert. Dies deutet darauf hin, dass PDR2 die Stärke der Phosphatmangelantwort kontrolliert, indem es die Aktivität von LPR1 begrenzt und somit eine vorzeitige Ausdifferenzierung des Primären Wurzelmeristems verhindert.

In dieser Arbeit wurde gezeigt, dass LPR1 eine im Apoplast des Wurzelmeristems lokalisierte Ferroxidase ist. Obwohl seine Funktionalität als Ferroxidase auf das Vorhandensein von Phosphatmangelbedingungen angewiesen ist, konnten keine Unterschiede in der Konzentration seiner mRNA oder im Proteinlevel nach dem Transfer auf -Pi Bedingungen im Vergleich zu +Pi festgestellt werden. Sogar in hypersensitiven *pd2*-Pflanzen unterscheiden sich mRNA-Level und korrespondierende Proteinkonzentrationen von *LPR1* nicht von denen im WT. Dies zeigt, dass die Regulation der LPR1 Funktion und die damit einhergehende Beschränkung der Eisenoxidation auf -Pi Bedingungen nicht durch anpassen der Transkription oder Translation erfolgt. Außerdem scheint die Lokalisierung von LPR1 im Apoplast nicht von der externen Phosphatverfügbarkeit abzuhängen, was eine Regulation der LPR1 Funktion über die Proteinverfügbarkeit sehr unwahrscheinlich macht. Obwohl bisher keine Beweise für eine Phosphorylierung oder Glykosylierung von LPR1 gefunden wurden, kann eine Regulation seiner Funktion über post-translationale Modifikationen nicht ausgeschlossen werden.

Im Verlauf der Arbeit konnte gezeigt werden, dass LPR1 konservierte Aminosäurereste für die Bindung seines Substrats verwendet und demnach wahrscheinlich ähnlich funktioniert wie Fet3p, ein homologes Protein aus Hefe. Höchstwahrscheinlich wird das Elektron von Fe^{2+} über den T1 *Cu cluster* zum terminalen Elektronenakzeptor O_2 , welcher im T2/T3-Trinuklearen *Cu cluster* gebunden ist. Es konnte gezeigt werden, dass eine Störung der Eisenbindung, vor allem durch die Aminosäureaustausche E269A und D462A zum Verlust der *in vitro* Ferroxidase-Aktivität von LPR1 führen. Austausch der Aminosäuren im T1 *Cu cluster* hingegen führen zu deutlich verringerten Proteinmengen, vermutlich verursacht durch Fehlfaltung und anschließendem Abbau des Proteins in der Zelle. Bemerkenswert ist die Tatsache, dass inaktive oder nur teilweise funktionstüchtige Varianten von LPR1 den Wurzelphänotypen von *lpr1* – Insensitivität des Primärwurzelwachstums

gegenüber -Pi-Bedingungen – nicht bzw. nur teilweise komplementieren können. Dies zeigt einmal mehr die Relevanz der LPR1-Funktion für die lokale Phosphatmangelantwort. Eine Reinigung von LPR1 könnte in Zukunft eine detaillierte Charakterisierung der Eigenschaften des Proteins und der von ihm katalysierten Reaktion ermöglichen und so neue Erkenntnisse über Ferroxidasen in Pflanzen liefern. Außerdem könnten Fe³-spezifische Farbstoffe genutzt werden, um die genaue Funktion von LPR1 in der Phosphatmangelantwort aufzuklären und gleichzeitig genauere Erkenntnisse über den Reaktionsablauf zu gewinnen.

Die Konstruktion von PDR2-GFP Expressionsvektoren ermöglichte es, die P5-Typ ATPase in ER-Membranen in Wurzelzellen von *Arabidopsis* zu lokalisieren. Trotz dessen war ein Komplementation des kurzen Wurzelphänotyps von *pdr2* in -Pi-Bedingungen mittels eines *35S::PDR2-GFP*-Konstruktes nicht erfolgreich. Der Grund dafür ist vermutlich das *Silencing* des *35S*-Promoters im Wurzelmeristem. Nichtsdestotrotz konnte durch Einbringen des *35S::PDR2-GFP*-Konstruktes in *pdr2* die gestörte Entwicklung der Schoten in *pdr2*-Pflanzen komplementiert werden. Als einzige P5-Typ ATPase in *Arabidopsis* mit einer Reihe von postulierten Funktionen ist PDR2 von besonderer Bedeutung für eine Reihe von Prozessen in der Pflanze. Außerdem sind die Funktionen von P5-Typ ATPasen in allen Organismen bisher kaum verstanden. Die Erkenntnisse im Zuge der Charakterisierung von PDR2 und seiner Funktion ist deshalb auch für Bereich außerhalb der Pflanzenforschung von Relevanz, weshalb die im Zuge dieser Arbeit generierten transgenen Linien wichtige Ressourcen für zukünftige Forschungen darstellen.

LPR1 und PDR2 bilden sind Zentrale Komponenten eines Signalnetzwerkes, welches Eisen nutzt, um die Verfügbarkeit von Phosphat im umliegenden Medium zu bestimmen. Das Zusammenspiel beider Enzyme beeinflusst maßgeblich die morphologischen Veränderungen des Wurzelsystems im Zuge der Anpassung der Pflanze an sinkende Phosphatkonzentrationen im Boden. Die derzeitige Forschung beginnt gerade erst, das komplexen Zusammenspiel zwischen den verschiedenen Nährstoffen im Boden, zu verstehen. Ein tieferes Verständnis, wie das relativ simple Netzwerk, welches Eisen und Phosphat in der Phosphatmangelantwort von *Arabidopsis* verknüpft, funktioniert, ist ein wichtiger Schritt, um zu verstehen, wie Pflanzen die Vielzahl verschiedener Umwelteinflüsse und Nährstoffkonzentrationen messen, verarbeiten und sich schließlich optimal an bestehende Umweltbedingungen anpassen.

4 Materials and methods

4.1 Chemicals and other supplies

If not indicated otherwise, all chemicals were obtained from the following suppliers: BD Difco, Carl Roth, Clontech Laboratories, Duchefa Biochemie, Merck, Sigma-Aldrich and Serva Electrophoresis. Molecular biology supplies including RNA/DNA purification kits and kits for cloning, including Gateway cloning reactions, were obtained from Thermo Scientific and Qiagen. Primer synthesis and sequencing of vectors and PCR products was carried out by Eurofins Genomics.

4.2 Media

All media were autoclaved at 121 °C for 20 min after preparation. Supplements were sterile filtered and added after autoclaving.

4.2.1 Preparation of washed agar

100 g Phyto agar (Duchefa Biochemie) was washed 5 times in 5 l ddH₂O. During the last washing step, the solution was dialyzed against Dowex 1X8 Ion exchanger (chloride form, strongly basic, 200 – 400 mesh [Sigma-Aldrich]) to remove residual ions. Subsequently the agar was air dried at 60°C for 2 – 3 days.

4.2.2 Solid Medium for sterile growth of *Arabidopsis* seedlings

For the sterile growth of *Arabidopsis* seedlings on agar plates, Solid Medium (SM) with the following composition was used.

Table 4: Composition of Solid Medium (SM)

Component	Final concentration
D-Sucrose	0,5 % (w/v)
Washed agar	1 % (w/v)
KNO ₃	5 mM
KH ₂ PO ₄	2.5 mM
Fe-EDTA	0.05 mM
MgSO ₄	2 mM
Ca(NO ₃) ₂	2 mM
MES-KOH pH 5.6	2.5 mM

For the preparation of –Pi medium KH₂PO₄ was omitted.

4.2.3 Murashige & Skoog medium for growth of *Arabidopsis* cell cultures

For growing *Arabidopsis* cell cultures, Murashige & Skoog (MS) medium (Duchefa) was used (Murashige and Skoog, 1962).

Table 5: Composition of Murashige & Skoog medium (MS)

Component	Final concentration
CaCl ₂	2.99 mM
KH ₂ PO ₄	1.25 mM
KNO ₃	18.79 mM
MgSO ₄	1.5 mM
NH ₄ NO ₃	20.61 mM
CoCl ₂ .6H ₂ O	0.11 µM
CuSO ₄ .5H ₂ O	0.1 mM
FeNaEDTA	100 µM
H ₃ BO ₃	100.27 µM
KI	5.00 µM
MnSO ₄ .H ₂ O	100 µM
Na ₂ MoO ₄ .2H ₂ O	1.03 µM
ZnSO ₄ .7H ₂ O	29.91 µM
Glycine	26.64 µM

After autoclaving the following sterile filtered supplements were added.

Table 6: MS medium supplements for *Arabidopsis* cell cultures

Component	Final concentration
Sucrose	3 % (w/v)
2,4-D	1 mg / l
Myo-Inositol	100 mg / l
Nicotinic acid	0.5 mg / l
Pyridoxin-HCl	0.5 mg / l
Thiamin-HCl	0.1 mg / l

4.2.4 Lysogeny broth medium

For cultivation of bacterial cells Lysogeny broth (LB) medium was used.

Table 7: Composition of Lysogeny broth (LB) medium

Component	Final concentration
Tryptone	1 % (w/v)
Yeast extract	0.5 %
NaCl	1 %

The preparation of LB agar plates was carried out by addition of Agar-agar to a total of 1.5 %. For selective growth the corresponding antibiotics were added after autoclaving.

4.2.5 S.O.B. and S.O.C. medium

For transformation of bacterial cells, Super Optimal Broth (S.O.B.) or S.O.C. medium was used.

Table 8: Composition of Super Optimal Broth medium

Component	Final concentration
Tryptone	2 % (w/v)
Yeast extract	5 % (w/v)
NaCl	10 mM
KCl	2.5 mM
	pH 7.0

MgCl₂ (10 mM) was added after autoclaving. For the preparation of S.O.C. medium, glucose was added to a total of 2 % (w/v).

4.2.6 Preparation of YPD medium for cultivation of yeast cells

For the preparation of YPD medium, YPD broth (Roth) was used according to the instruction manual.

Component	Final concentration
Casein (digested)	2 % (w/v)
Yeast extract	1 % (w/v)
Glucose	2 % (w/v)
	pH 6.5 ± 0.2

Agar-agar was added to a total of 1.5 % for preparation of YPD agar plates.

4.2.7 Preparation of Synthetic Defined (SD) medium

For the preparation of SD medium for selective growth of yeast cells Yeast Nitrogen Base without amino acids (Sigma) and -Ura Dropout supplement (Clontech) was used according to the instruction manuals. If not described otherwise, Glucose (2 % [w/v]) served as a carbon source. To prepare SD

plates a 4 % (w/v) stock of Agar-agar was autoclaved and diluted to a final concentration of 2 % (w/v) in the final medium. Other carbon sources and additional are described within the respective experiment. All ingredients and additional supplements were filter sterilized prior to addition.

4.3 Plant cultivation and growth conditions

4.3.1 Sterile growth of *Arabidopsis* seedlings on agar plates

Prior to seeding, *Arabidopsis* seeds were surface-sterilized with chlorine gas. Therefore, sodium hypochlorite (12% w/v NaClO) was mixed with fuming hydrochloric acid (37% v/v HCl) and incubated for 35 – 45 min. After removal of the gas the seeds were placed on the agar and stratified for at least 1 day at 8 °C in the dark. They were moved to light chambers or cabinets where they grew vertically under continuous light or long day conditions (16 h light and 8 h dark) at 20 - 22°C with ~ 130 $\mu\text{mol} / (\text{m}^2/\text{s})$ light fluency and ~ 55 % humidity.

4.3.2 Cultivation of *Arabidopsis thaliana* and *Nicotiana benthamiana* on soil

Unless stated otherwise, the cultivation of *Arabidopsis* and *Nicotiana* took place in the greenhouse under long day conditions at 18 – 20 °C and ~ 55 - 60 % relative humidity. “Einheitserde Typ GS 90” mixed with vermiculite (1 – 2 mm) in a 4:3 ratio served as substrate.

4.3.3 Sterile growth of *Arabidopsis thaliana* suspension cultures

Arabidopsis suspension cultures were originally generated by Dr. I. E. Somssich (MPIZ Cologne) and kindly cultured and provided by Sylvia Krüger.

4.3.4 Stable transformation of *Arabidopsis* via the floral dip method

For the generation of stable transgenic *Arabidopsis* lines flowering *Arabidopsis* plants were transformed via the *Agrobacterium tumefaciens* mediated floral dip method (Clough and Bent, 1998). *A. tumefaciens* strains carrying the plasmid which contains the genetic material to be transferred were cultivated 2 days on LB medium containing the respective antibiotics for selection. The bacteria were resuspended in 60 ml LB medium to an $\text{OD}_{600} = 2.0$. Sucrose and Silwet L-77 was added to a total concentration of 5 % (w/v) and 0.03 % (v/v), respectively. Flowering *Arabidopsis* plants were then dipped in the bacterial solution for 15 – 30 s under gentle slewing. The plants were placed horizontally in a tray and covered with saran wrap allowing them to dry for 1 – 3 days. The saran wrap was discarded and the plants were continued to be cultivated in the greenhouse for setting seeds.

To select positive T₁ seeds, all seeds derived from T₀ plants were grown on soil and repeatedly sprayed with BASTA. Surviving plants were then placed in individual pots for setting seeds again. 100 T₂ seeds were then placed on BASTA containing SM agar plates and the segregation ratio was determined by counting the ration between surviving and dead plants. 20 individual plants from lines showing a dead-to-alive ratio of 3:1 were transferred from the BASTA containing solid medium to soil, and their seeds were collected. T₃ seeds were then genotyped for the presence of the target construct. For lines containing the desired construct another segregation analysis on BASTA containing SM agar was carried out. 100 seeds were placed on the plates. If the survival rate was near 100 % the respective T₂ ancestor line was considered as homozygous for a single target construct insertion.

4.3.5 Transient transformation of *Nicotiana benthamiana* leaves

The transient transformation of *Nicotiana benthamiana* leaves was carried out using *Agrobacterium tumefaciens* strains that carried plasmids of choice and pCB301-p19 helper plasmid (Voinnet et al., 2003; Win and Kamoun, 2004). Bacteria were grown overnight in 4 ml LB medium containing the corresponding antibiotics to an OD₆₀₀ = 0.5 – 0.8. The cells were harvested at 10.000 g for 4 min. The pellet was washed 2 times with 2 ml Transformation buffer and subsequently dissolved in Transformation buffer to an OD₆₀₀ of 1. The bacteria carrying the expression construct were mixed 1:1 with the ones harboring the pCB301-p19 plasmid and incubated for 1 h at 20 °C. Afterwards, the bacteria were injected at the bottom side of leafs of 5 – 7-week old plants via a syringe. The plants were then placed in the greenhouse until further experiments were carried out.

Transformation buffer:

MES-KOH pH 5.5	10 mM
MgCl ₂	10 mM
Acetosyringe	150 µg / ml (w/v)

4.3.6 Determination of primary root growth of *Arabidopsis thaliana*

Arabidopsis seedlings were grown sterilely on agar plates for the indicated amount of time. Whole plates were photographed, and the root lengths were analyzed using ImageJ.

4.4 Bacterial and yeast general procedures

4.4.1 Cultivation of bacteria and yeast

4.4.1.1 Cultivation of *Escherichia coli*

E. coli cells were grown in liquid LB medium or on LB agar plates containing the appropriate antibiotics overnight at 37 °C at 120 – 160 RPM. For long term storage, liquid cultures were mixed with glycerol to a final concentration of 15 % (v/v), flash frozen in liquid nitrogen and stored at -80 °C.

4.4.1.2 Cultivation of *Agrobacterium tumefaciens*

A. tumefaciens cells were grown in liquid LB medium or on LB agar plates containing the appropriate antibiotics for 1 – 2 days at 28 °C at 120 – 160 RPM. For long term storage, liquid cultures were mixed with glycerol to a final concentration of 15 % (v/v), flash frozen in liquid nitrogen and stored at -80 °C.

4.4.1.3 Cultivation of *Saccharomyces cerevisiae*

S. cerevisiae cells were grown in liquid or solid YPD or Synthetic Defined (SD) medium lacking the appropriate amino acid for selection for 1 – 2 days at 30 °C at 120 – 160 RPM. For long term storage, liquid cultures were mixed with glycerol to a final concentration of 15 % (v/v), flash frozen in liquid nitrogen and stored at -80 °C.

4.4.1.4 Inducible gene expression in liquid *S. cerevisiae* cultures for protein production and complementation assays

A 2 ml preculture was inoculated with a colony of *S. cerevisiae* was picked from SD-U plates and grown overnight at 30 °C and 160 RPM in SD-U with 2 % Raffinose instead of Glucose and 50 µM FeCl₃. The OD₆₀₀ of all precultures was determined and adjusted to the same value. 100 ml of Yeast expression medium were inoculated with 0.5 ml of the indicated precultures and grown for 52 h at 160 RPM at 28 °C. The growth was determined via the OD₆₀₀ at different time points.

Yeast expression medium:

SD-U including following:

Galactose	2 % w/v
NaPO ₄ pH 6.0	100 mM
CuSO ₄	200 µM
BPS	80 µM

4.4.2 Transformation of bacteria and yeast

4.4.2.1 Transformation of chemical competent *Escherichia coli* cells

100 – 500 ng of plasmid were added to 50 µl chemically competent *E. coli* cells and incubated on ice for 30 min. The mixture was heat shocked for 45 s at 42 °C and immediately placed on ice. After addition of 300 µl S.O.C. medium the cells were incubated at 37 °C for 45 min at 350 RPM. Selection of positive clones took place overnight at 37 °C on LB Agar plates containing the corresponding antibiotics.

4.4.2.2 Transformation of chemical competent *Agrobacterium tumefaciens* cells

100 – 500 ng of plasmid were added to 50 µl chemically competent *A. tumefaciens* cells and incubated on ice for 30 min. The cells were incubated for 2 min in liquid nitrogen and thawed ~ 5 min at 37 °C. 300 µl of S.O.C. medium was added, and the mixture was incubated for 2 -4 h at 28 °C and 350 RPM. The selection of positive clones took place on LB Agar plates containing the corresponding antibiotics.

4.4.2.3 Transformation of *Saccharomyces cerevisiae*

For the transformation of *S. cerevisiae*, the Lithium acetate (LiOAc) method was used (Gietz and Schiestl, 2007). 200 ml YPD medium was inoculated with a single colony of *S. cerevisiae* and incubated over night at 30 °C at 120 – 160 RPM until the OD₆₀₀ reached 0.8 – 1.0. The cells were harvested by centrifugation at 5,000 g for 5 min and the supernatant was discarded. The pellet was washed with 10 ml sterile ddH₂O and centrifuged again as described above. The pellet was now washed in 1 ml ddH₂O, centrifuged again and resuspended in 1 ml TE/LiOAc. After a last centrifugation step, the pellet was dissolved in 250 µl TE/LiOAc. Salmon sperm DNA (ssDNA [Sigma]) was diluted in TE buffer (5 mg / ml [w/v]) and incubated at 95 °C for 20 min, placed on ice and used immediately for the next transformation step. 4 µl of the ssDNA was mixed with 20 µl cell suspension in a 96-well plate. 400 ng of the plasmid of choice and 100 µl PEG solution was added. The mixture was resuspended carefully and incubated for 1 h at 30 °C and 120 RPM. Next, the cells were heat shocked for 15 min at 42 °C and centrifuged for 5 min at 1.800 g. After carefully removing 100 µl of the supernatant the cells were washed by overlaying them with 180 µl TE buffer and immediately removing 130 µl of the supernatant. The cells were finally resuspended in the remaining 50 µl TE buffer and 10 µl were dropped on selective SD agar plates. After 2 – 4 days of growth at 30 °C single colonies were picked and streaked on a new selective SD plate. To verify the presence of the correct vector a colony PCR was carried out.

TE-Buffer:

Tris-HCl	10 mM
EDTA	1 mM
pH	7.5

TE/LiOAc:

Lithiumacetate	100 mM
Tris-HCl	10 mM
EDTA	1 mM
pH	7.5

PEG solution:

PEG 4000	40 % (w/v)
Lithiumacetate	100 mM
Tris-HCl	10 mM
EDTA	1 mM
pH	7.5

4.5 Molecular biological methods

4.5.1 DNA based methods

4.5.1.1 Isolation of plant DNA

All actions were carried out at RT. Approximately 100 mg of plant material (leaves, roots or whole seedlings) were grounded in a 1.5 ml reaction tube and 400 µl plant DNA extraction buffer was added. The samples were vortexed, centrifuged at 10.000 g for 5 min and the supernatant was transferred into a new tube. After the addition of 300 µl isopropanol the tubes were inverted several times, incubated for 2 min and centrifuged again at 10,000g for 5 min. The pellet was washed with 70 % Ethanol, air dried for 10 – 30 min and dissolved in 50 µl ddH₂O and incubated at 95 °C for 3 min. The DNA concentration was measured at a Nanoquant Infinite M200 (Tecan). The isolated DNA was stored at -20 °C.

Plant DNA extraction buffer:

Tris-HCl pH 7.25	200 mM
NaCl	250 mM
EDTA	25 mM
SDS	0.5 % (w/v)

4.5.1.2 Isolation of DNA from yeast

To isolate DNA from yeast a single colony was resuspended in 200 µl of 0.2 M LiOAc + 1 % SDS (w/v) and incubated for 5 min at 70 °C. After the addition of 300 µl EtOH (96 – 100 % [v/v]) the sample was vortexed and centrifuged at 15,000 g for 3 min at RT. The supernatant was discarded, and the pellet was washed in 200 µl EtOH (70 % [v/v]). The washing step was repeated and the pellet was dissolved in 100 µl ddH₂O and stored at -20 °C (Looke et al., 2011).

4.5.1.3 Isolation of plasmid DNA

For the isolation of plasmid DNA from bacteria, the GeneJET plasmid Mini Prep Kit (Thermo Fisher scientific) was used according to the manufacturer`s instruction. The isolated plasmid was eluted in 50 µl ddH₂O and stored at -20 °C.

4.5.1.4 Preparation of agarose gels for separation of DNA fragments

To separate DNA fragments agarose gel electrophoresis was used. Agarose (Biozym) was diluted 0.8 – 1.5 % (w/v) in TAE buffer and melted in a microwave oven. Stain G (Serva) was added to 0.003% (v/v) and after loading of the samples, the gels were run at 90 V for about 30 – 45 min. To analyze the separation pattern of the DNA fragments a Gene Genius (Syngene) UV table was used.

4.5.1.5 Purification of DNA fragments from agarose gels

Separated DNA fragments were purified from agarose gels via GeneJET Gel extraction Kit (Thermo Fisher Scientific) according to the manufacturer`s instructions. The purified DNA was stored at -20 °C.

4.5.1.6 Polymerase chain reaction (PCR)

For the amplification of DNA fragments PCR reaction was used. In general, Dream Taq Polymerase and 10 x Dream Taq Polymerase Green Buffer (Thermo Fisher Scientific) was used for analytical PCR reactions i.e. Colony PCR or genotyping of plant material. For amplification of DNA fragments for cloning purposes Phusion High Fidelity Polymerase and 5 x Phusion Green Buffer (Thermo Fisher Scientific) was used. Primers used are shown in Supplemental table 1. Specific reaction conditions are depicted at the individual experimental procedures. All PCR reactions were carried out in a Mastercycler pro S (Eppendorf) or a Veriti 96 well thermal cycler (Applied Biosystems).

4.5.1.7 Site directed mutagenesis of plasmids

To introduce point mutations in plasmids, site directed mutagenesis (SDM) was carried with the “Quick Change II Site directed mutagenesis Kit” (Agilent) according to the manufacturers instructions. Briefly, two complementary primers containing the desired mutation of the plasmid are used to amplify 2 overlapping, complementary strands of the plasmid with staggered nicks. After the amplification, the parental DNA is digested with DpnI and the mutated plasmids are transformed into *E. coli* Top 10 or XL1 Blue cells. The primers used to generate the different mutations are shown in Supplemental table 2.

4.5.2 RNA based methods

4.5.2.1 Isolation of plant RNA

For the isolation of plant RNA, “RNeasy Plant Mini Kit” (Qiagen) was used. In brief, 10 – 100 mg of plant material was frozen in liquid nitrogen and lysed using steel beads and a “Tissue Lyser II” (Retsch). Grounded material was then used for “Purification of Total RNA from Plant Cells and Tissues” according to the manufacturer manual. Eventually, the purified RNA was dissolved in 30 – 50 µl RNase-free ddH₂O. The concentration of the RNA was measured at a Nanoquant Infinite M200 (Tecan) and the isolated RNA was stored at -20 °C.

4.5.2.2 First strand cDNA synthesis from RNA samples

To generate cDNA samples from RNA Revert Aid Reverse Transcriptase (Thermo Scientific) was used according to the manufacturer manual. In short, 5 µg of total RNA was mixed with oligo(dT) primers in reaction buffer and the Revert Aid enzyme was added. The reverse transcriptase reaction was carried out for 60 min at 42 °C and terminated by a heat shock at 70 °C for 10 min. The cDNA samples were stored at -20 °C until usage.

4.5.2.3 Quantification of specific mRNA levels using quantitative Realtime-PCR (qRT-PCR)

To determine expression levels of specific genes qRT-PCR was used. The total RNA of a plant sample was extracted, and a Reverse Transcriptase reaction was carried out to generate cDNA samples (4.5.2.2). The cDNA was used as a template for the qRT-PCR reaction using the 7500 Fast Real-time PCR System (Thermo Fisher Scientific) in combination with the Fast SYBR™ Green Master Mix (Thermo Fisher Scientific) according to the manufacturer manual. In brief, 10 µM Primers specific for the target gene were mixed with 5 µl Fast SYBR Green Master Mix and cDNA template was added. Unless otherwise stated, the standard PCR was carried out using the following program:

Temperature	Time
95 °C	20 s
95 °C	3 s
60 °C	30 s

} X 40

The analysis of the results was carried out by using the 7500 Software v2.0. For some experiments the expression levels were calculated manually using the corresponding Ct values.

4.6 Protein biochemistry methods

4.6.1 Extraction from proteins from different organisms

4.6.1.1 Total protein extraction from plant material

100 – 500 mg of plant material from *A. thaliana* or *N. benthamiana* were frozen in liquid nitrogen and subsequently lysed using steel beads and a “Tissue Lyser II”. The grounded material was then dissolved in 1 – 2 µl of plant protein extraction buffer per mg plant material and incubated for 30 min on ice. Cell debris was pelleted for 10 min at 10.000 g at 4 °C and the supernatant was transferred to a new tube. The protein samples were stored at -20 °C until usage.

Plant protein extraction buffer:

Tris-HCl pH 8.0	50 mM
NaCl	100 mM
Glycerol	10 % (v/v)
PMSF	0.2 mM
Plant protease inhibitor cocktail (Sigma)	1 % (v/v)

4.6.1.2 Total protein extraction of *Arabidopsis thaliana* cell cultures

Arabidopsis thaliana cells grown sterilely in cell culture medium (4.3.3) were harvested by filtration through 3 layers of Miracloth with subsequent centrifugation at 200 g for 10 min at 4 °C. The pellet was washed 2 times with ddH₂O (3 ml g⁻¹ fresh weight), diluted in 1 x SDS sample buffer (3 ml g⁻¹ fresh weight) and incubated for 10 min at 95 °C. The protein extracts were stored at -20 °C.

1 X SDS sample buffer:

Tris-HCl pH 6.8	50 mM
EDTA	12.5 mM
SDS	2 % (w/v)
β -mercaptoethanol	1 % (v/v)
Glycerol	10 % (v/v)
Bromophenol blue	0.02 % (w/v)

4.6.1.3 Extraction of cell wall proteins from suspension cultured *Arabidopsis thaliana* cells

Cell wall proteins from suspension cultured *Arabidopsis* cells were extracted as described previously (Robertson et al., 1997). The cells were harvested 7 to 8 days after subculture via filtration through 3 layers of Miracloth with subsequent centrifugation at 200 g for 10 min at 4 °C. The medium fraction was prepared by collecting the supernatant and precipitating the proteins via acetone for 1 h at -20 °C. Afterwards, they were washed 3 times in ddH₂O (3 ml g⁻¹ fresh weight). All following steps were performed at 4 °C sequentially with the same cells. The first extraction was carried out by stirring the cells in 3 volumes of 0.2 M CaCl₂. After that the extracted proteins were collected via filtration through Miracloth and the cells were washed with ddH₂O as above. Three more extraction steps with 2 mM DTT, 1 M NaCl and 0.2 M borate (pH 7.5) followed in the same way as the first extraction, whereas the borate extraction was carried out at RT. The collected samples were dialyzed 2 times against 300 ml ddH₂O for 1 h at 4 °C. A third dialysis step was carried out overnight. The dialyzed samples were lyophilized for 2 to 3 days, subsequently diluted in 200 – 400 μ l of plant protein extraction buffer (4.6.1.1) and stored at -80 °C.

4.6.1.4 Total protein extraction from yeast cells

S. cerevisiae cells were harvested from the indicated liquid medium via centrifugation at 10,000 g for 10 min at 4 °C. The cells washed in 100 mM Tris-HCl pH 7.4, centrifuged at 4,000 g for 10 min at 4 °C and the supernatant was discarded. The pellet was frozen in liquid N₂ and stored at -20 °C for at least 1 h until it was resuspended in Protein extraction buffer. Zymolase was added to 1 mg / ml and the cells were incubated for 30 min at 29 °C while shaking slightly. Finally, the lysate was sonicated and centrifuged for 10 min at 10,000 g. The supernatant was then stored at -20 °C until further use.

Protein extraction buffer:

Tris-HCl pH 8.0	50 mM
NaCl	100 mM
Glycerol	10 % (v/v)

4.6.2 Determination of total protein content of samples

To determine the protein content of sample, 5 x Bradford reagent (Serva) was used according to the manufacturer manual for protein quantification in microtiter plates. After addition of the Bradford reagent, the samples were incubated 5 min at RT and the absorbance at 595 nm ($A_{595\text{nm}}$) was measured at a Nanoquant Infinite M1000 (Tecan).

4.6.3 Protein separation via SDS-PAGE (Laemmli, 1970)

Protein samples were loaded on an SDS Gel with the indicated concentration of Acrylamide and run for ~ 1.5 h until the lowest marker band reached the end of the gel. The gels were dismantled and subjected to further analysis.

4.6.4 Staining of SDS Gels with Coomassie Brilliant Blue

To visualize migrated proteins after an SDS-PAGE (4.6.3) the gels were stained for at least 1 h in Coomassie brilliant blue staining solution and subsequently destained in Coomassie destaining solution until distinct protein bands became visible against the cleared background.

Coomassie staining solution:

Methanol	50 % (v/v)
Glacial acetic acid	10 % (v/v)
Coomassie brilliant blue (Serva)	0.1 % (w/v)

Coomassie Destaining solution:

Methanol	50 % (v/v)
Glacial acetic acid	10 % (v/v)

4.6.5 Analysis of protein samples via Western Blot

To analyze the abundance of specific proteins within a protein sample, SDS gels were incubated in Towbin buffer for at least 10 min and the proteins were subsequently transferred to Protran Nitrocellulose membranes (GE Healthcare) via Semi Dry blotting for 1 h at 20 V. After the transfer the

blotting efficiency was evaluated via staining of the membranes in Ponceau S solution for 2 min. After unstaining of the membranes in ddH₂O they were exposed to blocking buffer (PBS-T + 2.5 % milk powder [w/v]) for 1 h at RT. The primary antibody (AB) was diluted as described for the respective experiment and incubated over night at 8 °C. The membranes were washed 3 times in PBS-T and exposed to the secondary AB for at least 3 hours at RT. They were washed 2 times in PBS-T and 2 times in PBS. The secondary AB was visualized with ECL Prime or ECL Select Western Blotting Detection Reagent (Amersham) and detected with the *MultiimagerII* (Alpha Innotech).

Towbin buffer:

Tris	25 mM
Glycine	192 mM
SDS	0.1 % (w/v)
Methanol	20 % (v/v)
	pH 8.3 (do not adjust)

Ponceau S solution

Glacial acetic acid	5 % (v/v)
Ponceau S	0.1 % (w/v)

PBS:

NaCl	137 mM
KCl	2.7 mM
Na ₂ HPO ₄	8 mM
KH ₂ PO ₄	2 mM

For preparation of PBS-T 0.05 % Tween 20 was added.

4.6.6 Stripping of nitrocellulose membranes after western blot analysis

For re-probing of a nitrocellulose membrane after western blot analysis with a different antibody, stripping of the antibodies from the first probing is necessary. After probing with the first set of antibodies the membrane was incubated 10 min in mild stripping buffer, twice. The buffer was discarded, and the membrane was washed 2 times 10 minutes in PBS before washing in TBS-T for 5 min, twice. After that the membrane was ready to be blocked again.

Mild stripping buffer:

Glycine	1.5 % (w/v)
SDS	0.1 % (w/v)
Tween 20	1 % (v/v)
pH	2.2

4.6.7 Determination of specific ferroxidase activity of a protein sample via Ferrozine assay

The specific ferroxidase activity of a protein sample was determined via Ferrozine assay (Erel, 1998). $\text{Fe}(\text{NH}_4)_2(\text{SO}_4) \times 6 \text{ H}_2\text{O}$ serves as the substrate and 3-(2-pyridyl)-5,6-bi(2-[5-furylsulfonic acid])-1,2,4-triazin (Ferrozine) as a specific chelator for Fe^{2+} . Chelation of the remaining substrate by Ferrozine quenches the reaction and leads to an absorption at 570 nm. A defined amount of protein was mixed in a 1, 5 ml reaction tube with Ferrozine substrate solution in Ferrozine reaction buffer to reach the desired concentration of substrate. 200 μl samples were taken in appropriate intervals and transferred to 96-well plates containing 14 μl of 18 mM Ferrozine. The addition of Ferrozine stopped the reaction and the absorbance at 570 nm was measured via the Nanoquant Infinite M1000 (Tecan). Using the specific molar absorption constant of 27.9 mM^{-1} for the Fe^{2+} -Ferrozine complex, the amount of remaining Fe^{2+} within the sample could be determined for each time point. The decline of substrate was then used as a proxy to calculate the oxidation rate of Fe^{2+} (de Silva et al., 1997).

Ferrozine reaction buffer:

Na-Acetate pH 5.8	450 mM
CuSO_4	100 μM

Ferrozine substrate solution:

Thiourea	130 mM
$\text{Fe}(\text{NH}_4)_2(\text{SO}_4) \times 6 \text{ H}_2\text{O}$	367 μM

Thiourea must be added prior to $\text{Fe}(\text{NH}_4)_2(\text{SO}_4) \times 6 \text{ H}_2\text{O}$ to prevent spontaneous oxidation of ferrous ions in water.

4.6.8 De-glycosylation assay

To examine possible glycosylation of proteins, a de-glycosylation assay was carried out using the Protein Deglycosylation Mix (NEB) according to the manufacturer manual. However, instead of using enriched or purified glycoprotein, whole root protein extracts of *Arabidopsis* seedlings were used. In brief, proteins were extracted in protein extractions buffer and Glycoprotein Denaturing Buffer was

added. Proteins were denatured at 90 °C for 10 min. After chilling the mixture on ice, GlycoBuffer 2, and NP-40 was added. After addition of Deglycosylation Enzyme Cocktail, the reaction was incubated for 4 h at 37 °C and the outcome was analyzed via Western Blotting.

4.6.9 Enrichment and purification of proteins

4.6.9.1 Protein purification via GFP-Trap (Chromotek)

For the purification of GFP-tagged proteins the GFP-Trap system from Chromotek was used according to the manufacturer manual. In brief, plant material was extracted as described in 4.6.1.1. Instead of using plant protein extraction buffer as described above, 1.5 µl GFP-Trap extraction buffer was used to dissolve 1 mg of plant material to obtain the crude extract. Subsequently, this extract was centrifuged for 10 min at 10,000 g at 4 °C, the supernatant was transferred to another tube and the step was repeated and used as Input for the purification. The binding of GFP-tagged proteins to the beads was carried for 90 min at 4 °C under slow rotation. After washing, the elution of bound proteins was facilitated by incubation of the beads in 0.2 M Glycine pH 2.5 for 30 s and subsequent centrifugation for 1 min at 1,000 g. The supernatant was transferred to a new tube and Tris-HCl pH 10.4 was added to neutralize the elution.

GFP-Trap extraction buffer:

Tris-HCl pH 7.5	20 mM
NaCl	150 mM
Glycerol	10 % (v/v)
PMSF	0.2 mM
Plant protease inhibitor cocktail (Sigma)	1 % (v/v)

4.6.9.2 Protein purification via Immunoprecipitation (IP) using antibody-coupled agarose beads

For the purification of untagged proteins, Protein A Agarose (Pierce) was used according to the manufacturer manual. In brief, a protein extract was incubated with the antibody against the target protein for 2 h or overnight at 4 °C under constant slow rotation. 100 µl of the Protein A resin was added to a new tube and briefly centrifuged. The supernatant was discarded and the beads were washed in IP buffer, twice. Subsequently, the sample containing the antigen-antibody complexes was added and incubated 2 h at RT under gentle mixing. The reaction was washed 2 times with IP buffer and incubated for 5 min in elution buffer. Subsequently, the sample was centrifuged and the supernatant containing the antigen-antibody complexes was collected in another tube, neutralized with ~ 10 µl Neutralization buffer and stored at -20 °C.

4.7 Microscopic analysis

4.7.1 Confocal laser scanning microscopy (cLSM)

For confocal laser scanning microscopy of *Arabidopsis* and *N. benthamiana* tissues, the cSLM700 (Zeiss) was used. If not stated otherwise, the c-Apochromat 40x/1.20 W Korr M27 objective was used. Zen Software (Zeiss) was used to operate the microscope and for the processing of the pictures.

5 References

- Abel, S.** (2017). Phosphate scouting by root tips. *Current opinion in plant biology* **39**, 168-177.
- Aisen, P., Enns, C., and Wessling-Resnick, M.** (2001). Chemistry and biology of eukaryotic iron metabolism. *Int J Biochem Cell B* **33**, 940-959.
- Askwith, C., and Kaplan, J.** (1997). An oxidase-permease-based iron transport system in *Schizosaccharomyces pombe* and its expression in *Saccharomyces cerevisiae*. *Journal of Biological Chemistry* **272**, 401-405.
- Askwith, C., Eide, D., Van Ho, A., Bernard, P.S., Li, L., Davis-Kaplan, S., Sipe, D.M., and Kaplan, J.** (1994). The FET3 gene of *S. cerevisiae* encodes a multicopper oxidase required for ferrous iron uptake. *Cell* **76**, 403-410.
- Attieh, Z.K., Mukhopadhyay, C.K., Seshadri, V., Tripoulas, N.A., and Fox, P.L.** (1999). ceruloplasmin ferroxidase activity stimulates cellular iron uptake by a trivalent cation-specific transport mechanism. *The Journal of biological chemistry* **274**, 1116-1123.
- Augustine, A.J., Kragh, M.E., Sarangi, R., Fujii, S., Liboiron, B.D., Stoj, C.S., Kosman, D.J., Hodgson, K.O., Hedman, B., and Solomon, E.I.** (2008). Spectroscopic studies of perturbed T1 Cu sites in the multicopper oxidases *Saccharomyces cerevisiae* Fet3p and *Rhus vernicifera* laccase: Allosteric coupling between the T1 and trinuclear Cu sites. *Biochemistry* **47**, 2036-2045.
- Balzergue, C., Dartevelle, T., Godon, C., Laugier, E., Meisrimler, C., Teulon, J.M., Creff, A., Bissler, M., Brouchoud, C., Hagege, A., Muller, J., Chiarenza, S., Javot, H., Becuwe-Linka, N., David, P., Peret, B., Delannoy, E., Thibaud, M.C., Armengaud, J., Abel, S., Pellequer, J.L., Nussaume, L., and Desnos, T.** (2017). Low phosphate activates STOP1-ALMT1 to rapidly inhibit root cell elongation. *Nature communications* **8**.
- Baxter, I., Tchieu, J., Sussman, M.R., Boutry, M., Palmgren, M.G., Gribskov, M., Harper, J.F., and Axelsen, K.B.** (2003). Genomic comparison of P-type ATPase ion pumps in *Arabidopsis* and rice. *Plant physiology* **132**, 618-628.
- Benfey, P.N., Ren, L., and Chua, N.H.** (1990). Combinatorial and Synergistic Properties of Camv 35s-Enhancer Subdomains. *Embo Journal* **9**, 1685-1696.
- Bonaccorsi di Patti, M.C., Paronetto, M.P., Dolci, V., Felice, M.R., Lania, A., and Musci, G.** (2001). Mutational analysis of the iron binding site of *Saccharomyces cerevisiae* ferroxidase Fet3. An in vivo study. *FEBS letters* **508**, 475-478.
- Bowler, M.W., Cliff, M.J., Waltho, J.P., and Blackburn, G.M.** (2010). Why did Nature select phosphate for its dominant roles in biology? *New J Chem* **34**, 784-794.
- Brachmann, C.B., Davies, A., Cost, G.J., Caputo, E., Li, J.C., Hieter, P., and Boeke, J.D.** (1998). Designer deletion strains derived from *Saccharomyces cerevisiae* S288C: a useful set of strains and plasmids for PCR-mediated gene disruption and other applications. *Yeast* **14**, 115-132.
- Brandizzi, F., Hanton, S., daSilva, L.L.P., Boevink, P., Evans, D., Oparka, K., Denecke, J., and Hawes, C.** (2003). ER quality control can lead to retrograde transport from the ER lumen to the cytosol and the nucleoplasm in plants. *Plant Journal* **34**, 269-281.
- Chen, D.L., Delatorre, C.A., Bakker, A., and Abel, S.** (2000). Conditional identification of phosphate-starvation-response mutants in *Arabidopsis thaliana*. *Planta* **211**, 13-22.
- Chen, H., Attieh, Z.K., Su, T., Syed, B.A., Gao, H., Alaeddine, R.M., Fox, T.C., Usta, J., Naylor, C.E., Evans, R.W., McKie, A.T., Anderson, G.J., and Vulpe, C.D.** (2004). Hephaestin is a ferroxidase that maintains partial activity in sex-linked anemia mice. *Blood* **103**, 3933-3939.
- Clough, S.J., and Bent, A.F.** (1998). Floral dip: a simplified method for *Agrobacterium*-mediated transformation of *Arabidopsis thaliana*. *Plant Journal* **16**, 735-743.

- Cordell, D., Drangert, J.O., and White, S.** (2009). The story of phosphorus: Global food security and food for thought. *Global Environ Chang* **19**, 292-305.
- Cronin, S.R., Rao, R.J., and Hampton, R.Y.** (2002). Cod1p/Spf1p is a P-type ATPase involved in ER function and Ca²⁺ homeostasis. *Journal of Cell Biology* **157**, 1017-1028.
- Cui, H.C., Levesque, M.P., Vernoux, T., Jung, J.W., Paquette, A.J., Gallagher, K.L., Wang, J.Y., Blilou, I., Scheres, B., and Benfey, P.N.** (2007). An evolutionarily conserved mechanism delimiting SHR movement defines a single layer of endodermis in plants. *Science* **316**, 421-425.
- Daudi, A., Cheng, Z.Y., O'Brien, J.A., Mammarella, N., Khan, S., Ausubel, F.M., and Bolwell, G.P.** (2012). The Apoplastic Oxidative Burst Peroxidase in Arabidopsis Is a Major Component of Pattern-Triggered Immunity. *The Plant cell* **24**, 275-287.
- de Silva, D., Davis-Kaplan, S., Fergestad, J., and Kaplan, J.** (1997). Purification and characterization of Fet3 protein, a yeast homologue of ceruloplasmin. *The Journal of biological chemistry* **272**, 14208-14213.
- di Patti, M.C.B., Pascarella, S., Catalucci, D., and Calabrese, L.** (1999). Homology modeling of the multicopper oxidase Fet3 gives new insights in the mechanism of iron transport in yeast. *Protein Eng* **12**, 895-897.
- Dong, J.S., Pineros, M.A., Li, X.X., Yang, H.B., Liu, Y., Murphy, A.S., Kochian, L.V., and Liu, D.** (2017). An Arabidopsis ABC Transporter Mediates Phosphate Deficiency-Induced Remodeling of Root Architecture by Modulating Iron Homeostasis in Roots. *Molecular plant* **10**, 244-259.
- Duan, K., Yi, K.K., Dang, L., Huang, H.J., Wu, W., and Wu, P.** (2008). Characterization of a sub-family of Arabidopsis genes with the SPX domain reveals their diverse functions in plant tolerance to phosphorus starvation. *Plant Journal* **54**, 965-975.
- Edgar, R.C.** (2004). MUSCLE: a multiple sequence alignment method with reduced time and space complexity. *Bmc Bioinformatics* **5**, 1-19.
- Erel, O.** (1998). Automated measurement of serum ferroxidase activity. *Clinical chemistry* **44**, 2313-2319.
- Franco-Zorrilla, J.M., Martin, A.C., Leyva, A., and Par-Ares, J.P.** (2005). Interaction between phosphate-starvation, sugar, and cytokinin signaling in arabidopsis and the roles of cytokinin receptors CRE1/AHK4 and AHK3. *Plant physiology* **138**, 847-857.
- Franco-Zorrilla, J.M., Valli, A., Todesco, M., Mateos, I., Puga, M.I., Rubio-Somoza, I., Leyva, A., Weigel, D., Garcia, J.A., and Paz-Ares, J.** (2007). Target mimicry provides a new mechanism for regulation of microRNA activity. *Nature genetics* **39**, 1033-1037.
- Frentzen, M.** (2004). Phosphatidylglycerol and sulfoquinovosyldiacylglycerol: anionic membrane lipids and phosphate regulation. *Current opinion in plant biology* **7**, 270-276.
- Fu, D.D., Beeler, T.J., and Dunn, T.M.** (1995). Sequence, Mapping and Disruption of Ccc2, a Gene That Cross-Complements the Ca²⁺-Sensitive Phenotype of Csg1 Mutants and Encodes a P-Type Atpase Belonging to the Cu²⁺-Atpase Subfamily. *Yeast* **11**, 283-292.
- Gietz, R.D., and Schiestl, R.H.** (2007). High-efficiency yeast transformation using the LiAc/SS carrier DNA/PEG method. *Nat Protoc* **2**, 31-34.
- Gonzalez, E., Solano, R., Rubio, V., Leyva, A., and Paz-Ares, J.** (2005). PHOSPHATE TRANSPORTER TRAFFIC FACILITATOR1 is a plant-specific SEC12-related protein that enables the endoplasmic reticulum exit of a high-affinity phosphate transporter in Arabidopsis. *The Plant cell* **17**, 3500-3512.
- Gruber, B.D., Giehl, R.F.H., Friedel, S., and von Wiren, N.** (2013). Plasticity of the Arabidopsis Root System under Nutrient Deficiencies. *Plant physiology* **163**, 161-179.
- Hawes, C., Saint-Jore, C., Martin, B., and Zheng, H.Q.** (2001). ER confirmed as the location of mystery organelles in Arabidopsis plants expressing GFP! *Trends in plant science* **6**, 245-246.
- Heppner, D.E., Kjaergaard, C.H., and Solomon, E.I.** (2014). Mechanism of the reduction of the native intermediate in the multicopper oxidases: insights into rapid intramolecular electron transfer in turnover. *Journal of the American Chemical Society* **136**, 17788-17801.

- Hiruma, K., Gerlach, N., Sacristan, S., Nakano, R.T., Hacquard, S., Kracher, B., Neumann, U., Ramirez, D., Bucher, M., O'Connell, R.J., and Schulze-Lefert, P.** (2016). Root Endophyte Colletotrichum tofieldiae Confers Plant Fitness Benefits that Are Phosphate Status Dependent. *Cell* **165**, 464-474.
- Hoehenwarter, W., Monchgesang, S., Neumann, S., Majovsky, P., Abel, S., and Muller, J.** (2016). Comparative expression profiling reveals a role of the root apoplast in local phosphate response. *BMC plant biology* **16**.
- Hoopes, J.T., and Dean, J.F.** (2004). ferroxidase activity in a laccase-like multicopper oxidase from *Liriodendron tulipifera*. *Plant physiology and biochemistry : PPB / Societe francaise de physiologie vegetale* **42**, 27-33.
- Jakobsen, M.K., Poulsen, L.R., Schulz, A., Fleurat-Lessard, P., Moller, A., Husted, S., Schiott, M., Amtmann, A., and Palmgren, M.G.** (2005). Pollen development and fertilization in *Arabidopsis* is dependent on the MALE GAMETOGENESIS IMPAIRED ANTHEARS gene encoding a type VP-type ATPase. *Genes & development* **19**, 2757-2769.
- Karimi, M., Inze, D., and Depicker, A.** (2002). GATEWAY vectors for *Agrobacterium*-mediated plant transformation. *Trends in plant science* **7**, 193-195.
- Karthikeyan, A.S., Ballachanda, D.N., and Raghothama, K.G.** (2009). Promoter deletion analysis elucidates the role of cis elements and 5'UTR intron in spatiotemporal regulation of *AtPht1;4* expression in *Arabidopsis*. *Physiol Plantarum* **136**, 10-18.
- Karthikeyan, A.S., Jain, A., Nagarajan, V.K., Sinilal, B., Sahi, S.V., and Raghothama, K.G.** (2014). *Arabidopsis thaliana* mutant *lpsi* reveals impairment in the root responses to local phosphate availability. *Plant Physiol Bioch* **77**, 60-72.
- Kellermeier, F., Armengaud, P., Seditas, T.J., Danku, J., Salt, D.E., and Amtmann, A.** (2014). Analysis of the Root System Architecture of *Arabidopsis* Provides a Quantitative Readout of Crosstalk between Nutritional Signals. *The Plant cell* **26**, 1480-1496.
- Koncz, C., and Schell, J.** (1986). The Promoter of Tl-DNA Gene 5 Controls the Tissue-Specific Expression of Chimeric Genes Carried by a Novel Type of *Agrobacterium* Binary Vector. *Mol Gen Genet* **204**, 383-396.
- Kruger, M., Teste, F.P., Laliberte, E., Lambers, H., Coghlan, M., Zemunik, G., and Bunce, M.** (2015). The rise and fall of arbuscular mycorrhizal fungal diversity during ecosystem retrogression. *Molecular ecology* **24**, 4912-4930.
- Krumbein, W.E., and Altmann, H.J.** (1973). New Method for Detection and Enumeration of Manganese Oxidizing and Reducing Microorganisms. *Helgoland Wiss Meer* **25**, 347-356.
- Laemmli, U.K.** (1970). Cleavage of structural proteins during the assembly of the head of bacteriophage T4. *Nature* **227**, 680-685.
- Lambers, H., Martinoia, E., and Renton, M.** (2015). Plant adaptations to severely phosphorus-impooverished soils. *Current opinion in plant biology* **25**, 23-31.
- Lambers, H., Shane, M.W., Cramer, M.D., Pearse, S.J., and Veneklaas, E.J.** (2006). Root structure and functioning for efficient acquisition of phosphorus: Matching morphological and physiological traits. *Annals of botany* **98**, 693-713.
- Liebinger, E., Grass, J., Altmann, F., Mach, L., and Strasser, R.** (2013). Characterizing the Link between Glycosylation State and Enzymatic Activity of the Endo-beta 1,4-glucanase KORRIGAN1 from *Arabidopsis thaliana*. *Journal of Biological Chemistry* **288**, 22270-22280.
- Lin, S.I., Chiang, S.F., Lin, W.Y., Chen, J.W., Tseng, C.Y., Wu, P.C., and Chiou, T.J.** (2008). Regulatory network of microRNA399 and PHO2 by systemic signaling. *Plant physiology* **147**, 732-746.
- Looke, M., Kristjuhan, K., and Kristjuhan, A.** (2011). Extraction of genomic DNA from yeasts for PCR-based applications. *Biotechniques* **50**, 325-+.
- Lopez-Arredondo, D.L., Leyva-Gonzalez, M.A., Gonzalez-Morales, S.I., Lopez-Bucio, J., and Herrera-Estrella, L.** (2014). Phosphate Nutrition: Improving Low-Phosphate Tolerance in Crops. *Annu Rev Plant Biol* **65**, 95-123.
- Lynch, J.P., and Brown, K.M.** (2001). Topsoil foraging - an architectural adaptation of plants to low phosphorus availability. *Plant Soil* **237**, 225-237.

- Marino, K., Bones, J., Kattla, J.J., and Rudd, P.M.** (2010). A systematic approach to protein glycosylation analysis: a path through the maze. *Nat Chem Biol* **6**, 713-723.
- Martin-Hernandez, A.M., and Baulcombe, D.C.** (2008). Tobacco rattle virus 16-kilodalton protein encodes a suppressor of RNA silencing that allows transient viral entry in meristems. *Journal of virology* **82**, 4064-4071.
- Martin, A.C., del Pozo, J.C., Iglesias, J., Rubio, V., Solano, R., de la Pena, A., Leyva, A., and Paz-Ares, J.** (2000). Influence of cytokinins on the expression of phosphate starvation responsive genes in Arabidopsis. *Plant Journal* **24**, 559-567.
- Meyer, S., De Angeli, A., Fernie, A.R., and Martinoia, E.** (2010). Intra- and extra-cellular excretion of carboxylates. *Trends in plant science* **15**, 40-47.
- Muller, J., Toev, T., Heisters, M., Teller, J., Moore, K.L., Hause, G., Dinesh, D.C., Burstenbinder, K., and Abel, S.** (2015). Iron-dependent callose deposition adjusts root meristem maintenance to phosphate availability. *Developmental cell* **33**, 216-230.
- Murashige, T., and Skoog, F.** (1962). A Revised Medium for Rapid Growth and Bio Assays with Tobacco Tissue Cultures. *Physiol Plantarum* **15**, 473-497.
- Mzhel'skaya, T.I.** (2000). Biological functions of ceruloplasmin and their deficiency caused by mutation in genes regulating copper and iron metabolism. *B Exp Biol Med+* **130**, 719-727.
- Nelson, B.K., Cai, X., and Nebenfuhr, A.** (2007). A multicolored set of in vivo organelle markers for co-localization studies in Arabidopsis and other plants. *Plant Journal* **51**, 1126-1136.
- Norris, S.R., Meyer, S.E., and Callis, J.** (1993). The Intron of Arabidopsis-Thaliana Polyubiquitin Genes Is Conserved in Location and Is a Quantitative Determinant of Chimeric Gene-Expression. *Plant molecular biology* **21**, 895-906.
- Peret, B., Desnos, T., Jost, R., Kanno, S., Berkowitz, O., and Nussaume, L.** (2014). Root architecture responses: in search of phosphate. *Plant physiology* **166**, 1713-1723.
- Plaxton, W.C., and Tran, H.T.** (2011). Metabolic Adaptations of Phosphate-Starved Plants. *Plant physiology* **156**, 1006-1015.
- Porder, S., and Ramachandran, S.** (2013). The phosphorus concentration of common rocks-a potential driver of ecosystem P status. *Plant Soil* **367**, 41-55.
- Qi, W., Manfield, I.W., Muench, S.P., and Baker, A.** (2017). AtSPX1 affects the AtPHR1-DNA-binding equilibrium by binding monomeric AtPHR1 in solution. *The Biochemical journal* **474**, 3675-3687.
- Radisky, D., and Kaplan, J.** (1999). Regulation of transition metal transport across the yeast plasma membrane. *Journal of Biological Chemistry* **274**, 4481-4484.
- Reymond, M., Svistoonoff, S., Loudet, O., Nussaume, L., and Desnos, T.** (2006). Identification of QTL controlling root growth response to phosphate starvation in Arabidopsis thaliana. *Plant Cell and Environment* **29**, 115-125.
- Robertson, D., Mitchell, G.P., Gilroy, J.S., Gerrish, C., Bolwell, G.P., and Slabas, A.R.** (1997). Differential extraction and protein sequencing reveals major differences in patterns of primary cell wall proteins from plants. *Journal of Biological Chemistry* **272**, 15841-15848.
- Rubio, V., Linhares, F., Solano, R., Martin, A.C., Iglesias, J., Leyva, A., and Paz-Ares, J.** (2001). A conserved MYB transcription factor involved in phosphate starvation signaling both in vascular plants and in unicellular algae. *Genes & development* **15**, 2122-2133.
- Sabatini, S., Heidstra, R., Wildwater, M., and Scheres, B.** (2003). SCARECROW is involved in positioning the stem cell niche in the Arabidopsis root meristem. *Genes & development* **17**, 354-358.
- Sanchez-Calderon, L., Lopez-Bucio, J., Chacon-Lopez, A., Cruz-Ramirez, A., Nieto-Jacobo, F., Dubrovsky, J.G., and Herrera-Estrella, L.** (2005). Phosphate starvation induces a determinate developmental program in the roots of Arabidopsis thaliana. *Plant and Cell Physiology* **46**, 174-184.
- Schachtman, D.P., Reid, R.J., and Ayling, S.M.** (1998). Phosphorus uptake by plants: From soil to cell. *Plant physiology* **116**, 447-453.

- Schroeder, G.K., Lad, C., Wyman, P., Williams, N.H., and Wolfenden, R.** (2006). The time required for water attack at the phosphorus atom of simple phosphodiester and of DNA. *Proceedings of the National Academy of Sciences of the United States of America* **103**, 4052-4055.
- Sedlak, E., Zoldak, G., and Wittung-Stafshede, P.** (2018). Synergistic Effects of Copper Sites on Apparent Stability of Multicopper Oxidase, Fet3p. *International journal of molecular sciences* **19**.
- Shin, W., Sundaram, U.M., Cole, J.L., Zhang, H.H., Hedman, B., Hodgson, K.O., and Solomon, E.I.** (1996). Chemical and spectroscopic definition of the peroxide-level intermediate in the multicopper oxidases: Relevance to the catalytic mechanism of dioxygen reduction to water. *Journal of the American Chemical Society* **118**, 3202-3215.
- Singh, A.P., Fridman, Y., Holland, N., Ackerman-Lavert, M., Zananiri, R., Jaillais, Y., Henn, A., and Savaldi-Goldstein, S.** (2018). Interdependent Nutrient Availability and Steroid Hormone Signals Facilitate Root Growth Plasticity. *Developmental cell* **46**, 59-+.
- Sorensen, D.M., Moller, A.B., Jakobsen, M.K., Jensen, M.K., Vangheluwe, P., Buch-Pedersen, M.J., and Palmgren, M.G.** (2012). Ca²⁺ Induces Spontaneous Dephosphorylation of a Novel P5A-type ATPase. *Journal of Biological Chemistry* **287**, 28336-28348.
- Stearman, R., Yuan, D.S., Yamaguchi-Iwai, Y., Klausner, R.D., and Dancis, A.** (1996). A permease-oxidase complex involved in high-affinity iron uptake in yeast. *Science* **271**, 1552-1557.
- Stefanovic, A., Ribot, C., Rouached, H., Wang, Y., Chong, J., Belbahri, L., Delessert, S., and Poirier, Y.** (2007). Members of the PHO1 gene family show limited functional redundancy in phosphate transfer to the shoot, and are regulated by phosphate deficiency via distinct pathways. *Plant Journal* **50**, 982-994.
- Stoj, C.S., Augustine, A.J., Zeigler, L., Solomon, E.I., and Kosman, D.J.** (2006). Structural basis of the ferrous iron specificity of the yeast ferroxidase, Fet3p. *Biochemistry* **45**, 12741-12749.
- Svistoonoff, S., Creff, A., Reymond, M., Sigoillot-Claude, C., Ricaud, L., Blanchet, A., Nussaume, L., and Desnos, T.** (2007). Root tip contact with low-phosphate media reprograms plant root architecture. *Nature genetics* **39**, 792-796.
- Taylor, A.B., Stoj, C.S., Ziegler, L., Kosman, D.J., and Hart, P.J.** (2005). The copper-iron connection in biology: structure of the metallo-oxidase Fet3p. *Proc Natl Acad Sci U S A* **102**, 15459-15464.
- Thibaud, M.C., Arrighi, J.F., Bayle, V., Chiarenza, S., Creff, A., Bustos, R., Paz-Ares, J., Poirier, Y., and Nussaume, L.** (2010). Dissection of local and systemic transcriptional responses to phosphate starvation in Arabidopsis. *Plant Journal* **64**, 775-789.
- Ticconi, C.A., and Abel, S.** (2004). Short on phosphate: plant surveillance and countermeasures. *Trends in plant science* **9**, 548-555.
- Ticconi, C.A., Delatorre, C.A., and Abel, S.** (2001). Attenuation of phosphate starvation responses by phosphite in Arabidopsis. *Plant physiology* **127**, 963-972.
- Ticconi, C.A., Delatorre, C.A., Lahner, B., Salt, D.E., and Abel, S.** (2004). Arabidopsis pdr2 reveals a phosphate-sensitive checkpoint in root development. *Plant Journal* **37**, 801-814.
- Ticconi, C.A., Lucero, R.D., Sakhonwasee, S., Adamson, A.W., Creff, A., Nussaume, L., Desnos, T., and Abel, S.** (2009). ER-resident proteins PDR2 and LPR1 mediate the developmental response of root meristems to phosphate availability. *Proc Natl Acad Sci U S A* **106**, 14174-14179.
- Tiessen, H., International Council of Scientific Unions. Scientific Committee on Problems of the Environment, and United Nations Environment Programme.** (1995). Phosphorus in the global environment : transfers, cycles, and management. (Chichester ; New York: Published on behalf of the Scientific Committee on Problems of the Environment (SCOPE) of the International Council of Scientific Unions (ICSU), and of the United Nations Environment Programme (UNEP) by Wiley).

- Urbanowski, J.L., and Piper, R.C.** (1999). The iron transporter *fth1p* forms a complex with the Fet5 iron oxidase and resides on the vacuolar membrane. *Journal of Biological Chemistry* **274**, 38061-38070.
- Varki, A.** (1993). Biological Roles of Oligosaccharides - All of the Theories Are Correct. *Glycobiology* **3**, 97-130.
- Voinnet, O.** (2001). RNA silencing as a plant immune system against viruses. *Trends in Genetics* **17**, 449-459.
- Voinnet, O., Rivas, S., Mestre, P., and Baulcombe, D.** (2003). An enhanced transient expression system in plants based on suppression of gene silencing by the p19 protein of tomato bushy stunt virus. *The Plant journal : for cell and molecular biology* **33**, 949-956.
- Vulpe, C.D., Kuo, Y.M., Murphy, T.L., Cowley, L., Askwith, C., Libina, N., Gitschier, J., and Anderson, G.J.** (1999). Hephaestin, a ceruloplasmin homologue implicated in intestinal iron transport, is defective in the *sla* mouse. *Nature genetics* **21**, 195-199.
- Ward, J.T., Lahner, B., Yakubova, E., Salt, D.E., and Raghothama, K.G.** (2008). The effect of iron on the primary root elongation of *Arabidopsis* during phosphate deficiency. *Plant physiology* **147**, 1181-1191.
- Wass, M.N., Kelley, L.A., and Sternberg, M.J.E.** (2010). 3DLigandSite: predicting ligand-binding sites using similar structures. *Nucleic acids research* **38**, W469-W473.
- Waterhouse, A.M., Procter, J.B., Martin, D.M.A., Clamp, M., and Barton, G.J.** (2009). Jalview Version 2-a multiple sequence alignment editor and analysis workbench. *Bioinformatics* **25**, 1189-1191.
- White, P.J., and Hammond, J.** (2008). *The ecophysiology of plant-phosphorus interactions.* (Dordrecht ; London: Springer).
- Wild, R., Gerasimaite, R., Jung, J.Y., Truffault, V., Pavlovic, I., Schmidt, A., Saiardi, A., Jessen, H.J., Poirier, Y., Hothorn, M., and Mayer, A.** (2016). Control of eukaryotic phosphate homeostasis by inositol polyphosphate sensor domains. *Science* **352**, 986-990.
- Win, J., and Kamoun, S.** (2004). pCB301-p19: A Binary Plasmid Vector to Enhance Transient Expression of Transgenes by Agroinfiltration. <http://www.Kamounlab.net>.
- Wirth, J., Chopin, F., Santoni, V., Viennois, G., Tillard, P., Krapp, A., Lejay, L., Daniel-Vedele, F., and Gojon, A.** (2007). Regulation of root nitrate uptake at the NRT2.1 protein level in *Arabidopsis thaliana*. *Journal of Biological Chemistry* **282**, 23541-23552.
- Wrzaczek, M., Brosche, M., and Kangasjarvi, J.** (2013). ROS signaling loops - production, perception, regulation. *Current opinion in plant biology* **16**, 575-582.
- Yu, B., Xu, C.C., and Benning, C.** (2002). *Arabidopsis* disrupted in SQD2 encoding sulfolipid synthase is impaired in phosphate-limited growth. *Proceedings of the National Academy of Sciences of the United States of America* **99**, 5732-5737.
- Zhang, Z.Y., Wang, Y.A., and Dixon, J.E.** (1994). Dissecting the Catalytic Mechanism of Protein-Tyrosine Phosphatases. *Proceedings of the National Academy of Sciences of the United States of America* **91**, 1624-1627.
- Ziegler, L., Terzulli, A., Sedlak, E., and Kosman, D.J.** (2010). Core glycan in the yeast multicopper ferroxidase, Fet3p: A case study of N-linked glycosylation, protein maturation, and stability. *Protein Science* **19**, 1739-1750.
- Zipfel, C., Robatzek, S., Navarro, L., Oakeley, E.J., Jones, J.D.G., Felix, G., and Boller, T.** (2004). Bacterial disease resistance in *Arabidopsis* through flagellin perception. *Nature* **428**, 764-767.

5.1 Acknowledgements

I would like to thank Prof. Steffen Abel for providing me the opportunity to work at this complex topic under his supervision and for being my mentor during all this. I am especially thankful for all the discussions we had over the years that enabled me to develop confidence in my own work and ideas which was a crucial step in my life as a young scientist. I also want to thank him for being first reviewer of my thesis.

Additionally, I would like to thank Prof. Gary Sawers as the second reviewer of my thesis and also being a mentor for me since my time as a diploma student in his lab at the university.

I would also like to thank Prof. Thierry Desnos for being the third reviewer of my thesis.

Furthermore, I would like to thank all the people at our department that helped me with all the many tiny and bigger problems that occur in and outside the lab. Special thanks to Dr. Katharina Bürstenbinder, Dr. Jörg Ziegler and Dr. Jens Müller for many hours of discussions and priceless advices.

I would also like to thank all my colleagues in our department and the whole IPB for the friendly atmosphere and so many hours of fun during work. Special thanks therefore to my lab colleagues Dr. Christin Naumann and Carolin Alfs. I really enjoyed the time we spent together in and outside the lab.

I would also like to mention my fellow PhD student colleagues throughout the whole institute. Especially Paul, Martin, Micha, Stefan, Jakob, Juliane, Andreas, Linda and all the other people who already left the institute. It was a pleasure to work with you.

Of course, a very special thanks goes out to my family and friends. You helped me to become the person that I am. Thank you for your support for all these years.

The last and most important “Thank You” is addressed to my mother and father. You made all this possible. I will always be grateful. Danke für Alles.

6 Appendix

6.1 Eidesstattliche Erklärung / Declaration under Oath

Ich erkläre an Eides statt, dass ich die Arbeit selbstständig und ohne fremde Hilfe verfasst, keine anderen als die von mir angegebenen Quellen und Hilfsmittel benutzt und die den benutzten Werken wörtlich oder inhaltlich entnommenen Stellen als solche kenntlich gemacht habe.

I declare under penalty of perjury that this thesis is my own work entirely and has been written without any help from other people. I used only the sources mentioned and included all the citations correctly both in word or content.

Datum/Date

Unterschrift des Antragstellers/ Signature of applicant

6.2 Supplemental tables

Supplemental table 1: General primers and their respective sequences used in this work

Name	Gene	Description	Sequence 5' -> 3'
MH84	<i>PDR2</i>	Genomic <i>PDR2</i> forward + 5' cacc	CACCATGTCGAGCTTTCGTGT
MH85	<i>PDR2</i>	Genomic <i>PDR2</i> revers - stop	AACTTCTCTTCTTCTCCAGATTTGC
MH93	<i>PP2A</i>	qPCR <i>PP2A</i> in tobacco for	GACCCTGATGTTGATGTTTCGCT
MH94	<i>PP2A</i>	qPCR <i>PP2A</i> in tobacco rev	GAGGGATTGAAGAGAGATTTTC
P071	<i>LPR1</i>	qPCR <i>LPR1</i> for	GCCGACGCGTGGTTCACCTGCC
P072	<i>LPR1</i>	qPCR <i>LPR1</i> rev	AGGCGCTACCAAACCGCAAGG
TT038	<i>LPR1</i>	Semi-quantitative PCR	CACCGAGCTCGAGGACCAACTATTC

Supplemental table 2: Overview of all generated *LPR1* variants and the primers used for site directed mutagenesis.

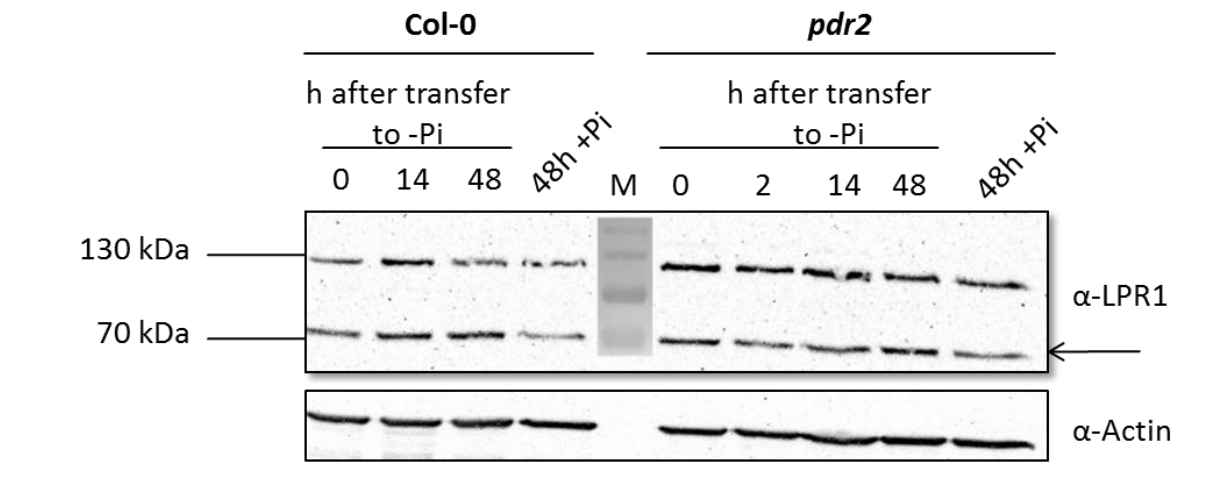
Mutation #	amino acid exchange	Primer for (5'->3')	Primer rev (5' -> 3')
1	E269A	GATTCACCCGACAGTGGCAACCGCCTATTTGGCGA TGTGATAATCG	CGATTATCACATCGCCAAAATAGGCCGTTGCCACTG CGGGTGAATC
2	D370A	CACCATATCCTTACCTAGTGGTGCCCTGTCAACGA AGAAAATGGCAAG	CTTGCCATTTTCTCGTTGACAGGGGCACCACTAGGG TAAGGATATGGTG
3	D462A	GTATGGGAAGTGATAAATTTGACGGAAGCCAACCA TCCGTTACACATTC	GAATGTGTAACGGATGGTTGGCTCCGTCAAATTTAT CACTTCCCATAC
4	H464A	GTGATAAATTTGACGGAAGATAACGCCCGTTACAC ATTCATCTAGG	CCTAGATGAATGTGTAACGGGGCGTTATCTTCCGTCA AATTTATCAC
5	H568A	CCATTGTCACATATTGGACGCCGAGGACAATATGAT GATGAGG	CCTCATCATCATATTGCTCGGCCGTCCAATATGTGA CAATGG
6	C563A	GGAACCGGGCTATGTCTACCATGCCACATATTGGA CCATGAGG	CCTCATGGTCCAATATGTGGGCATGGTAGACATAGC CCGGTTCC
7	P365A	GCTTGCTAATGACGCACCATATGCCTACCCTAGTGG TGATCCTGTCAACG	CGTTGACAGGATCACCACTAGGGTAGGCATATGGTG CGTCATTAGCAAGC
13	E269A D462A	see above	see above
123	E269A D370A D462A	see above	see above

6.3 Supplemental figures

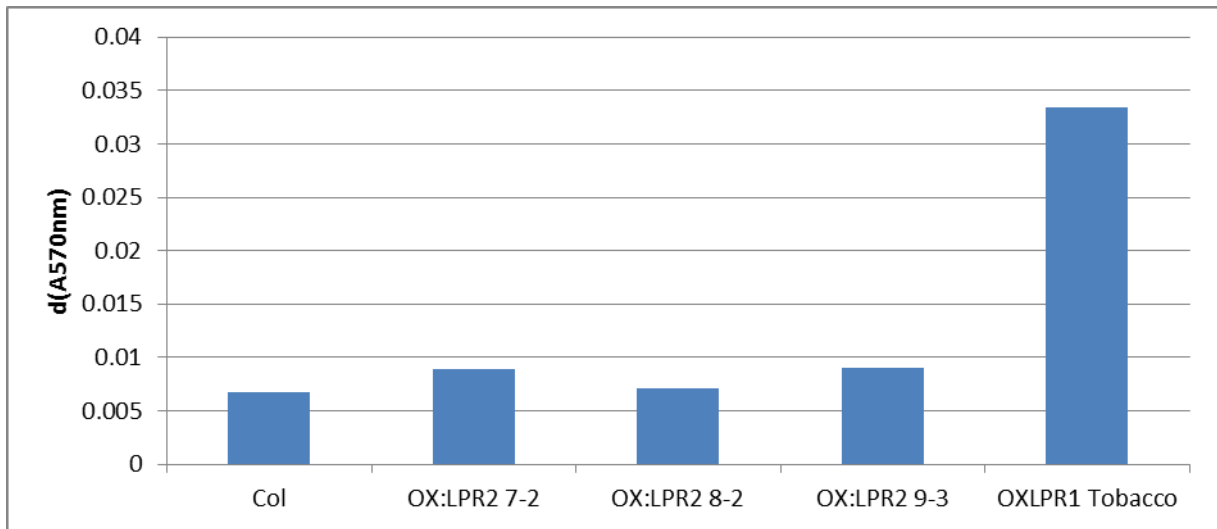
```

1/1-50      1 MESLLCRRRI - KRVMVLIAL - TWLRSTCGEL - EDQLFEVGLK - KMFVDDL PDM
101/1-50   1 PGPTIETVYG - VDTYVTWRNH - LPKSHILPVD - PTISPATPKH - GG IPTVVHLH
151/1-50   1 GGIHEPTSDG - NADAWFTAGF - RETGPKWTKT - TLHYENKQQP - GNMWYHDHAM
201/1-50   1 GLTRVNLLAG - LVGAYILRHH - AVESPFQLPT - GDEFDRPLII - FDRSFRKDG S
251/1-50   1 IYMNATGN NP - SIHPQWQPEY - FGDVIVVNGK - AWPRLNVRRR - KYRFRIINAS
301/1-50   1 NARFFKFFFS - NGLDFIVVGS - DSAYLSK PVM - TKSILLSPSE - IVDVVVDFYK
351/1-50   1 SPSRTVVLAN - DAPYPYPSGD - PVNEENGKVM - KFIINNESED - DTCTIPKKLI
401/1-50   1 NYPNADV SNA - VLTRYISMYE - YVSN SDEPTH - LLVNGLPYEA - PVTETPKSGT
451/1-50   1 TEVWEVINLT - EDNHPLHLHL - GLFKVVEQTA - LLAAGLEEFK - ECMTKQNDAV
501/1-50   1 KCQISKYARG - KKTAVTAHER - GWKNVFKMMP - GHVTRILVRF - SYIHTNASYP
551/1-31   1 FDPTQEPGYV - YHCHILDHED - NMMMRPLKVI - I . . . . .
  
```

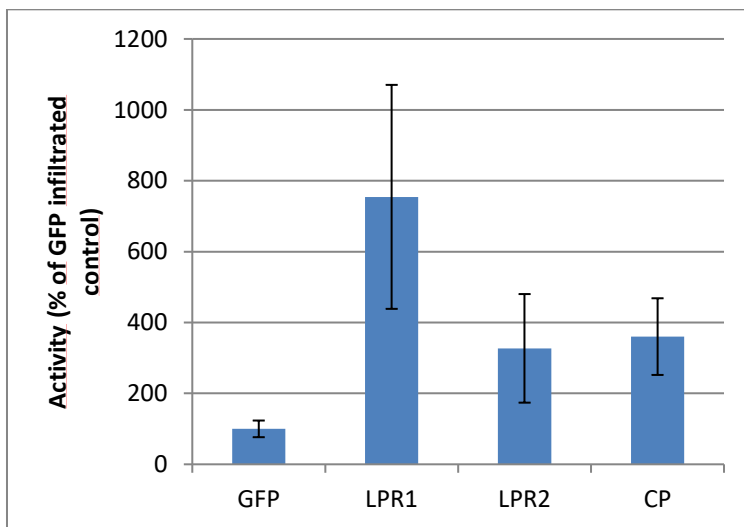
Supplemental Figure 1: AA sequence of *Arabidopsis* LPR1 including ER signal peptide and antibody binding epitope. The amino acid sequence of LPR1 is depicted. Predicted ER signal peptide is marked in green. The peptide that was used to generate the α -LPR1 AB is marked in red.



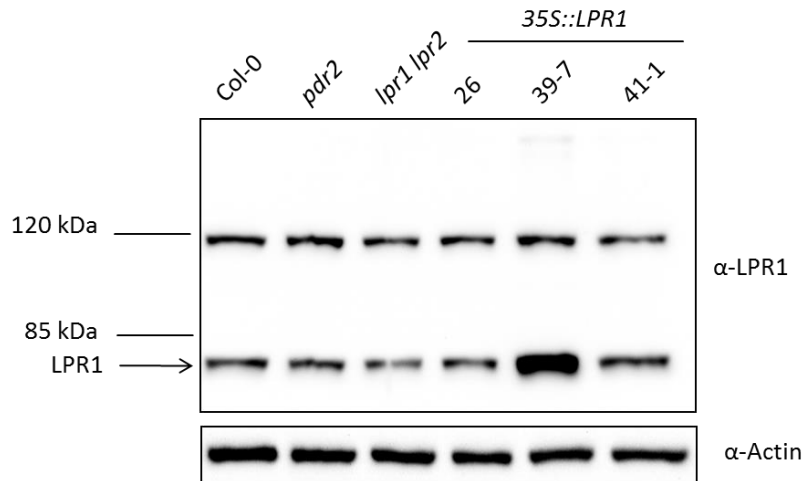
Supplemental figure 2: LPR1 levels in Col-0 and *pdr2* roots upon transfer to -Pi medium



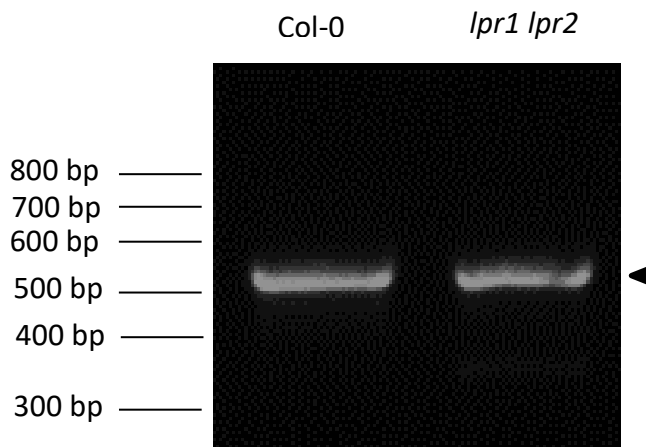
Supplemental figure 3: Decreasing amount of A570nm min-1 in different 35S::LPR2 lines. Col-0 and 3 different 35S::LPR2 lines were grown sterilely on agar plates for 6 days. Protein extracts from whole roots were prepared and Ferrozine assays were carried out. The decreasing amount of absorbance at 570 nm was used as a proxy for the relative ferroxidase activities of the samples in comparison to roots of Col-0. Protein extract from tobacco leaves transiently overexpressing LPR1 was used as a positive control. No elevated ferroxidase activity could be detected in extracts of 35S::LPR2 lines. Representative experiment 1 of 2.



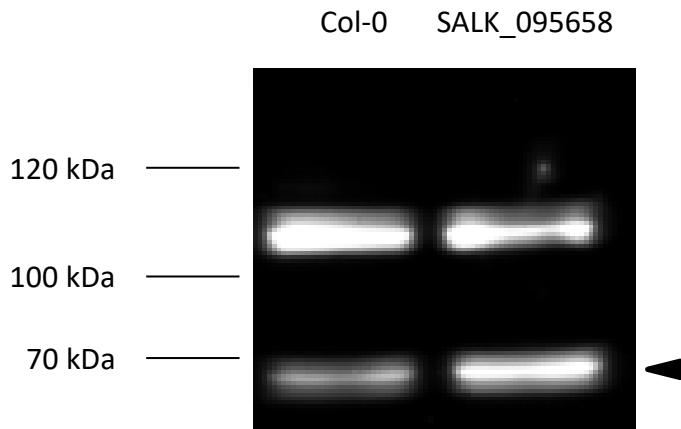
Supplemental figure 4: Ferrozine activity of tobacco leaves transiently expressing GFP, LPR1-GFP and LPR2-GFP. Protein extracts of tobacco leaves that transiently express GFP, LPR1-GFP and LPR2-GFP under the control of the CamV 35S promoter were extracted after 5 days of expression and subjected to Ferrozine assays. GFP infiltrated leaves and purified ceruloplasmin served as negative and positive control, respectively. N=3, error bars indicated Standard deviation



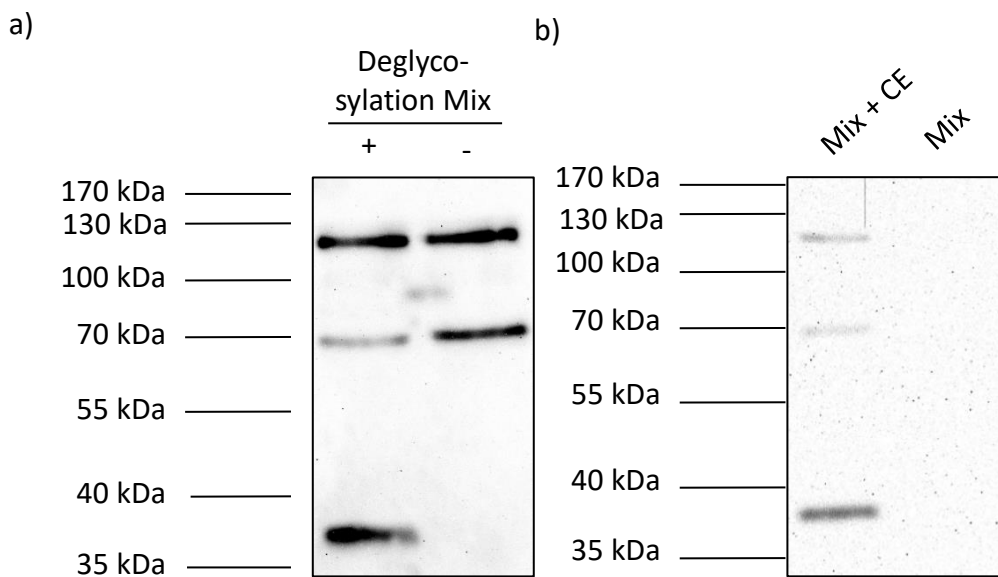
Supplemental figure 5: Protein levels of LPR1 in different genetic backgrounds. Seedlings of Col-0, *pdr2-1*, *lpr1 lpr2*, and 3 different *35S::LPR1* overexpression lines were grown sterilely on +Pi agar plates for 6 days. Total protein extracts were prepared from whole roots and 70 μg of protein were loaded on a 10 % SDS gel. Subsequently, samples were analyzed via Western Blot using α-LPR1 Antibody. LPR1 has a molecular weight of 66 kDa. A second, unspecific band, appeared in all *Arabidopsis*-derived samples at a molecular weight of ~ 120 kDa and served as a loading control.



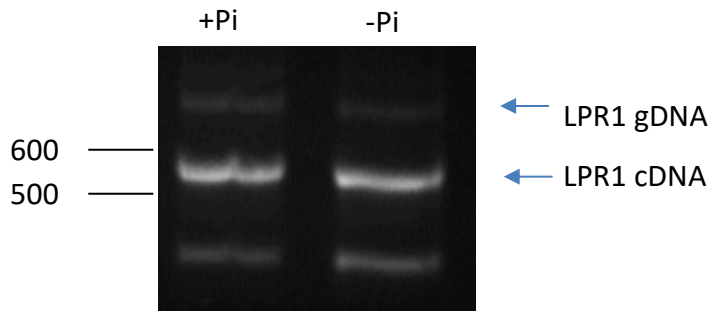
Supplemental figure 6: *LPR1* mRNA levels in Col-0 and *lpr1 lpr2* roots. RNA was extracted from roots of Col-0 and *lpr1 lpr2* plants and first strand cDNA was generated using Revert Aid Reverse Transcriptase. To establish *LPR1* mRNA levels of the original samples, a PCR was carried using primers (TT38 & P072) that bind in 2 neighboring exons. Therefore, PCR products that are originate from gDNA have a size of 880 bp whereas cDNA-derived products have a size of 563 bp and are marked with ◀. Although *lpr1 lpr2* is homozygous for the T-DNA insertion that disrupts the *LPR1* gene, *lpr1* levels were not decreased in this mutant line.



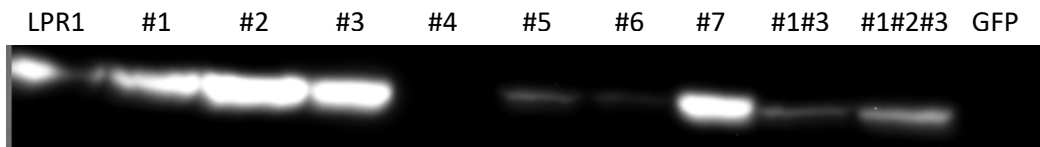
Supplemental figure 7: LPR1 levels in roots of Col-0 and SALK_095658 (*lpr1-2*). Seedlings of Col-0 and *lpr1-2* were grown sterilely on +Pi medium for 6 days. Roots were harvested and total proteins extracted. 70 μ g of protein were loaded on a 10 % SDS gel and subsequently transferred to a nitrocellulose membrane. After Western Blotting, the membrane was probed with 0.1 μ g/ ml α -LPR1 AB. Goat- α -rabbit was used as a secondary AB. Theoretical MW of LPR1 is \sim 66 kDa and the corresponding band on the blot is marked with an \blacktriangleleft .



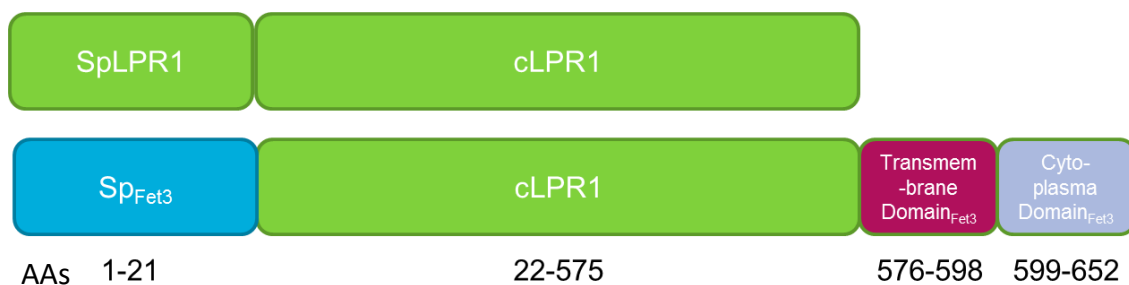
Supplemental figure 8: Western Blot of Deglycosylation Assays of total root extracts from *Arabidopsis* seedlings. Col-0 seedlings were grown for 6 days on +Pi conditions and total protein extracts from roots were prepared. Subsequently, the total protein extracts were subjected to a Deglycosylation assay using Protein Deglycosylation Mix (NEB). All samples were then loaded on an SDS gel and a Western Blot using α -LPR1 AB (0.1 μ g/ml). a) Samples treated with Deglycosylation mix (+) show a fainter band at 70 kDa corresponding to LPR1 than samples without treatment (-). Additionally, an extra band appeared after the treatment at around 35 kDa. b) To exclude an unspecific reaction of the LPR1 AB with PNGaseF that is included in the kit, another western blot was carried out using α -LPR1 AB (0.1 μ g/ml) including a sample that contained Extracted proteins + Protein Deglycosylation Mix and a sample that only included the Protein Deglycosylation Mix. No signals were visible in the Mix only fraction indicating that additional signals in both de-glycosylated samples derived from a product of deglycosylation.



Supplemental figure 9: Semi-quantitative RT-PCR of LPR1 in suspension cultures. After 6 days of growth in + or -Pi medium, suspension culture cells were harvested and the RNA was extracted. cDNA was synthesized and 250 ng used as template for a semi-qRT-PCR. For amplification of LPR1 cDNA, Primers TT038 and P072 were used. The expected amplified PCR product, derived from cDNA has a size of 563 bp. PCR products derived from gDNA have a size of 880 bp.



Supplemental figure 10: Western Blot probed with Anti-LPR1 AB after transient expression of 35S::LPR1 variants in tobacco. *LPR1* and all generated SDM variants including GFP as a negative control were transiently overexpressed in tobacco under the control of a 35S promoter for 4 days. To estimate the amount of LPR1 in each sample, protein crude extracts were generated from 200 – 300 mg leaf material and 70 µg of total protein was loaded on a 10% SDS gel. Subsequently the gels were blotted on a nitrocellulose membrane and probed with an α-LPR1 AB (0,1 mg/ ml [Immunoglobulin]).



Supplemental figure 11: Native LPR1 and chimeric constructs generated for expression in yeast and complementation of a Δ fet3 strain. WT *Arabidopsis* LPR1 consisting of ER signal peptide and coding sequence (a). Chimeric construct of the coding sequence of LPR1 (cLPR1) fused to ER signal peptide of Fet3p. Additionally, Fet3ps transmembrane and cytoplasmic domain was fused to c-terminus of LPR1 to provide membrane anchorage of the chimera.